## ABSTRACT

The electron and nuclear magnetic resonance techniques are now well established and are extensively applied to the investigation of the solid state. We are at present largely concerned with the investigation of defect sites in ionic crystals which are associated with unpaired electronic spins.

Phosphor and semiconductor physics are concerned in many instances with the behaviour of an impurity ion in a host lattice. An impurity cation will, in general, enter a host lattice substitutionally and in some cases may cause distortion of the lattice. Charge compensation must occur when the charge on the impurity cation and the host cation are not the same and the mechanism by which this is achieved is of interest. Accurate information about the behaviour of paramagnetic impurities may be obtained from the resonance spectrum.

Many irradiation induced defects in alkali halides are paramagnetic and may be investigated by the electron resonance technique; addition of impurities extends the range of irradiation induced defects which may be produced. The stability of irradiation centres is temperature dependent and the variety of centres is enhanced by irradiation at low temperature.

The nuclear magnetic resonance technique may be used to determine non-nuclear properties of materials. We are concerned here with magnetic interactions in paramagnetic iron group fluorides using the fluorine nucleus as a probe.

The techniques which have been used to detect electron and nuclear magnetic resonance are outlined.

## RESULTS

### Iron Group Impurities in NaF

Crystals of NaF were grown containing chromium, manganese, iron, cobalt or nickel ions. The paramagnetic resonance spectra of $Mn^{2+}$ and $Co^{2+}$ ions were observed. The divalent ions replace $Na^{+}$ ions and are presumably accompanied by positive ion vacancies to balance the excess charge. Four different types of $Mn^{2+}$ spectrum are observed with D values of 89, 225, 325 and 380 x $10^{-4}$ $cm^{-1}$. The non cubic symmetry arises from association with positive ion vacancies; the variation in D arises from variation in the degree of association. The $Co^{2+}$ spectrum has rhombic symmetry. The failure to observe the non-Kramers ions $Cr^{2+}$, $Fe^{2+}$ and $Ni^{2+}$ may be due to the reduced symmetry produced by a vacancy. The ions $Cr^{+}$, $Fe^{+}$, $Co^{+}$ and $Ni^{+}$ are observed in cubic surroundings after X, $\gamma$ or electron irradiation at room temperature and the resonance spectra have properties which are familiar from previous investigations of the corresponding isoelectronic divalent ions. It appears that divalent iron group ions are effective electron traps at room temperature in NaF. The electron deficient centres which are the source of the trapped electrons have not been determined. The monovalent ions are annealed out by heating to about 140°C and the original state of the crystal is restored.

Most of the spectra investigated show a resolved fluorine structure due to weak covalent bonding of the magnetic electrons with the surrounding fluorine ions. Analysis of this structure gives information about the environment of the impurity ion and indicates that the magnetic electrons spend about 2 of the time in n = 2 orbitals on each of the

nearest neighbour fluorine ions.

Nuclear Magnetic Resonance in $FeF_2$ and $CoF_2$

The paramagnetic ions of $FeF_2$ and $CoF_2$ acquire a considerable mean magnetisation in an external magnetic field and it is expected that the time averaged dipolar field of the magnetic ions at the fluorine nuclear positions will displace the fluorine nuclear magnetic resonance line by several gauss from its normal value of $\omega/\gamma_N$. Measurements made at 30 mcs show however that in addition to the expected anisotropic dipolar shift, an extremely large isotropic shift occurs; this shift has the same temperature dependence as the bulk paramagnetism and in the case of $FeF_2$ at 195°K is 5% of the applied magnetic field while in the case of $CoF_2$ at 90°K a fractional shift of 8% is found. The large internal fields at the fluorine nuclei responsible for this shift are produced by the weak covalency of the $Fe^{2+}$ and $Co^{2+} - F^-$ bond. It may be shown that at a frequency $\nu$, the fluorine magnetic resonance line will occur at magnetic fields given by

$$h\nu = g_N \beta_N H (1 + \alpha)$$

where $\beta_N$ is the nuclear magneton, $g_N$ is the fluorine nuclear g-factor and the fractional field shift is $\alpha$ where

$$\alpha = \frac{1338\chi}{g} \sum_N A^N$$

if $A$ is in units of $cm^{-1}$; here $\chi$ is the molar susceptibility, $g$ is the electronic g-factor and $A^N$ is the h.f.s. constant for the interaction between the fluorine nucleus and the $N^{th}$ paramagnetic ion. Values of $g$

and $A^N$ are available from electronic magnetic resonance measurements on $Fe^{2+}$ and $Co^{2+}$ ions present as trace impurities in $ZnF_2$ and we may compare calculated values of $a$ with the measured values. In the case of $FeF_2$ the measured values of $a$ are a few per cent larger than the calculated values but with $CoF_2$ the agreement is very poor; this is not unexpected since the expression for $a$ was derived assuming 'spin-only' magnetism and this condition does not hold in the case of $CoF_2$.

Paramagnetic Impurities in $CaF_2$

Rare earth impurities were introduced into the cubic $CaF_2$ lattice and the paramagnetic resonance spectra of $Ce^{3+}$, $Eu^{2+}$, $Gd^{3+}$ and $Er^{3+}$ ions were observed. The trivalent ions replace $Ca^{2+}$ ions and charge compensation is generally achieved by the introduction of an $F^-$ ion into the nearest interstitial site; this introduces tetragonal symmetry about a cube edge into the crystal field at the impurity ion and there are three distinguishable centres with similar spectra in the magnetic unit cell. The g-values of $Ce^{3+}$ are $g_{\parallel} = 3.038 \pm 0.003$, $g_{\perp} = 1.396 \pm 0.002$. Transitions within two doublets of $Er^{3+}$ in a tetragonal field were observed with (a) $g_{\parallel} = 7.76 \pm 0.02$, $g_{\perp} = 6.253 \pm 0.006$, (b) $g_{\parallel} = 6.76 \pm 0.02$, $g_{\perp} = 9.11 \pm 0.01$; the doublet which gives rise to (b) is about 36k above the ground doublet which gives rise to (a). $Er^{3+}$ ions also occur in a cubic field with $g = 6.78 \pm 0.01$; in this case the cubic symmetry is not reduced presumably because of remote charge compensation. A complete analysis of the $Gd^{3+}$ spectrum was not possible because of the large overall zero field splitting ($\sim 2$ cm$^{-1}$) of the ground octuplet which is largely due to the tetragonal field. The cubic crystal

symmetry is maintained in the case of $Eu^{2+}$ and the constants of the spectrum are $g = 1.989 \pm 0.002$, $^{151}A = 34.5 \pm 0.2 \times 10^{-4}$ cm$^{-1}$, $^{153}A = 15.3 \pm 0.4 \times 10^{-4}$ cm$^{-1}$; the overall zero field splitting of the octuplet is 0.186 cm$^{-1}$.

Iron group ions were also introduced into the $CaF_2$ lattice. $Mn^{2+}$ ions are present with cubic symmetry and a complete analysis of the spectrum shows that the cubic field splitting is small ($a = + 0.6 \pm 0.4 \times 10^{-4}$ cm$^{-1}$). Spectra have also been observed which have been assigned to $Cr^{2+}$ and $Co^{2+}$ ions but a local distortion of the lattice makes the interpretation of the spectra difficult.

The iron group ions show a resolved fluorine structure characteristic of weak covalent bonding with nearest fluorines but this is not evident with rare earth ions because the magnetic electrons are more localised. In the case of the rare earths, a fluorine satellite structure is observed due to the simultaneous flipping of the electron spin and the nuclear spin of a nearest fluorine ion; this effect arises from a weak magnetic coupling, partly dipolar in origin, between the electron spin and the nuclear spin.

V-centres in Alkali Halides

Crystals of KCl and KBr containing $Ba^{2+}$, $Sr^{2+}$ or $Ca^{2+}$ ions were X-irradiated at 195°K and the paramagnetic resonance spectra investigated without warming the crystals. Spectra were observed which have been assigned to $Cl_2^-$ and $Br_2^-$ molecule ions (these centres are described as V-centres, hole centres or electron deficient centres) alined approximately along a cube edge. The electrons released by the

irradiation are trapped as F-centres. These results are in contrast with measurements on pure crystals or crystals containing good electron traps such as silver, thallium or lead where $Cl_2^-$ and $Br_2^-$ centres are observed alined accurately along a face diagonal. It is proposed that the approximate cube edge alinement arises from the trapping of the V-centres at positive ion vacancies associated with the divalent impurity ions.

The spectra may be approximately fitted to the spin Hamiltonian

$$\mathcal{H} = g_{\parallel} \beta H_z S_z + g_{\perp} \beta (H_x S_x + H_y S_y) + A I_z S_z + B(I_x S_x + I_y S_y)$$

where $S = \frac{1}{2}$ and $I = I_1 + I_2$ where $I_1 = I_2 = \frac{3}{2}$ is the spin of the halogen nuclei. There are three resolved $Cl_2^-$ isotopic species, 35-35, 35-37, 37-37; the $Br_2^-$ isotopic species 79-79, 79-81 and 81-81 are also resolved. The constants of the spectrum of $Cl_2^-$ (35-35) are $g_{\parallel} = 2.005 \pm 0.003$, $g_{\perp} = 2.04 \pm 0.01$, $A = 89.0 \times 10^{-4}$ cm$^{-1}$, $B = 13 \times 10^{-4}$ cm$^{-1}$. The only measurable constants of $Br_2^-$ (81-81) are $g_{\parallel} = 1.991 \pm 0.003$ and $A = 419 \times 10^{-4}$ cm$^{-1}$.

Potassium Chloride Containing Silver

When crystals of KCl containing $Ag^+$ ions are X-irradiated at 77°K, $Cl_2^-$ ions alined along a crystal face diagonal are rapidly produced because $Ag^+$ ions are efficient electron traps. A $Ag^+$ ion which traps an electron becomes a neutral paramagnetic silver atom ($Ag^\circ$). The resonance spectra of both $Cl_2^-$ and $Ag^\circ$ have been observed, the latter showing a resolved chlorine structure. Silver has two isotopes, $^{107}Ag$ and $^{109}Ag$ each with $I = \frac{1}{2}$. The constants of the spectrum of $^{109}Ag$ are

$g = 1.997 \pm 0.003$, $A = 620 \pm 2 \times 10^{-4}$ cm$^{-1}$.

When the crystals are warmed to 208°K a luminescent glow is observed and the spectrum changes. The $Cl_2^-$ centres disappear, the $Ag^0$ concentration is reduced by about 20% and a new paramagnetic hole centre is produced. The hole is localised mostly on a silver ion and two chlorine ions (for this reason we refer to the centre as $AgCl_2$) and within the accuracy of measurement has axial symmetry about a cube edge; there are three distinguishable centres in the magnetic unit cell, each with similar spectra. The spectrum may be fitted to the spin Hamiltonian

$$\mathcal{H} = g_{\parallel} \beta H_z S_z + g_{\perp} \beta (H_x S_x + H_y S_y) + A I_z S_z$$
$$+ B (I_x S_x + I_y S_y) + A' [(I_{oz}^{I} + I_{oz}^{II}) S_z]$$
$$+ B' [(I_{ox}^{I} + I_{ox}^{II}) S_x + (I_{oy}^{I} + I_{oy}^{II}) S_y]$$

where $S = \frac{1}{2}$, $I = \frac{1}{2}$ is the spin of the silver nucleus, $I_o^I = I_o^{II} = \frac{3}{2}$ is the spin of the chlorine nucleus, $g_{\parallel} = 2.196 \pm 0.006$, $g_{\perp} = 2.038 \pm 0.005$,

$$A = 38 \pm 2 \times 10^{-4} \text{ cm}^{-1}, \quad B = 30 \pm 4 \times 10^{-4} \text{ cm}^{-1}$$
$$A' < 4 \times 10^{-4} \text{ cm}^{-1} \quad \text{and} \quad B' = 30 \pm 4 \times 10^{-4} \text{ cm}^{-1}.$$

On heating to 373°K, electrons are released from $Ag^0$ centres forming $Ag^+$ ions and are captured by the $AgCl_2$ hole centres with the emission of a luminescent glow; the $AgCl_2$ centres are destroyed and the crystal is restored to its condition before irradiation.

# FURTHER APPLICATIONS OF MAGNETIC RESONANCE

THESIS FOR

THE DEGREE OF DOCTOR OF PHILOSOPHY

AT THE UNIVERSITY OF OXFORD

SUBMITTED BY

W. HAYES

OF ST. JOHN'S COLLEGE




HILARY TERM, 1959

## ACKNOWLEDGMENTS

The author is deeply indebted to:

The late Professor Lord Cherwell, the late Professor Sir Francis Simon and Professor B. Bleaney for provision of research facilities at the Clarendon Laboratory;

Professor B. Bleaney and Dr. J.M. Baker who supervised the work carried out in the Clarendon Laboratory, for much helpful advice;

Dr. M.C.M. O'Brien, Dr. J. Owen and Dr. B.R. Judd for many helpful discussions;

Dr. D.A. Jones of the University of Aberdeen and Professor J.W. Stout of the University of Chicago who supplied crystals;

The Atomic Energy Research Establishment, Harwell, and Mr. J.E. Ortem for the provision of irradiation facilities;

Mr. L.J. Arundel for assistance with electronic equipment;

Mr. E.J. Jenkinson and the workshop staff of the Clarendon Laboratory for building items of apparatus;

The Commissioners for the Exhibition of 1851 for the award of an Overseas Scholarship (1955-57);

Dr. O.C. Simpson for general hospitality during the tenure of a Resident Research Associateship at the Argonne National Laboratory (1957-58);

Dr. P.H. Yuster, Dr. C.J. Delbecq and Dr. G.M. Nichols for friendly cooperation in research projects;

Dr. B. Smaller for the loan of apparatus;

Mr. E. Avery and Mr. E. Yasaitis for assistance with experiments.

## CONTENTS


| | | Page |
|---|---|---|
| INTRODUCTION | | 1 |
| | **Chapter I. Experimental Techniques** | |
| I.1 | The Paramagnetic Resonance Spectrometers | 6 |
| I.2 | Irradiation of Crystals with Polarised Light | 12 |
| I.3 | The Nuclear Magnetic Resonance Spectrometer | 12 |
| I.4 | Crystal Growing Techniques | 13 |
| | **Chapter II. Iron Group Impurities in NaF** | |
| II.1 | Introduction | 17 |
| II.2 | The Interaction of the Magnetic Ions with the Lattice | 18 |
| II.3 | Chromium | 23 |
| II.4 | Manganese | 27 |
| II.5 | Iron | 31 |
| II.6 | Cobalt | 32 |
| II.7 | Nickel | 34 |
| II.8 | Copper | 37 |
| II.9 | Discussion | 37 |
| | **Chapter III. Nuclear Magnetic Resonance in $FeF_2$ and $CoF_2$** | |
| III.1 | Introduction | 44 |
| III.2 | Crystal Structure | 45 |
| III.3 | Experimental Results | 46 |
| III.4 | Interpretation | 48 |

Page

Chapter IV. Paramagnetic Impurities in $CaF_2$.

IV.1 Introduction 57

IV.2 Manganese 58

IV.3 Impurities of the 4f group 63

IV.4 Cerium 64

IV.5 Europium 65

IV.6 Gadolinium 71

IV.7 Erbium 74

IV.8 Other Impurities 75

IV.9 Fluorine Satellite Structure of Rare Earths 76

IV.10 Discussion 82

Chapter V. V-centres in Alkali Halides

V.1 Introduction 88

V.2 Optical Absorption Spectrum of KCl 92

V.3 Paramagnetic Resonance Spectrum of KCl 92

V.4 Optical Absorption Spectrum of KBr 94

V.5 Paramagnetic Resonance Spectrum of KBr 94

V.6 Correlation between Optical and Resonance Spectra 95

V.7 Discussion 96

Chapter VI. Potassium Chloride Containing Silver

VI.1 Introduction 104

VI.2 Effect of $\lambda$-irradiation on KCl:Ag at 77°K 104

| | | Page |
|---|---|---|
| VI.3 | Changes in the properties of the KCl:Ag crystals with increasing temperature | 107 |
| VI.4 | Discussion | 110 |

## INTRODUCTION

The basic theory of the electron magnetic resonance phenomenon has been described in review articles. Bleaney and Stevens[1] have primarily concerned themselves with salts containing transition group ions where the unpaired electrons are in unfilled d or f shells. Bowers and Owen[2] have collected available paramagnetic resonance data on these salts. The work described in these reviews is largely concerned with the properties of the energy levels of the paramagnetic ion within a few $cm^{-1}$ of the ground level and with the determination of nuclear properties of the transition ion. Nuclear spins and approximate values of nuclear magnetic dipole moments and electric quadrupole moments may be obtained if there is a hyperfine structure in the electron resonance spectrum from interaction between the electrons and the nucleus.

During the past few years the paramagnetic resonance technique has been extensively applied to the investigation of the solid state. A review of work on such problems as cyclotron resonance in semiconductors, the properties of conduction electrons in metals and defect sites in solids has been given by Bagguley and Owen[3]. This present thesis is largely concerned with the investigation of defect sites in ionic crystals.

The behaviour of an impurity ion in a host lattice is of interest in phosphor and semiconductor physics. The luminescence of many phosphors is associated with the presence of impurities and in some cases these are paramagnetic, for example Zn S and Cd S activated with copper or

manganese ions and $CaF_2$ with rare earths. The degree to which an impurity ion is incorporated into a host lattice is determined to a considerable extent by its bonding characteristics and size. An impurity cation will in general enter a host lattice substitutionally and if its size is not comparable with that of the host cation, considerable local distortion of the lattice may occur. An impurity may also enter a lattice interstitially. In cases where the charge on the impurity cation and the host cation are not the same, charge compensation must occur since the crystal as a whole must remain neutral and the mechanism by which this is achieved is of interest.

When the impurity ion is paramagnetic and the electron resonance spectrum is observable it is sometimes possible to obtain precise information about its environment. The nature of the resonance spectrum gives information about the spectroscopic state of the ion and the symmetry and strength of the crystalline electric field in which it is placed. In the course of the present work the properties of iron group ions in MgF and $CaF_2$ were investigated and a fluorine hyperfine structure observed in the resonance spectrum due to the formation of a weak covalent complex with the nearest neighbour fluorine ions; this structure arises from the interaction of the magnetic electrons with fluorine nuclei through bond formation. Analysis of the fluorine structure enables one to estimate the percentage covalent character of the bonds and gives information about the ligands of the impurity ion.

When insulating crystals are irradiated with ionising radiations such as X-rays or $\gamma$-rays, then, electrons excited to a conduction band

are eventually trapped at a defect centre in the lattice. Normally a crystal contains positive and negative ion vacancies in equal number and the latter may trap electrons forming F-centres. An imperfection in a crystal which has one or more unpaired electrons associated with it gives rise in general to a resonance spectrum. Both the electron excess centres (trapping centres) and the electron deficient centres (V-centres or holes) are of interest.

The irradiation of alkali halides has flourished for many years[4,5] and these crystals have provided a rich field for investigation. The diversity of defect centres which may be produced by irradiation is greatly increased by the addition of impurities. Many impurities are efficient electron traps and assist the formation of hole centres. The stability of electron excess centres and of hole centres is temperature dependent and the variety of these centres is enriched by irradiation at low temperatures.

Defect centres in alkali halides have been investigated through their optical absorption spectra, luminescence spectra, dielectric loss, electrical conductivity and by the application of optical microscopy. Where applicable, the paramagnetic resonance technique is a powerful tool because of its high resolution, and combination with the above techniques sometimes enables one to give very extensive descriptions of the structure of defect centres. Any nucleus of spin I associated with a defect is 'labelled' by the $2I + 1$ hyperfine splitting of the paramagnetic resonance spectrum; the magnitude of the splitting indicates the time spent by the unpaired electron in the vicinity of the nucleus. This is the most powerful method of 'labelling' a defect. The behaviour of the resonance

spectrum as the crystal is rotated in the external magnetic field gives information about the symmetry properties of the defect. The line width gives information about magnetic interactions with the surroundings and spin-lattice relaxation effects. The departure of the spectroscopic splitting factor from the free spin value, $\Delta g = g - 2.002\ 3$, is usually determined by spin-orbit interactions for the unpaired electron and is normally negative for electrons and may be positive for holes. Recently (Watkins, private communication), the correlation of dielectric loss measurements with paramagnetic resonance measurements enabled the dielectric loss peaks of divalent-vacancy pairs in monovalent lattices to be unambiguously established. In the present work it will be shown how the optical spectra of some defect centres may be established by correlation with resonance measurements.

The nuclear magnetic resonance technique has found many applications in the study of ionic and covalent solids; useful information may be obtained concerning the structure and other non-nuclear properties of the material. The protons in hydrated paramagnetic and antiferromagnetic crystals have provided magnetic probes for the study of the magnetic properties of these crystals. We are concerned here with magnetic interactions in iron group fluorides, e.g. $FeF_2$, using the fluorine nucleus as a probe and it is shown how electron resonance measurements on iron group impurity ions present in trace quantities in the isomorphous diamagnetic $ZnF_2$ may be correlated with the nuclear resonance measurements. The theory and general applications of nuclear magnetic resonance have been described by Andrew[6].

Each chapter in this thesis is supplied with an individual table of references.

## References


1. Kleaney, B. and Stevens, K.W.H., Rep. Prog. Phys., (1953), 16, 108.
2. Bowers, K.D. and Owen, J., Rep. Prog. Phys., (1955), 18, 304.
3. Baggulley, D.M.S. and Owen, J., Rep. Prog. Phys., (1957), 20, 304.
4. Seitz, F., Rev. Mod. Phys., (1946), 18, 384.
5. Seitz, F., Rev. Mod. Phys., (1954), 26, 7.
6. Nuclear Magnetic Resonance by E. R. Andrew, Cambridge University Press, (1955).

# Chapter I

## EXPERIMENTAL TECHNIQUES

### 1.1 The Paramagnetic Resonance Spectrometers

A detailed description of a sensitive X-band paramagnetic resonance spectrometer has been given by Llewellyn[1,2]. A similar spectrometer has been built by the present author.

In a conventional paramagnetic resonance apparatus the detector crystal noise sets the limit on sensitivity. Over a wide range of frequencies the noise power is approximately proportional to $1/f$ and detection of the resonance signal at a high frequency will therefore reduce the noise density[1,2,3]. In a pass band from $f_1$ to $f_2$ the noise power is proportional to

$$P = \int_{f_1}^{f_2} f^{-1}\, df = \ln f_2/f_1 . \qquad 1.1$$

In a simple type of paramagnetic resonance spectrometer the signal is detected at 50 cs and displayed on an oscilloscope screen[4]. For satisfactory oscilloscope display a receiver bandwidth of at least 5 kcs is required. In the spectrometer of Llewellyn the signal is detected at 115 kcs and we may compare the noise power with a 5 kcs bandwidth at this frequency with a simple system taken from 25 cs to 5 kcs. Formula 1.1 shows that the noise power is reduced by a factor of about 100 and hence the signal to noise will be a factor of ten better than that obtainable with the simpler system. Such an improvement has

been realised in practice[1,2]. The performance of the high frequency modulated system is even better with narrow band detection. In this case, for a given bandwidth, the noise power reduction is proportional to the ratio of the centre band frequencies and if we compare a 50 cs system with a 115 kcs system there is an improvement of signal to noise of almost 50 to 1. Because of the commercial availability of I.F. transformers tuneable to 465 kcs it was decided to build a field modulated spectrometer operating at this frequency. The r.f. oscillator, pre-amplifier and detector were built after designs by L. J. Arundel. Apart from the r.f. stages, the spectrometer resembled the 115 kcs spectrometer of Llewellyn very closely.

A block diagram of the spectrometer is shown in fig. 1.1. The X-band microwave power is supplied by a CV129 klystron which is capable of delivering about 50 mw; the mechanical tuning provides a coarse frequency adjustment and a fine adjustment is made by varying the reflector voltage. A stabilised klystron power supply designed by L. J. Arundel gives - 1.4 kv for the cathode and 0 → - 500 v relative to the cathode for the reflector; the ripple on the reflector and grid leads is less than 200 μv. The power from the klystron is coupled into a wave guide which has a backing plunger for proper matching. The klystron power is monitored by a directional coupler and a silicon-tungsten crystal rectifier. An attenuator isolates the klystron from the resonant cavity and controls the power level in the cavity. The wave length of the radiation is measured with a coaxial line wavemeter. The wave guide is terminated by a section with a backing plunger which

couples out power into a coaxial line which is part of the resonant cavity assembly. A rectangular transmission cavity oscillating in the $TE_{101}$ mode is used. A detailed description of the cavity assembly and the method of introducing the high frequency modulation into the cavity has been given by Llewellyn.

The paramagnetic resonance signal appears as a 465 kcs modulation of the microwaves. The microwaves are rectified by a silicon-tungsten crystal and fed to a 465 kcs pre-amplifier. This consists of four stages of amplification with a tuned input which matches the crystal impedance to that of the input grid. The pass-band of each stage is about 8 kcs centred on 465 kcs. The maximum gain is 140 db which is sufficient to saturate the input noise. The output is matched to a 70 ohm load. The output signal passes through an adjustable phase shifter, another stage of amplification, and is finally detected in a phase sensitive manner using a 1V reference signal from the 465 kcs oscillator. The detector output, which is proportional to the derivative of the absorption, may be passed through an adjustable RC time constant and d.c. amplifier to operate a chart recorder for sensitive slow-sweep work; the time constants employed in the RC network varied from 0.1 to 10 seconds in switched steps. If we are not interested in the highest sensitivity and wish to use the 8 kcs bandwidth for visual presentation, we may impress a 50 cs modulation on the external magnetic field using auxiliary coils on the magnet pole faces and apply the detector output directly to an oscilloscope. If we are working with specimens containing $10^{16}$ or more spins, we may dispense with r.f.

modulation, use 50 cs modulation only and apply the crystal detector output through an a.f. amplifier to an oscilloscope.

The current providing the slow sweep of the magnetic field for sensitive work is fed through the auxiliary magnet coils and is obtained from a rectifier supplied by a motor driven variac. During the slow sweep, drift of the steady magnetic field is reduced by floating a bank of accumulators across the coil windings of the magnet. This system provides voltage stabilisation and at 4 kG the 'jitter' may be reduced to about $^1/_{10}$ gauss and the slow drift, after a warming time of one hour, to less than 10 gauss per hour. We measure the magnetic field in which electron resonance is observed by finding the frequency at which proton resonance occurs in the same field; the proton resonance frequency is measured with a BC 221 wavemeter.

To achieve the ultimate sensitivity using 465 kcs modulation it is necessary to suppress 'pick-up' signals at this frequency. The 465 kcs generator is contained in a $\frac{1}{8}$" copper box which is earthed at one point only. The entire first stage of the 465 kcs preamplifier is also in a $\frac{1}{8}$" copper box and the coupling transformer between the first and second stage is screened with copper. The leads from the generator to the modulating coil and from the crystal rectifier to the preamplifier are double screened and the connections from the crystal rectifier to the preamplifier are heavily screened. The klystron is also screened. Earth loops which can pick up 465 kcs signals must be eliminated and d.c. breaks are provided in the waveguide before and after the resonant cavity assembly.

Llewellyn calibrated the 115 kcs spectrometer with a $^{56}Co$ source of

known concentration and estimated that, at maximum sensitivity, $3 \times 10^{11}$ molecules of dpph would give a signal to noise ratio of 2 to 1 at $90^{\circ}K$; this value is close to the theoretical sensitivity. A direct comparison of the noise figure of the receiver systems at 465 kcs and 115 kcs showed that the former was about 5 times better. However, it was not always possible to use the available sensitivity of the 465 kcs system. Eddy currents in the cavity limit the magnetic field modulation depth to about 20 gauss peak to peak even with 8 amps r.m.s. in the modulating coil. With r.f. currents of this magnitude there is a rapid evaporation of liquid hydrogen. However, this effect is not very serious since line widths are in general of the order of 5 to 10 gauss. A more important effect is an increase in temperature of the specimens when the modulation amplitude is more than about 5 gauss peak to peak. This effect is observed in cases where the line width is determined by the spin-lattice relaxation, e.g. $Co^{2+}$ at $20^{\circ}K$. The increase in temperature may be demonstrated by displaying the cobalt spectrum visually using 50 cs modulation only and at the same time subjecting the crystal to a 465 kcs r.f. field. At r.f. field amplitudes of about 10 gauss the line width increases to about 100 gauss and at greater modulation amplitudes the spectrum may be made to disappear altogether. If the r.f. field is switched off the spectrum returns after a few seconds. The heating arises from dissipation of power in the sample, presumably from dielectric loss. No such effect was found using the 115 kcs modulation.

Measurements at K-band were made with a spectrometer using 50 cs modulation only; the construction was similar to that of the simple type

of X-band system already described.

An illustrated description of the X-band paramagnetic resonance spectrometer used at the Argonne National Laboratory has already been given[5]. The dewar-cavity system was especially useful for investigating the effects of irradiation on crystals at low temperatures. The unsilvered tail of the dewar projected into an evacuated reflection cavity operating in the $TE_{102}$ mode and crystals could be kept at 20°K within the cavity without cooling the cavity itself. The alkali halide crystals to be irradiated were accurately cleaved to the dimensions 2.5 x 2.5 x 10 mm. The crystals were then submerged to a shallow depth in liquid nitrogen or other suitable refrigerant and exposed to X-rays produced in a Machlett tube operating with a tungsten target at 50 kv and 50 ma; a quarts filter 1 mm thick was used to reduce excess surface absorption in the crystal. After irradiation the crystals were tightly wedged into a rectangular aperture at the end of a lucite rod, while still covered with refrigerant. The rod was subsequently inserted into the dewar quickly and it is estimated that the temperature of the sample does not change more than a few degrees during the transfer. This technique avoids the difficulties encountered in the irradiation of crystals within a cooled cavity. The crystal could be oriented in the magnetic field in a measurable fashion by rotating the lucite rod about a vertical axis.

A dual modulation system[6] operating at 17 kcs and 25 cs was incorporated into the system. Phase sensitive detection was used at both frequencies and the second derivative of the absorption signal displayed. It was estimated[5] that the limiting detectability of

dpph at 80°K was about $2 \times 10^{12}$ spins.

## I.2. Irradiation of Crystals with Polarized Light

In many cases it was of interest to study the effect of polarised light at a low temperature on the magnetic centres of X-irradiated alkali halide crystals. Polarised bleaching experiments were done while the crystal, mounted on a lucite holder, was immersed in a dewar flask filled with refrigerant. The light entered the dewar flask through quartz windows. In general, the polarising prism was mounted with its axis parallel to one of the cubic axes of the alkali halide crystal and the prism could be rotated about this axis so that the electric vector of the transmitted polarised light made any desired angle with the other two cubic axes of the crystal.

## I.3. The Nuclear Magnetic Resonance Spectrometer

The nuclear resonance spectrometer incorporates a bridge arrangement of the type described by Bloembergen, Purcell and Pound[7]. The purpose of a bridge is to reduce the r.f. carrier level to a sufficiently low value to permit considerable amplification before rectification and to cancel noise arising from spurious modulation of the output of the signal generator. It normally suffices that the carrier level at the output of the bridge be reduced to about 1% of its value in either arm. A block diagram of the spectrometer is given in fig. I.2. The r.f. signal generator and detector and the low frequency phase sensitive detector were designed and built by L. J. Arundel.

The r.f. signal generator is crystal controlled at 5, 10 and 30 mcs and has a maximum output at each of these frequencies of about 2v. All

the measurements described in Chapter III were carried out at 30 mcs. The condition of the bridge which determines the nature of the signal curve displayed, is maintained by observation of the r.f. detector current. The nuclear resonance line widths encountered in paramagnetic crystals may be of the order of 10 to 30 gauss. To display the resonance absorption we may modulate the external magnetic field at a low audio frequency, e.g. 75 cs, with an amplitude greater than the line width using the auxiliary magnet coils. After rectification, the audio signal is amplified and displayed on an oscilloscope. In the present case the modulation was supplied by an a.f. signal generator followed by a power amplifier. In the experiments described in Chapter III the lines were almost 30 gauss wide and were too weak for visual display. A phase sensitive detector was used operating on a 1V reference signal from the a.f. generator. A 2 second time constant was employed and the signal was displayed on a chart recorder driven by a d.c. amplifier.

It was necessary for some measurements to immerse the coil in a refrigerant. The coil was electrically screened and isolated from the refrigerant by a brass cup which also reduced the Q of the coil by a factor of about 3. During the operation of the spectrometer, difficulties were encountered in maintaining the balance of the bridge and interference by outside sources of r.f. radiation sometimes caused trouble. Effective elimination of outside interference would require screening of the entire spectrometer.

## I.4. Crystal Growing Techniques

Crystals of NaF (see Chapter II) and crystals of $CaF_2$ (see Chapter IV)

were grown by D. A. Jones using the Stockbarger technique[8]. The $CaF_2$ crystals were grown from colourless natural fluorite which was crushed before loading into the graphite crucible. The impurities were introduced by mixing the appropriate amount of salt containing the element required with the powdered fluorite. Where possible, fluorides were used but if these were not available 1% $PbF_2$ was added to the mixture to remove unwanted electronegative ions. Any excess $PbF_2$ evaporates from the melt and the crystal contains less than 1 in $10^6$ of lead.

The procedure adopted for growing these crystals was as follows. The furnace was evacuated and when the pressure was less than 5μ the temperature was raised to about 100°C and left under these conditions for 24 hours. This was to ensure thorough drying of the powdered fluorite before it was raised to temperatures at which hydrolysis occurs. The temperature was then increased at a rate of 100°C per hour to about 1250°C. At this temperature a stream of oxygen free nitrogen was passed through the furnace to raise the pressure to about 30μ to avoid undue loss of material due to evaporation. The furnace was then raised to about 20°C above the melting point of fluorite (1360°C) and left at this temperature for an hour to ensure complete melting. The crystal was then grown by lowering the crucible in the furnace at a rate of 1 mm per hour and when the melt was completely solidified it was cooled to room temperature at about 50°C per hour.

Crystals of NaF were grown in a similar fashion. However, no attempt was made to remove unwanted electronegative ions by the addition of $PbF_2$ because under the conditions of temperature and pressure at which

the NaF crystals were grown, this salt does not completely evaporate off. The salt was held at a pressure less than 5μ and a temperature of about 100°C for 24 hours. The temperature was then raised at a rate of 100°C per hour to about 850°C at which temperature a stream of oxygen-free nitrogen was passed through the furnace to raise the pressure to 6 mm. of mercury. The temperature was increased to 1000°C (M.P. of NaF 980°C) and the crystal grown by lowering the crucible at a rate of 1 mm. per hour. When growth was complete the furnace was cooled to room temperature at a rate of 50°C per hour.

Estimates of the number of impurity atoms present in the NaF and $CaF_2$ crystals were made from the intensity of the paramagnetic resonance spectrum. The apparatus was calibrated using a $^{56}Co$ source of known concentration[1] and the estimates are expected to be in error by about a factor of five.

Alkali halide crystals were grown at the Argonne National Laboratory by E. Hutchinson using the Kyropoulos method[9] (see Chapter V and VI). The powdered salt with impurity mixed was melted in a platinum crucible exposed to the atmosphere. A seed crystal attached to the end of a platinum rod was then partly inserted into the melt and slowly withdrawn.

Crystals of $CoF_2$ and $FeF_2$ were supplied by J. W. Stout (see Chapter III).

REFERENCES

1. Llewellyn, P.M., J. Sci. Instr., (1957), 34, 236.

2. Llewellyn, P.M., Thesis, Oxford, (1956).

3. Tinkham, M., Proc. Roy. Soc., (1956), A236, 535.

4. Bleaney, B. and Stevens, K.W.H., Rep. Prog. Phys., (1953), 16, 108.

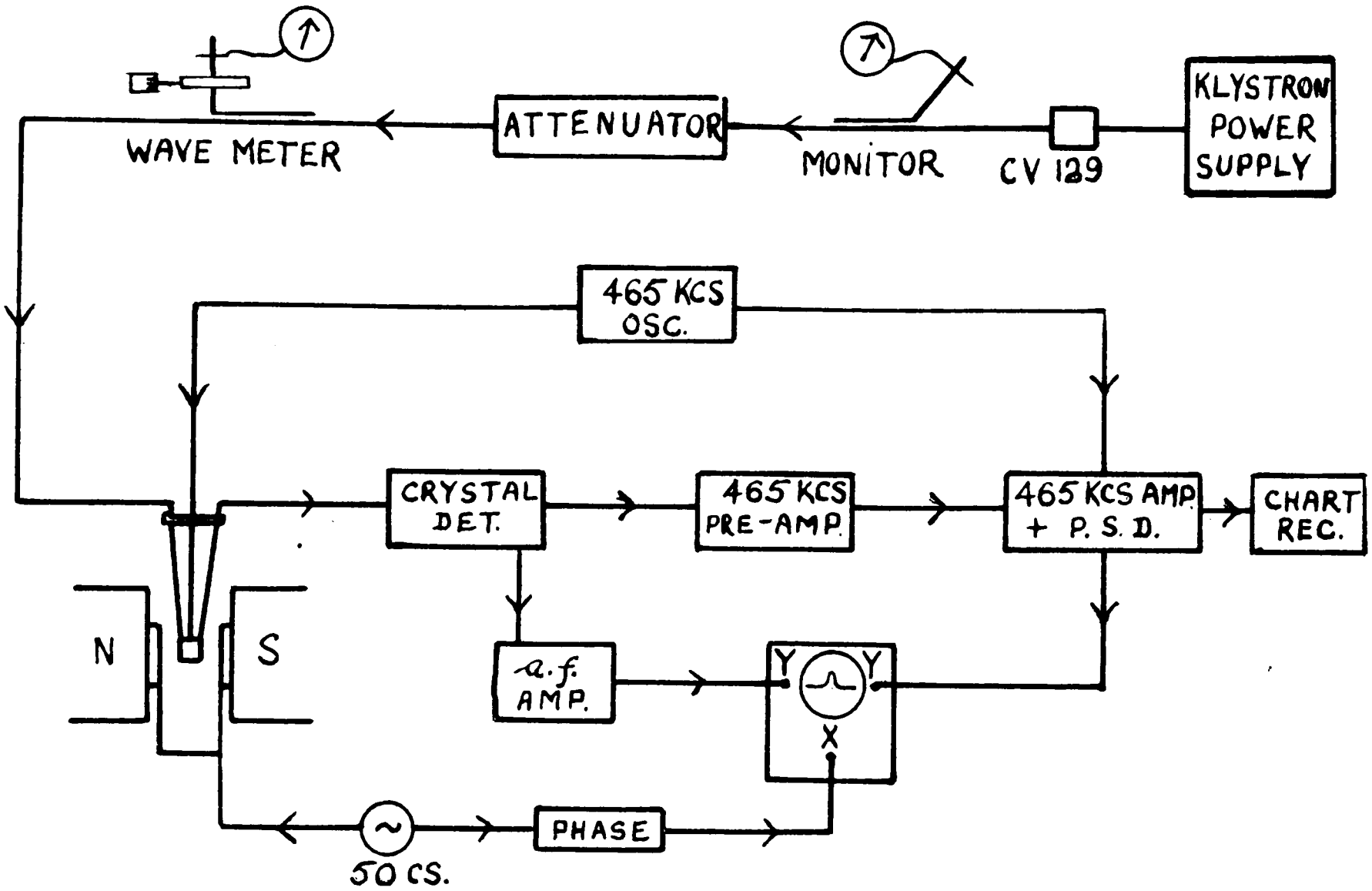
5. Delbecq, C.J., Smaller, B., Yuster, P.H., Phys. Rev., (1956), 104, 599.

6. Smaller, B. and Yasaitis, E., Rev. Sci. Inst., (1953), 24, 991.

7. Bloembergen, N., Purcell, E.M., Pound, R.V., Phys. Rev., (1948), 73, 679.

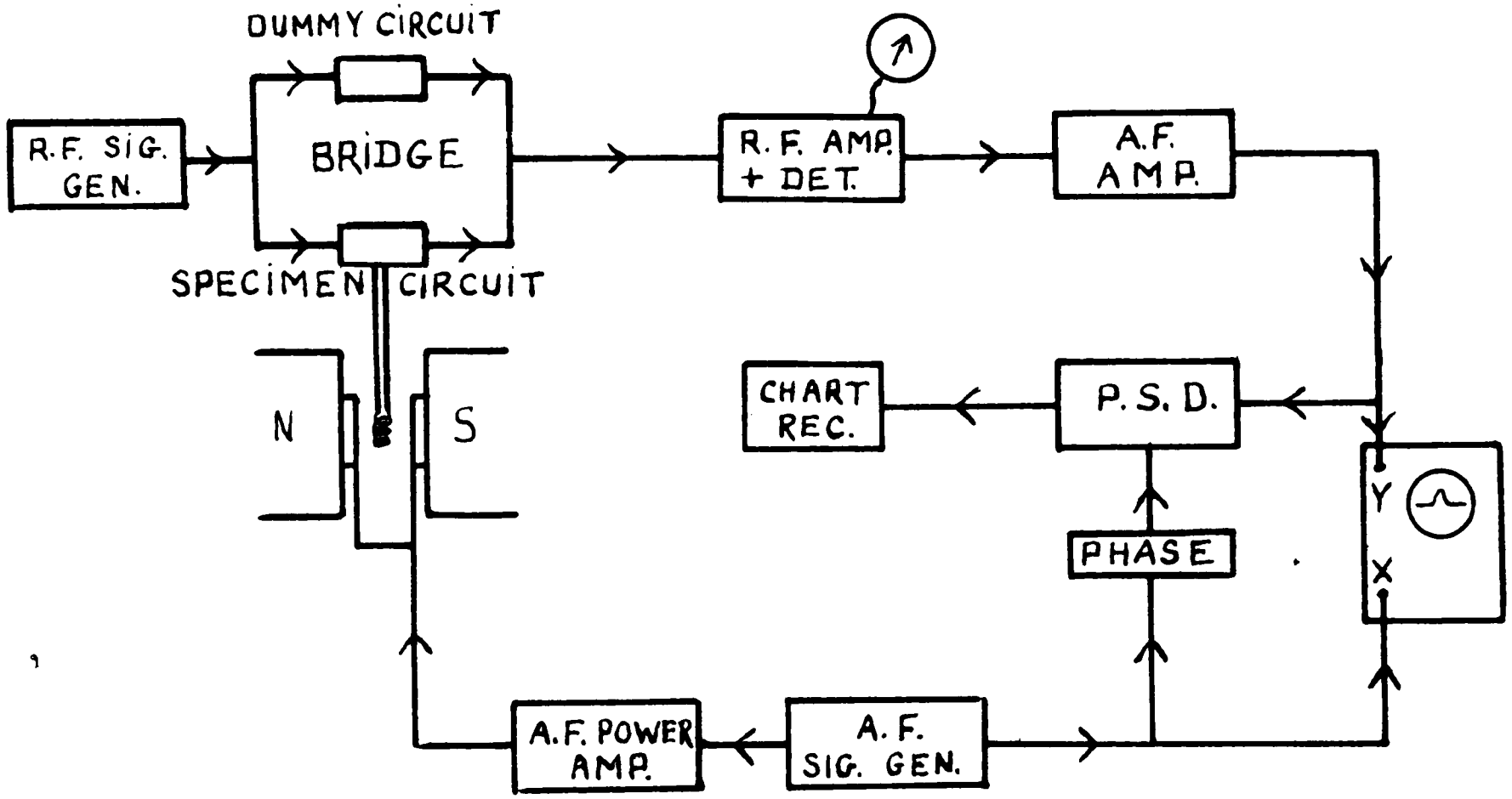
8. Stockbarger, D.C., J. Opt. Soc. Am., (1949), 39, 731.

9. Kyropoulos, S., Zeit. f. Anorg. Allgem. Chemie, (1926), 154, 308.




X-BAND ELECTRON MAGNETIC RESONANCE SPECTROMETER

FIG. 1.1




NUCLEAR MAGNETIC RESONANCE SPECTROMETER

FIG 1.2

# CHAPTER II

## IRON GROUP IMPURITIES IN NaF

### II.1. Introduction

Alkali halides and silver halides containing divalent metal impurities present interesting problems in colour centre research[1,2]. The divalent ions generally substitute for monovalent cations in the lattice and are accompanied by positive ion vacancies to balance the excess charge. The degree of association of the vacancies and impurities is of interest. The divalent ions may form effective electron traps; the positive ion vacancies may trap holes and form V-centres. We are at present concerned with the properties of iron group impurities in NaF and the effect of ionising radiations on the crystals. In NaF a fluorine structure is observed in the resonance spectra of the impurity ions due to the interaction of the magnetic electrons with fluorine nuclei through bond formation. This structure gives information about the environment of the impurity ion.

The NaF crystals were grown by the Stockbarger technique[3]. A salt containing the element required as impurity was mixed with NaF powder before loading into the graphite crucible. The type of salt used and the molar concentration of impurity added are given in Table II.1. The molar concentration of impurity present in the crystals is also given in Table II.1; this was estimated from the intensity of the paramagnetic resonance spectrum.

TABLE II.1

Iron Group Impurities in NaF

| Salt added to the melt | molar concentration of impurity added | molar concentration of impurity observed |
|---|---|---|
| $CrCl_3.n\,H_2O$ | .01% Cr | .003% |
| $Mn\,F_2$ | .01% Mn | .002% |
| $Fe\,SO_4.7H_2O$ | .01% Fe | .0001% |
| $CoCl_2.6H_2O$ | 1.0 % Co | .0004% |
| $NiCl_2.6H_2O$ | .02% Ni | .002% |

The irradiation of the NaF crystals was performed with (a) $^{60}Co$ γ-rays at 40°C or (b) 150 kv X-rays at room temperature, or (c) about 5 μa of 1 Mev electrons for 2 minutes at room temperature. The observed effects produced by each of these radiations were substantially the same.

Brief accounts of the general results have already been given[4,5]. A detailed discussion of the bonding and valence properties of the impurities has also been given[6].

## II.2. The Interaction of the Magnetic Ions with the Lattice

NaF has the cubic NaCl structure and each sodium ion is surrounded by a regular octahedron of fluorine ions. When singly charged impurity cations enter the lattice substitutionally the octahedral cubic symmetry will in general be maintained. Consider however a solid solution of $MnF_2$ in NaF in which $Mn^{2+}$ ions occupy sites normally occupied by $Na^+$ ions. In order to conserve charge the crystal will in general contain one cation vacancy for each $Mn^{2+}$ ion incorporated into the lattice.

Vacancies are expected to occur near doubly charged impurity ions because of the electrostatic attraction between them. The degree of association of the vacancy-impurity complex appears to depend on the technique of crystal growth and on the concentration of impurity added. A vacancy in positions P or Q (fig. II.1) will introduce an axial component about a cube edge into the crystal field seen by the impurity ion at A; the lower symmetry will be apparent in the resonance spectrum and three distinguishable magnetic complexes will be observed since there are three distinguishable cube edges. A vacancy in position R or S will introduce rhombic symmetry with principal axes along two face diagonals and a cube edge and six distinguishable magnetic centres will be found. A vacancy may also occur along a body diagonal to the impurity ion but such a situation has not been observed.

Charge compensation for doubly charged impurity cations may also be achieved by introducing doubly charged impurity anions, for example $O^{2-}$, $S^{2-}$. An example of such a system is described by Watkins[7] who suggests that charge compensation for $Mn^{2+}$ ions in NaCl results from the presence of a doubly charged impurity anion at T (fig. II.1). With NaF a check on this type of system is possible since the number of nearest neighbour fluorine ions may be determined from an analysis of the fluorine structure.

The first detailed description of extra-nuclear structure in the spectrum of a paramagnetic ion was given for $Ir^{4+}$ ($5d^5$) in the complex $(IrCl_6)^{2-}$.[8,9,10] Subsequently a fluorine structure was observed in the spectra of iron group (3d) impurity ions in $ZnF_2$[11] and in $CaF_2$[12].

The fluorine structure arises from a partial transfer of the unpaired d electrons to orbits on fluorine ions and its order of magnitude may be estimated from the product of the h.f.s. of the free fluorine atom and the probability of finding the d electrons on fluorines. The following discussion of the bonding follows Van Vleck[13], Owen[10] and Tinkham[11].

Consider a complex $AX_6$ where A is an iron group ion ($3d^n$) surrounded by a regular octahedron of fluorine ions X. If we consider the bonding to be perfectly ionic then the orbitals of the magnetic electrons on A are of the form $d_{x^2-y^2}$, $d_{3z^2-r^2}$, $d_{xy}$, $d_{yz}$, $d_{zx}$. The first two orbitals ($d_\gamma$ type) have a higher energy than the remaining three ($d_\varepsilon$ type) which form a ground orbital triplet. For $Mn^{2+}$ ($d^5$) each of these orbitals is singly occupied and the ground state ($^6S$) has zero angular momentum. If we consider the mixing which occurs between the central $d_\gamma$ orbitals on A and the 2s and 2p orbitals on X then the modified $d_\gamma$ orbitals become

$$\sigma_{3z^2-r^2} = N_\sigma \{d_{3z^2-r^2} + [\alpha_\sigma/12^{\frac{1}{2}}](p_x^1 - p_x^4 + p_y^2 - p_y^5 - 2p_z^3 + 2p_z^6)\}_\sigma \qquad (2.1)$$

$$\sigma_{x^2-y^2} = N_\sigma \{d_{x^2-y^2} + \tfrac{1}{4}\alpha_\sigma(-p_x^1 + p_x^4 + p_y^2 - p_y^5)\}_\sigma . \qquad (2.2)$$

The numbers 1,2,3 and 4,5,6 refer to nearest neighbour fluorine positions on positive and negative x, y, z axes respectively. The p orbitals are made up of 2s and 2p orbitals on X and $\alpha_\sigma^2 = \alpha_s^2 + \alpha_{p\sigma}^2$. The mixing between $d_\varepsilon$ orbitals on A and $p_\pi$ orbitals on X will

lead to augmented dπ orbitals of the form

$$\pi_{xy} = N_\pi \{d_{xy} + \tfrac{1}{2}a_\pi (p^1_y - p^4_y + p^2_x - p^3_x)\}_\pi . \qquad 2.3$$

The admixtures in this case are expected to be smaller than for $\sigma$-bonds and do not contribute measurably to the bonding in the cases to be described.

The interaction between the magnetic electrons and the fluorine nuclei may be expressed by including the term

$$\sum_N I^N_o \cdot A^N . S$$

in the appropriate spin Hamiltonian; $I_o = \frac{1}{2}$ is the spin of the fluorine nucleus and the summation is over the six nearest neighbour fluorine ions. Fluorine structure components occur at energies displaced from the zero interaction position by

$$\delta\nu = \sum_N I^N_s A^N_s = \sum_N I^N_s \{A^N_s + A^N_p (3\cos^2\theta_{s,p} - 1)\} \qquad 2.4$$

where $\theta_{sp}$ is the angle between the external magnetic field and the bond axis to the $N^{th}$ fluorine ion. The term $A^N_s$ arises from the s-electron contact interaction through the fluorine 2s orbital. When the orbital angular momentum is completely quenched and when, as for $Cr^+$, $Mn^{2+}$ and $Fe^+$, both $\sigma$-bonding orbitals are singly occupied this becomes

$$A^N_s = \frac{8\pi\beta\mu^N}{9SI^N} N^2_\sigma \alpha^2_s |s(0)|^2 . \qquad 2.5$$

In this expression $\beta$ is the Bohr magneton, $\mu^N$ is the nuclear moment

of the $N^{th}$ fluorine nucleus, S is the true electronic spin and s(0) is the amplitude at the fluorine nucleus of the fluorine 2s orbital. Where the observed multiplicity of the ground state is 2 an effective spin $S' = \frac{1}{2}$ may be used to describe the resonance spectrum[14]. In such cases a correction factor $2\langle|S|\rangle\, g_s/2$ must be introduced such that $(g_s/2)\, A_S^N = A_S^{N\prime}$. This correction factor is unity for $Cr^+$, $Mn^{2+}$ and $Ni^+$ and 1.6 for $Fe^+$ where $S = \frac{1}{2}$. The term $A_p^N$ includes (a) the coupling $A_{p\sigma}^N$ with the $N^{th}$ fluorine nucleus through the $p\sigma$ orbital and (b) the direct magnetic dipole interaction $g_n\beta_n\, g\beta/r^3$ between the $N^{th}$ fluorine nucleus and the electronic wave function located on the central ion; g and $g_n$ are the electronic and nuclear g-factors and $\beta_n$ is the nuclear magneton. Both interactions have the same angular dependence and in general are comparable in magnitude ($g_n\beta_n\, g\beta/r^3 = 2.0 \times 10^{-4}$ cm$^{-1}$ for $g = 2$). If the orbital angular momentum is completely quenched, then the expression for $A_{p\sigma}^N$ becomes

$$A_{p\sigma}^N = \frac{2}{5}\,\frac{\mu_0^N}{SI^N}\,\langle r^{-3}\rangle\, N_\sigma^2\, \alpha_{p\sigma}^2 \qquad 2.6$$

where r is the radius of the 2p wavefunction. In the calculations of section 2.9 we assume n = 2 orbitals and take $|s(0)|^2 = 75 \times 10^{24}$ cm$^{-3}$ and $\langle r^{-3}\rangle = 38 \times 10^{24}$ cm$^{-3}$.[15,16] In cases where the quenching approximation is poor and the g-value departs considerably from 2 then the interaction between the electronic orbital magnetic moment and the fluorine nuclear spin should be considered; ignoring the effect will introduce errors of about 20 into the calculation of the anisotropic bonding in the case of $Fe^+$ and $Ni^+$ and it will be neglected.

When the external magnetic field is in the [111] orientation, $(3\cos^2\theta_{s,p} - 1) = 0$ and the interactions with six equivalent fluorines will give a seven line structure with intensities in the ratio 1 :6 :15: 20 :15 : 6 : 1;[4] the spacing of the lines gives a direct measurement of $A_s$. The parameter $A_p$ may now be determined by examination of the spectra in other orientations. Since both σ-bonding orbitals are occupied in the case of $Cr^+$, $Mn^{2+}$ and $Fe^+$ the probability that the magnetic electrons will be found in a fluorine 2s orbital is $\frac{1}{3} N_\sigma^2 \alpha_s^2$ and in a 2pσ orbital is $\frac{1}{3} N_\sigma^2 \alpha_{p\sigma}^2$.

Description of the Paramagnetic Resonance Spectra

## 2.3 Chromium

Clear crystals of NaF to which $Cr^{3+}$ ions were added do not show a resonance spectrum down to 20°K. In the case of $Cr^{3+}$ ($d^3$ $^4F$) a cubic field leaves an orbital singlet lowest with a fourfold spin degeneracy; fields of lower symmetry split this into two Kramers doublets. It is not surprising that chromium is not present as $Cr^{3+}$ because of the large charge discrepancy; it seems likely that the impurity enters the lattice as $Cr^{2+}$ ($d^4$ $^5D$). Since this is a non-Kramers ion the degeneracy is completely lifted by fields of rhombic symmetry and a resonance may not be observed; a field of rhombic symmetry may be produced by a charge compensating positive ion vacancy.

After irradiation however, a single isotropic line with a resolved fluorine structure is observed at 90°K with $g = 2.000$. The crystals are now a pink colour which is associated with an optical absorption band at 500 mμ and probably arises from M-centres[1,17]. The pink colour

has been observed in all NaF crystals irradiated and is a property of the host lattice. The resonance spectrum is assigned to $Cr^+$ which is isoelectronic with $Mn^{2+}$ ($d^5$ $^6S$).

Detailed discussions of the level scheme of $Mn^{2+}$ given by several authors[7,18,19] are expected to apply to $Cr^+$. The $^6S_{5/2}$ ground state is only slightly effected by the environment; the g-value is close to the free electron g-value (2.0023) and is isotropic. $^{53}Cr$ is 9.5% abundant and has a nuclear spin $I = \frac{3}{2}$; a weak four line h.f.s. is observed and the h.f.s. interaction constant A is isotropic. The spin Hamiltonian for the ion in an external magnetic field may be written

$$\mathcal{H} = g\beta H.S + AI.S. \qquad 2.7$$

Transitions to second order occur at fields[20]

$$H = H_o - Am - \frac{A^2}{2H_o}[I(I+1) - m^2 + m(2M-1)] \ldots M \leftrightarrow M-1. \qquad 2.8$$

where m and M are the nuclear and electronic magnetic quantum numbers. In NaF the cubic crystalline environment adds a small term[21]

$$F(a) = \frac{a}{6}\{S_x^4 + S_y^4 + S_z^4 - \frac{1}{5}S(S+1)(3S^2 + 3S - 1)]\} \qquad 2.9$$

to the spin Hamiltonian. This adds terms to the right hand side of 2.8 which are given to first order in a by

$$\begin{aligned} \Delta H &= 0 && M = +\tfrac{1}{2} \leftrightarrow -\tfrac{1}{2} \\ \Delta H &= \pm \tfrac{5}{2} pa && M = \pm \tfrac{3}{2} \leftrightarrow \pm \tfrac{1}{2} \\ \Delta H &= \mp 2\, pa && M = \pm \tfrac{5}{2} \leftrightarrow \pm \tfrac{3}{2} \end{aligned} \qquad 2.10$$

where $p = 1 - 5\varphi$ and $\varphi = \ell^2 m^2 + m^2 n^2 + n^2 \ell^2$ and $\ell$, m, n are the direction cosines of the external magnetic field with the cubic axes. A defect near the ion destroys the cubic symmetry and a large splitting of the fine structure results. The additional interaction may be written[18]

$$\mathcal{H}_{\text{non-cubic}} = D\{S_z^2 - \tfrac{1}{3}S(S+1)\} + E(S_x^2 - S_y^2). \qquad 2.11$$

The term in E vanishes if the field has axial symmetry. This interaction leads to terms which must be added to 2.8 and are given to second order in D and E by[7]

$$\Delta H = \mp 4a_0 - \frac{32\,|a_1|^2 - 16\,|a_2|^2}{H_0} \qquad M = \pm\tfrac{5}{2} \longleftrightarrow \pm\tfrac{3}{2}$$

$$\Delta H = \mp 2a_0 + \frac{4\,|a_1|^2 - 20\,|a_2|^2}{H_0} \qquad M = \pm\tfrac{3}{2} \longleftrightarrow \pm\tfrac{1}{2} \qquad 2.12$$

$$\Delta H = + \frac{16\,|a_1|^2 - 32\,|a_2|^2}{H_0} \qquad M = +\tfrac{1}{2} \longleftrightarrow -\tfrac{1}{2}$$

where

$$a_0 = D\,\frac{(3\ell^2 - 1)}{2} + \frac{3E}{2}(m^2 - n^2)$$

$$|a_1|^2 = D^2\ell^2(1-\ell^2) + E^2\{(1-\ell^2) - (m^2 - n^2)^2\} - 2DE\ell^2(m^2 - n^2) \qquad 2.13$$

$$|a_2|^2 = \tfrac{1}{16}[D^2(1-\ell^2)^2 + E^2\{4\ell^2 + (m^2 - n^2)^2\} + 2DE(\ell^2 + 1)(m^2 - n^2)]$$

and $\ell$, m, n are the direction cosines of the external field relative

to the principal axis of the interaction. These non-cubic terms reveal the presence of a defect near the impurity ion.

In the present case, the $Cr^+$ ion is in a cubic environment and the spectrum at $90^{\circ}K$ may be fitted to the spin Hamiltonian

$$\mathcal{H} = g\beta H.S + F(a) + AI.S + \sum_N I_o^N . A^N . S \qquad 2.14$$

with $S = \frac{5}{2}$, $I = \frac{3}{2}$, $I_o = \frac{1}{2}$, $g = 2.000 \pm 0.002$,

$A = 14.0 \pm 0.5 \times 10^{-4}\ cm^{-1}$, $a = 3.6 \pm 0.6 \times 10^{-4}\ cm^{-1}$,

$A_s = 12.8 \pm 0.2 \times 10^{-4}\ cm^{-1}$ and $A_{po} = 0 \pm 1.5 \times 10^{-4}\ cm^{-1}$.

The line width is 5 gauss.

The $^{53}Cr$ h.f.s. is observed on the extreme fluorine structure lines and confirms that chromium is the source of the spectrum. The g-value for $Cr^{3+}$ in a cubic field is expected to be less than two because of the positive sign of the spin-orbit coupling constant and $Cr^{3+}$ will not have a fluorine structure from $\sigma$-bonding[11]. $Cr^{2+}$ in a cubic field will also have a g-value less than two and one may conclude that the chromium is present as $Cr^+$.

If there were no essential difference between $Mn^{2+}$ and $Fe^{3+}$ ions, then, according to Watanabe[23], one might expect the same order of magnitude of the cubic field splitting parameter a for both ions in the same environment. However, the value of a for $Fe^{3+}$ in several crystals is about ten times larger than for $Mn^{2+}$.[14] For $Mn^{2+}$ we find[23] that

$$a = 8\,(Dq)^2 \times 10^{-4}\ cm^{-1} \qquad 2.15$$

where Dq is a parameter determined by the strength of the crystal field.[24]

The value of $a$ for $Mn^{2+}$ in MgO is $+ 18.6 \pm 0.3 \times 10^{-4}$ cm$^{-1}$.[25] The crystal field in NaF should be about $\frac{1}{3}$ as strong as in MgO and a value of about $1.8 \times 10^{-4}$ cm$^{-1}$ is predicted for $a$. This is reasonably close to the value found for $Cr^{+}$. However, the agreement may be fortuitous since MgO is strongly covalent and NaF is strongly ionic and the effect of covalency has been neglected in the theory of Watanabe.

It is interesting to note that in NaF the ratio $A(^{55}Mn^{2+})/A(^{53}Cr^{+}) = 6.5$ whereas $g_n(^{55}Mn)/g_n(^{53}Cr) = 4.6$ where $g_n$ is the nuclear g-factor so that the mechanism responsible for the h.f.s.[26,27] is not equally potent in the two cases (the spectrum of $Mn^{2+}$ is described in the next section).

The analysis of the fluorine structure shows that the $Cr^{+}$ ion is on a cation site and is surrounded by a regular octahedron of fluorine ions. When H is in the [110] or [100] orientations a seven line structure characteristic of the interaction with six equivalent fluorines is observed. In these orientations the effects due to $p\sigma$ bonding and dipole-dipole interaction are not resolved and broaden the lines sufficiently to prevent resolution of the cubic field splitting. When H is in the [111] orientation these effects disappear and the cubic field splitting is resolved.

## II.4 Manganese

The spectrum of manganese in alkali halides has been extensively studied[7,28,29,30]. Forrester and Schneider[28] find three types of $Mn^{2+}$ spectrum in alkali halides:

(1) A single line of half-width about 400 gauss. They suggest that this line arises partly from isolated $Mn^{2+}$ ions in

distorted fields near dislocations and partly from aggregates at dislocations.

(2) An isotropic six line h.f.s. from the nuclear spin $I = \frac{5}{2}$ of $^{55}Mn$. This is assigned to isolated $Mn^{2+}$ ions on cation sites where the cubic symmetry is maintained.

(3) A complex spectrum with a large fine structure splitting (D = 500 gauss) due to the presence of a positive ion vacancy nearby.

Watkins[7] has observed five different manganese spectra in NaCl.

(1) A single line 130 gauss wide from $Mn^{2+}$ ions in an aggregated state leading to exchange narrowing.

(2) A spectrum from isolated $Mn^{2+}$ ions in a cubic field.

(3) A spectrum from isolated $Mn^{2+}$ ions in a rhombic field which arises from the presence of a positive ion vacancy on a nearest neighbour cation site (D = - 144 gauss, E = 43.5 gauss).

(4) A spectrum from isolated $Mn^{2+}$ ions in an axial field due to a vacancy on a second nearest cation site (D = - 140 gauss).

(5) A spectrum from isolated $Mn^{2+}$ ions with a doubly charged impurity charge compensator, e.g. $O^{2-}$, on a nearest anion site (D = - 548 gauss, E = + 20 gauss).

Watkins finds that the spectra (3) and (4) occur in equal concentration in the same crystal and that the binding energies of the vacancy - $Mn^{2+}$ pairs are the same for each. This is in agreement with recent calculations[31].

In NaF before irradiation we find four different types of $Mn^{2+}$ spectrum

the spectra observed depend on the crystal growing technique:

(a) Stockbarger technique

(i) A spectrum from isolated $Mn^{2+}$ ions with a principal axis of symmetry along a cube edge.

(ii) A spectrum similar to a(i) but with a larger fine structure splitting.

(b) Kyropoulos technique

(i) A spectrum similar to a(i), a(ii), but with a larger fine structure splitting.

(ii) A spectrum similar to b(i) but with a larger fine structure splitting.

The (a) and (b) type spectra are mutually exclusive. In both (a) and (b) categories the type (ii) spectra are about 2 of the concentration of type (i). Each spectrum shows a resolved fluorine structure. The fluorine structure could not be analysed in type a(ii) and b(ii) spectra due to lack of intensity. The analysis of the fluorine structure for the type a(i) and b(i) spectra shows that the octahedron of fluorine ions surrounding the $Mn^{2+}$ ion is complete in both cases.

The measured constants of the resonance spectra are given in Table II.2. To determine the position of the vacancies which produce the fine structure splitting it is first necessary to know the detailed symmetry of the spectra. This appears to be almost impossible in the present case because of the great complexity of the spectra and the large line width (50 gauss) due to the fluorine structure. The values of the parameter D in Table II.2 are determined by equating 8D to the

separation of the extreme fine structure components when the external magnetic field is along a cube edge.

TABLE II.2

SPIN HAMILTONIAN CONSTANTS OF $Mn^{2+}$ SPECTRA IN MgF AT 90°K

| Spectrum | g | A | D | $A_s$ | $A_{pc}$ |
|---|---|---|---|---|---|
| a(i) | 1.996 ± 0.006 | 91± 4 | 89 ± 5 | 14.4±0.3 | 0.8± 0.7 |
| a(ii) | 2.00 ± 0.01 | 92± 4 | 225 | - | - |
| b(i) | 1.998 ± 0.006 | 88± 4 | 325±5 | 14.1±0.3 | 1.7 ± 0.7 |
| b(ii) | 2.00 ± 0.01 | 90± 4 | 380 | - | - |

The parameters A, D, $A_s$ and $A_{pc}$ are in units of $10^{-4}$ $cm^{-1}$.

Upon irradiation, the $Mn^{2+}$ spectra are reduced to a limiting intensity of about 10% of their original value. No new resonance is observed down to 4°K. It may be that $Mn^{2+}$ ions capture electrons forming $Mn^{+}$ ions which are isoelectronic with $Fe^{2+}$ ($3d^6$ $^5D$). In the case of $Fe^{2+}$ the cubic field leaves an orbital triplet lowest which is also five-fold degenerate in spin. Spin-orbit coupling gives a sextuplet ground state[14]. A field of rhombic symmetry will raise the degeneracy completely and Tinkham[11] has observed a transition within a low lying slightly split doublet ($\Delta$ = 0.2 $cm^{-1}$) in $ZnF_2$. Low[32] observed a sharp line in MgO due to $Fe^{2+}$ with g = 3.4277; this was superimposed on a broad line with the same g-value. He attributed the sharp line to $Fe^{2+}$ ions in cubic surroundings and the broad line to $Fe^{2+}$ ions in slightly distorted cubic surroundings. Failure to observe a resonance from $Mn^{+}$ ions in the present

case may be due either to crystal distortions or a short spin-lattice relaxation time.

II.5 Iron

Before irradiation a weak isotropic line about 50 gauss wide is observed at $4^{\circ}K$ with $g = 4.28 \pm 0.06$, arising from about $3 \times 10^{14}$ centres. After irradiation of the same crystal a line with an isotropic g-value ($g = 4.344 \pm 0.002$) appears at $20^{\circ}K$ with a well resolved fluorine structure; the fluorine interaction constants are $A_{\parallel} = 28.3 \pm 1.0 \times 10^{-4} cm^{-1}$ and $A_{per} = 6.0 \pm 1.0 \times 10^{-4} cm^{-1}$. The intensity corresponds to about $2 \times 10^{15}$ centres. The line width is 5 gauss. The broad line remains visible after annealing and on reirradiating the resolved structure at $g = 4.344$ reappears with the same intensity. This g-value is close to that of $Co^{2+}$ in the cubic field of MgO ($g = 4.278$)[33]. In the case of $Co^{2+}$ a large 8 line h.f.s. is observed due to the spin $I = \frac{7}{2}$ of $^{57}Co$; in the present case no h.f.s. due to the nucleus of the paramagnetic ion is found. Since MgO has the NaF structure these results suggest that the magnetic centre in NaF is $Fe^{+}$ which is isoelectronic with $Co^{2+}$ ($3d^{7}\ ^{4}F$). The analysis of the fluorine structure (Fig. II.2) shows that the $Fe^{+}$ ion is on a normal cation site.

The theory for the $d^{7}$ configuration in an octahedral cubic field has been discussed by Low[33]. The cubic field leaves an orbital triplet lowest followed by another triplet and a singlet highest. The lowest orbital triplet is four-fold spin degenerate and spin-orbit coupling partly raises the twelve-fold degeneracy leaving a doublet lowest with the g-value

$$g = \frac{10}{3} + k - \frac{15}{2}\frac{\lambda'}{\Delta} \qquad 2.16$$

where $\frac{10}{3}$ is the spin contribution $g_s$ to the $g$-value and $k$ is the orbital contribution $g_L$. If the ion is perfectly ionic then $k = 1$ but if there is some covalent bonding then $k < 1$. The third term arises from an admixture of the next highest Stark triplet at a distance $\Delta$; $\lambda'$ is the effective spin-orbit coupling constant in the solid which in general is less than that of the free ion.

Spectrochemical analysis of the crystals showed iron present in concentration 2 parts per million. Comparison with the magnetic resonance intensity indicates that in the irradiated sample all the iron is present as $Fe^{+}$ ions while before irradiation or after annealing less than 10% is in this form if we ascribe the broad line at $g = 4.28$ to such ions. The remainder may then be present as $Fe^{2+}$ ions although no trace of a spectrum due to $Fe^{2+}$ ions has been found down to $4^{\circ}K$, presumably for reasons outlined in the discussion on $Mn^{+}$.

## II.6 Cobalt

Before irradiation a complex spectrum from $Co^{2+}$ ions is observed at $20^{\circ}K$. There are six types of magnetic ion with similar spectra. Each ion has rhombic symmetry with two face diagonals and a cube edge as principal axes. The spectrum of each ion is described by the following spin Hamiltonian with $S = \frac{1}{2}$ and $I = \frac{7}{2}$:

$$\mathcal{H} = \beta\, S.g.H + I.A.S. \qquad 2.17$$

The measured constants are $g_x = 4.3$, $g_y = 3.3$, $g_z = 5.7$,

$A_y = 82 \times 10^{-4}$ cm$^{-1}$ and $A_z = 250 \times 10^{-4}$ cm$^{-1}$. Confusion due to overlap prevented the measurement of $A_x$. These measurements are consistent with the presence of $Co^{2+}$ ions in an octahedral cubic field with a rhombic distortion.[34]

A noticeable feature in the complex fluorine structure of the ion which has its z axis parallel to the external magnetic field is the presence of three lines with intensities in the ratio 1:2:1 and spacing $62 \times 10^{-4}$ cm$^{-1}$. A detailed analysis of the fluorine structure was not possible but it appears that the interaction with two fluorines is stronger than the interaction with the remaining four; this suggests that the $Co^{2+}$ ion is on a cation site but displaced slightly along a face diagonal. The observed symmetry of the spectrum and the displacement of the small $Co^{2+}$ ion may be due to the presence of a positive ion vacancy on a nearest neighbour cation site (Fig. II.1, Pos. S).

On irradiation the spectrum described above disappears completely and two isotropic lines are observed. One line occurs at 20°K with a g-value of 4.5, is about 400 gauss wide and has no resolved structure; this line is assigned to $Co^{2+}$ ions in slightly distorted cubic surroundings. The second line is observed at 90°K with a g-value of 2.31 ± 0.02 and has a flat top about 200 gauss long. The g-value is close to that observed by Low[35] for $Ni^{2+}$ in MgO ($g = 2.227 \pm 0.002$) suggesting that the magnetic centre is $Co^{+}$ which is isoelectronic with $Ni^{2+}$ ($3d^9\ ^2F$). A discussion of the theory of $Ni^{2+}$ in the cubic field of MgO has been given by Low[35]. The seven-fold orbital degeneracy is partly raised by the cubic field leaving a ground singlet and two excited triplets. The ground orbital singlet is triply degenerate in the spin and this degeneracy is not

raised by the combined action of the cubic field and spin-orbit coupling. In a trigonal or tetragonal field the spin triplet is split into a singlet and an upper doublet with splittings of the order of 0.1 to 0.5 $cm^{-1}$. [14] Rhombic symmetry components in the Tutton salts split the triplet into three singlets with an overall spacing of about 3 $cm^{-1}$. [36] In a cubic field we expect to get a single line with[35,37]

$$g = g_0 - \frac{8\lambda'}{\Delta} \qquad 2.18$$

where $g_0$ is the free electron g-value, $\lambda'$ is the effective spin-orbit coupling constant and $\Delta$ is the separation of the ground state and the first excited Stark triplet.

The absence of a resolved structure on the $Co^+$ line may be due to the simultaneous presence of cobalt h.f.s. (a value of $A = 30 \times 10^{-4}$ $cm^{-1}$ is estimated from the line shape which may be compared with the value $A = 97.7 \pm 0.2 \times 10^{-4}$ $cm^{-1}$ found for $Co^{2+}$ in MgO[33]), fluorine structure and line broadening due to slight distortions of the crystal field.

## II.7 Nickel

No lines are observed before irradiation down to 20°K. This is not surprising if the nickel is present as $Ni^{2+}$ since a charge compensating vacancy may introduce a rhombic splitting sufficiently large to prevent observation of a resonance. After irradiation a spectrum with a resolved fluorine structure appears at 20°K. There are three magnetic ions with similar spectra, each with axial symmetry about a cube edge. The spectrum is assigned to $Ni^+$ ions which are isoelectronic with $Cu^{2+}$ ions ($3d^9$ $^2D$). The theory of $Cu^{2+}$ in an octahedral cubic field has been described[37,38].

A field of cubic symmetry splits the D state into a lower doublet and an upper triplet. Spin-orbit coupling does not raise the orbital degeneracy of the ground state which is therefore four-fold degenerate in a cubic field. An isotropic spectrum is expected with

$$g = 2 - \frac{4\lambda'}{\Delta} - 5\left(\frac{\lambda'}{\Delta}\right)^2 \qquad 2.19$$

where $\lambda'$ and $\Delta$ have the usual meanings. However, when there is orbital degeneracy it is reasonable to assume that some distortion of the complex may occur in accordance with the theorem of Jahn and Teller[39]. Such an effect has been observed in the case of $Cu^{2+}$.[40]

A tetragonal distortion splits the lower orbital doublet ($x^2 - y^2$, $3z^2 - r^2$) into two singlets ($x^2 - y^2$ is lowest if the octahedron is extended along a cube edge and $3z^2 - r^2$ is lowest if the octahedron is flattened) and the upper triplet into a doublet (yz, zx) and a singlet (xy). When $x^2 - y^2$ is the ground state the g-values are

$$g_{//} = 2 - \frac{8\lambda'}{\Delta}$$

$$g_{\perp} = 2 - \frac{2\lambda'}{\Delta} . \qquad 2.20$$

When the $3z^2 - r^2$ level is lowest the g-values are

$$g_{//} = 2$$

$$g_{\perp} = 2 - \frac{6\lambda'}{\Delta} . \qquad 2.21$$

$\Delta$ is now the mean distance of the upper triplet.

In the course of the work on NaF, $Cu^{2+}$ ions were diffused into MgO

powder by heating at 1300°C for two hours. A spectrum with a four line h.f.s. due to $Cu^{2+}$ was found with $g = 2.190 \pm 0.002$ and $A = 19 \pm 1 \times 10^{-4}$ $cm^{-1}$ at 90°K. The line width was 10 gauss indicating that the departure from cubic symmetry was small. It has been pointed out however[41] that the system may be expected to resonate between distortions of equivalent energy leading to an isotropic g-value although the g-value for a static distortion would be anisotropic. Bleaney and Bowers[42] find that the spectrum of $Cu^{2+}$ in $ZnSiF_6 \cdot 6H_2O$ is isotropic at 90°K but between 60°K and 20°K three equivalent static tetragonal distortions become 'frozen out'. The spectrum of $Cu^{2+}$ in MgO remains isotropic down to 12°K however.

In the case of $Ni^+$, three equivalent tetragonal distortions of the lattice are observed. The g-values indicate that the octahedron of fluorines surrounding the $Ni^+$ ion is extended along a cube edge. The possibility that the tetragonal distortion arises from a positive ion vacancy on a cube edge is discounted since this would result in g-values similar to those of a flattened octahedron. The spectrum is fitted to the spin Hamiltonian

$$\mathcal{H} = \beta\, S.g.H + \sum_N I_o^N . A^N . S \qquad 2.22$$

with $S = \frac{1}{2}$, $I_o = \frac{1}{2}$, $g_{//} = 2.766 \pm 0.002$, $g_\perp = 2.114 \pm 0.002$, $A_s^I = 41 \pm 2 \times 10^{-4}$ $cm^{-1}$, $A_s^{II} = 10 \pm 1 \times 10^{-4}$ $cm^{-1}$, $A_{p\sigma}^{I} = 16 \pm 2 \times 10^{-4} cm^{-1}$ and $A_{p\sigma}^{II} = 0^{+2}_{-0} \times 10^{-4}$ $cm^{-1}$. The superscript I on the fluorine interaction constants refers to the four fluorines in the plane perpendicular to the symmetry axis and the superscript II to the two fluorines on the axis. If the distortion of the octahedron is pure tetragonal then the unpaired

electron is expected to be in the $x^2 - y^2$ state and bonding only to four type I fluorines should occur. However, an appreciable interaction with the two type II fluorines on the axis is observed and the mechanism by which this is achieved is not yet clear. The interaction with the type I and type II fluorine ions is shown in fig. 2.3.

## II.8 Copper

No resonance was observed before or after irradiation. It is believed that copper enters alkali halide crystals as $Cu^+$ [43] which is non-magnetic and $Cu^+$ ions may not be stable electron traps under the conditions of irradiation.

## II.9 Discussion

Earlier investigations of the effect of divalent impurity ions, for example $Ca^{2+}$ and $Sr^{2+}$, in alkali halides showed the presence of $Z_1$ optical absorption bands following irradiation. These bands were attributed by Seitz[1] to electrons trapped on the divalent ions. It was further assumed that the positive ion vacancy which was initially associated with the divalent ion moves away, possibly to join the electron deficient centre left behind by the captured electron. In the present case the spectra of two divalent ions, $Mn^{2+}$ and $Co^{2+}$, have been observed. In both cases the symmetry of the surroundings is less than cubic due to association with positive ion vacancies. No effects due to rotional diffusion of the vacancies have been observed at the temperature of measurement. The onset of line broadening due to vacancy diffusion was observed by Watkins[7] for $Mn^{2+}$ in NaCl at about 200°C. The fact that no spectra are observed from the non-Kramers ions $Cr^{2+}$, $Fe^{2+}$ and $Ni^{2+}$ may be

due in part to the reduced symmetry produced by an associated vacancy. The observation of $Cr^+$, $Fe^+$ and $Co^+$ ions with symmetry close to cubic indicates that vacancies which may have been originally associated with the divalent ions have migrated. Some of the electrons released during the irradiation are trapped as F-centres and M-centres. No resonances have been observed which can be attributed to the electron deficient centres and the nature of these centres is unknown. The metastable monovalent ions are annealed out by heating to $140^{\circ}C$ and the initial condition of the crystal is restored. The trapping efficiency of the iron group ions may be due in part to the fact that the radii of the ions are less than that of $Na^+$ and the strain energy of the lattice due to misfit of the impurity ion will be less in the monovalent form.

The effect of irradiation on MgO crystals containing iron group ions has also been investigated[43]. Irradiation with ultra-violet light or X-rays causes electron transfer to occur among the impurities and the monovalent ions $Fe^+$ and $Ni^+$ have been observed.

The measured $g$-values indicate that the values of $\frac{\lambda'}{\Delta}$ for the monovalent ions in NaF are larger than the values for the isoelectronic divalent ions in MgO. It is possible to write $\lambda' = k\lambda$ where $\lambda$ is the spin-orbit coupling constant for the free ion and $k$ is a reduction factor determined by the chemical bonding in the solid[44,45]. Approximate values of $\lambda$ for iron group ions are given in Table II.3; these were estimated from the ground multiplets[46] of the free ions assuming Russel-Saunders coupling to hold. Values of $k$ in NaF are expected to be greater than in MgO because of weaker covalent bonding and values of $\lambda$ for

monovalent ions are less than for the isoelectronic divalent ions. The increased values of $\frac{\lambda'}{\Delta}$ in NaF are

TABLE II.3

Spin-Orbit Coupling Constant ($\lambda$) of Iron Group Ions

| Ion | $\lambda$ ($cm^{-1}$) |
|---|---|
| $Fe^{2+}$ | - 101 |
| $Fe^{+}$ | - 119 |
| $Co^{2+}$ | - 178 |
| $Co^{+}$ | - 228 |
| $Ni^{2+}$ | - 324 |
| $Ni^{+}$ | - 603 |
| $Cu^{2+}$ | - 829 |

due to the smaller values of $\Delta$ expected in the singly charged lattice, and rough estimates of $\Delta$ in the case of $Fe^{+}$ and $Co^{+}$ indicate splittings of about 5000 $cm^{-1}$. It is unlikely that these splittings can be observed optically because of the small impurity concentration. Direct determinations of $\Delta$ for $Co^{2+}$ [33] and $Ni^{2+}$ [35] in MgO have been made by Low from the optical absorption spectrum and he finds values of 8470 $cm^{-1}$ and 8600 $cm^{-1}$ respectively.

The analysis of the fluorine h.f.s. shows that the largest interaction comes from magnetic electrons in fluorine 2s orbitals. The smaller anisotropic contribution from 2p orbitals comes mainly from $\sigma$-bonding; the contribution from $\pi$-bonding is inside the error of measurement. The probability that the magnetic electron will be found in a fluorine 2s

orbital and a fluorine 2p orbital is given in Table II.4 for $Cr^{+}$, $Mn^{2+}$ and $Fe^{+}$. The charge transfer has not been calculated for $Ni^{+}$ since the nature of the ground state is not known. It is seen that the probability of finding the magnetic electrons of the impurity ions on a nearest neighbour fluorine ion is about 2%. This value is consistent with the ionic nature of the crystal and should be an indication of the charge transfer which occurs in the pure crystal.

TABLE II.4

Charge Transfer of Iron Group Ions in NaF

| Ion | Probability of occupation of a fluorine 2s orbital | Probability of occupation of a fluorine 2p orbital |
|---|---|---|
| $Cr^{+}$ | .42% | - |
| $Mn^{2+}$ | .47% | 1.0% |
| $Fe^{+}$ | .35% | 2.0% |

REFERENCES


1. Seitz, F., Rev. Mod. Phys., (1954), 26, 7.
2. Seitz, F., " " " , (1951), 23, 328.
3. Stockbarger, D.C., J. Opt. Soc. Am., (1949), 39, 731.
4. Kleaney, B., Hayes, W., Proc. Phys. Soc., (1957), 70, 626.
5. Hayes, W., Jones, D.A., " " " (1958), 71, 503.
6. Hayes, W., Faraday Soc. Discussions, in the press.
7. Watkins, G.W., (private communication) to be published.
8. Griffiths, J.H.E., Owen, J., Proc. Roy. Soc., (1954), A226, 96.
9. Owen, J., Proc. Roy. Soc., (1953), A227, 183.

10. Owen, J., Faraday Soc. Discussions, (1955), 19, 127.

11. Tinkham, M., Proc. Roy. Soc., (1956), A236, 535, 549.

12. Baker, J.M., Bleaney, B., Hayes, W., Proc. Roy. Soc., (1958), A247, 141.

13. van Vleck, J.H., J. Chem. Phys., (1935), 3, 807.

14. Bowers, K.D., Owen, J., Rep. Prog. Phys., (1955), 18, 304.

15. Hartree, D.R., Proc. Roy. Soc., (1935), A151, 96.

16. Lowdin, P.O., Phys. Rev., (1935), 90, 120.

17. Yuster, P.H. (private communication).

18. Bleaney, B., Ingram, D.J.E., Proc. Roy. Soc., (1951), A205, 336.

19. Low, W., Phys. Rev., (1957), 105, 793.

20. Bleaney, B., Phil. Mag., (1951), 42, 441.

21. Bleaney, B., Stevens, K.W.H., Rep. Prog. Phys., (1953), 16, 108.

22. Bleaney, B., (private communication).

23. Watanabe, H., Prog. Theor. Phys. Japan, (1957), 18, 405.

24. Schlapp, R., Penney, W.G., Phys. Rev., (1932), 42, 666.

25. Low, W., Bull. Am. Phys. Soc., Ser. II, (1956), 1, 283.

26. Abragam, A., Horowitz, J., Pryce, M.H.L., Proc. Roy. Soc., (1955), A230, 169.

27. Heine, V., Phys. Rev., (1957), 107, 1002.

28. Forrester, P.A., Schneider, E.E., Proc. Phys. Soc. (1956), B69, 833.

29. Schneider, E.E., Cafyn, J.E., Defects in crystalline solids, (1955), p. 74. (London Physical Society).

30. Low, W., Proc. Phys. Soc., (1956), B96, 837.

31. Tosi, M.P., Airoldi, G., Il Nuovo Cim., (1958), 8, 584.

32. Low, W., Phys. Rev., (1956), 101, 1827.

33. Low, W., Phys. Rev., (1958), 109, 256.

34. Abragam, A., Pryce, M.H.L., Proc. Roy. Soc., (1951), A206, 173.

35. Low, W., Phys. Rev., (1958), 109, 247.

36. Griffiths, J.H.E., Owen, J., Proc. Roy. Soc., (1952), A213, 459.

37. Owen, J., Thesis, Oxford (1953).

38. Bleaney, B., Bowers, K.D., Pryce, M.H.L., Proc. Roy. Soc., (1955), A288, 166.

39. Jahn, H.A., Teller, E., Proc. Roy. Soc. (1937), A161, 220.

40. Bleaney, B., Bowers, K.D., Trenam, R.S., Proc. Roy. Soc., (1955), A228, 157.

41. Abragam, A., Pryce, M.H.L., Proc. Phys. Soc., (1950), A63, 409.

42. Bleaney, B., Bowers, K.D., Proc. Phys. Soc., (1952), A65, 667.

43. Wertz, J.E., Auzins, P., Griffiths, J.H.E., Orton, J.W., Disc. of Faraday Soc., (1958), in the press.

44. Stevens, K.W.H., Proc. Roy. Soc., (1953), A219, 542.

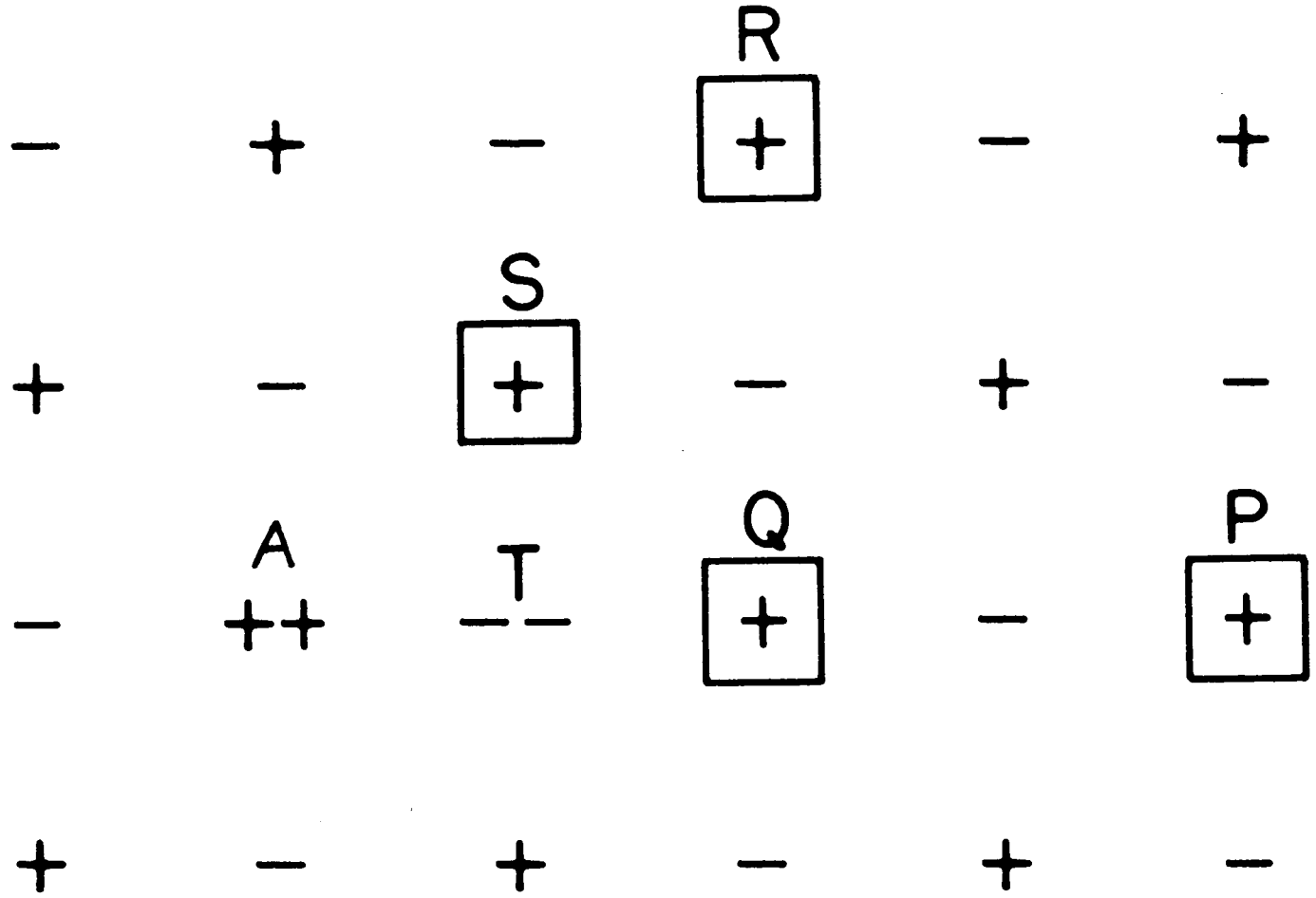
45. Owen, J., Proc. Roy. Soc., (1955), A227, 183.

46. Atomic Energy Levels, Vol. II, (1952), Circular of the National Bureau of Standards 467.

Fig. II.1. Methods by which charge compensation may be achieved for a doubly charged cation A in NaF. P, Q, R, S are positive ion vacancies; T is a doubly charged anion.

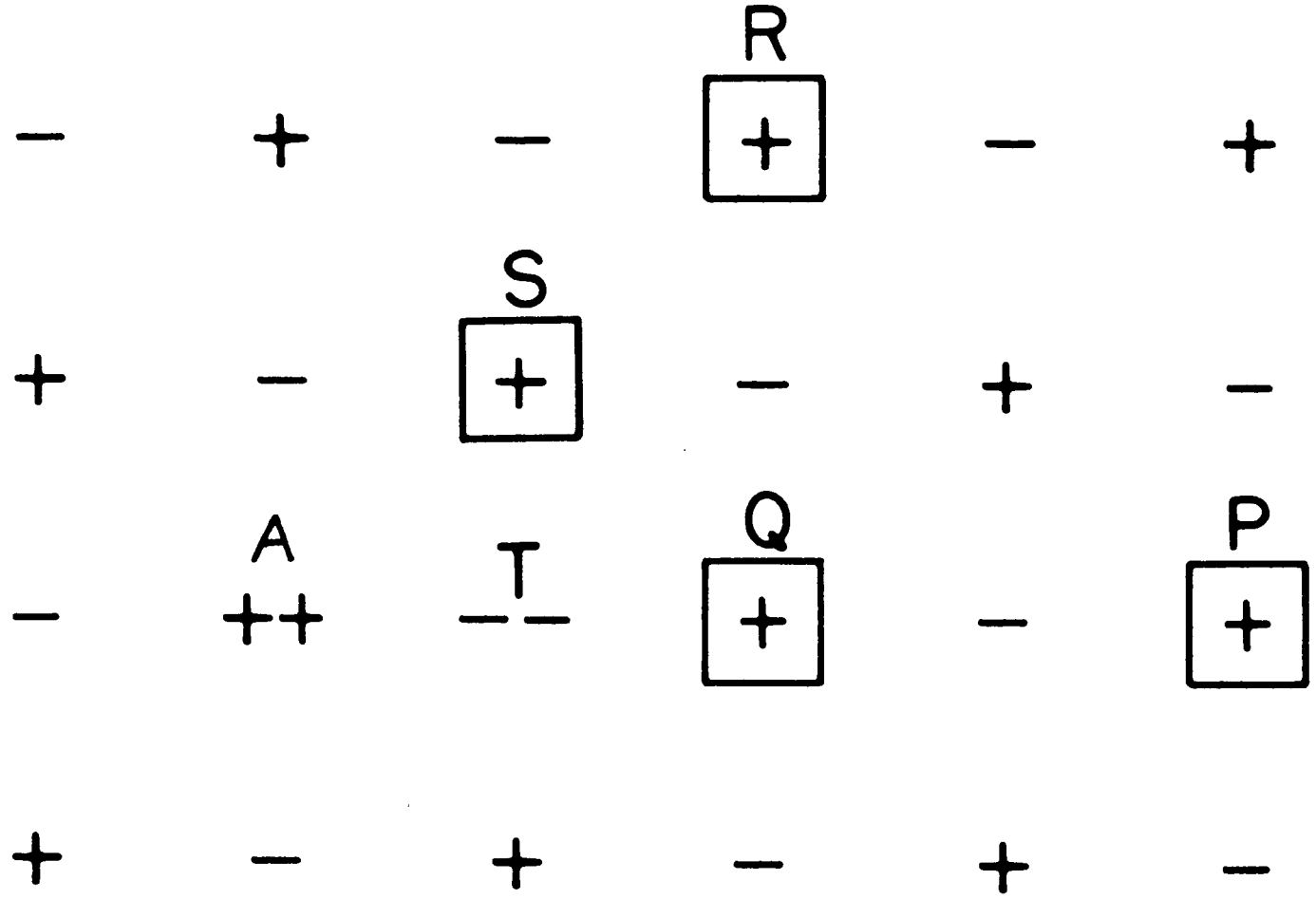
Fig. II.2. Fluorine structure of $Fe^+$ in chart recording of differential of absorption lines. The calculated pattern for the [111] direction predicts seven lines with relative intensities 1 : 6 : 15 : 20 : 15 : 6 : 1 characteristic of an interaction with six equivalent fluorines. The calculated patterns for the [100] and [110] directions have been constructed using the approximate ratio $A_o/A_s = 2/5$ which gives simple ratios for the line separations. The observed spectra are in good agreement with the calculated patterns.

Fig. II.3. The spectrum of the $Ni^+$ ion whose axis is directed along [001] for the [110] orientation of the external magnetic field. The interaction with the four type I fluorines splits the resonance line into five components with intensities in the ratios 1 : 4 : 6 : 4 : 1; a further splitting of each of these lines into three components with intensities in the ratios 1 : 2 : 1 is produced by the weaker interaction with the type II fluorine ions (see text).




CHARGE COMPENSATION IN NaF

FIG. 2.1




CHARGE COMPENSATION IN NaF

FIG. 2.1

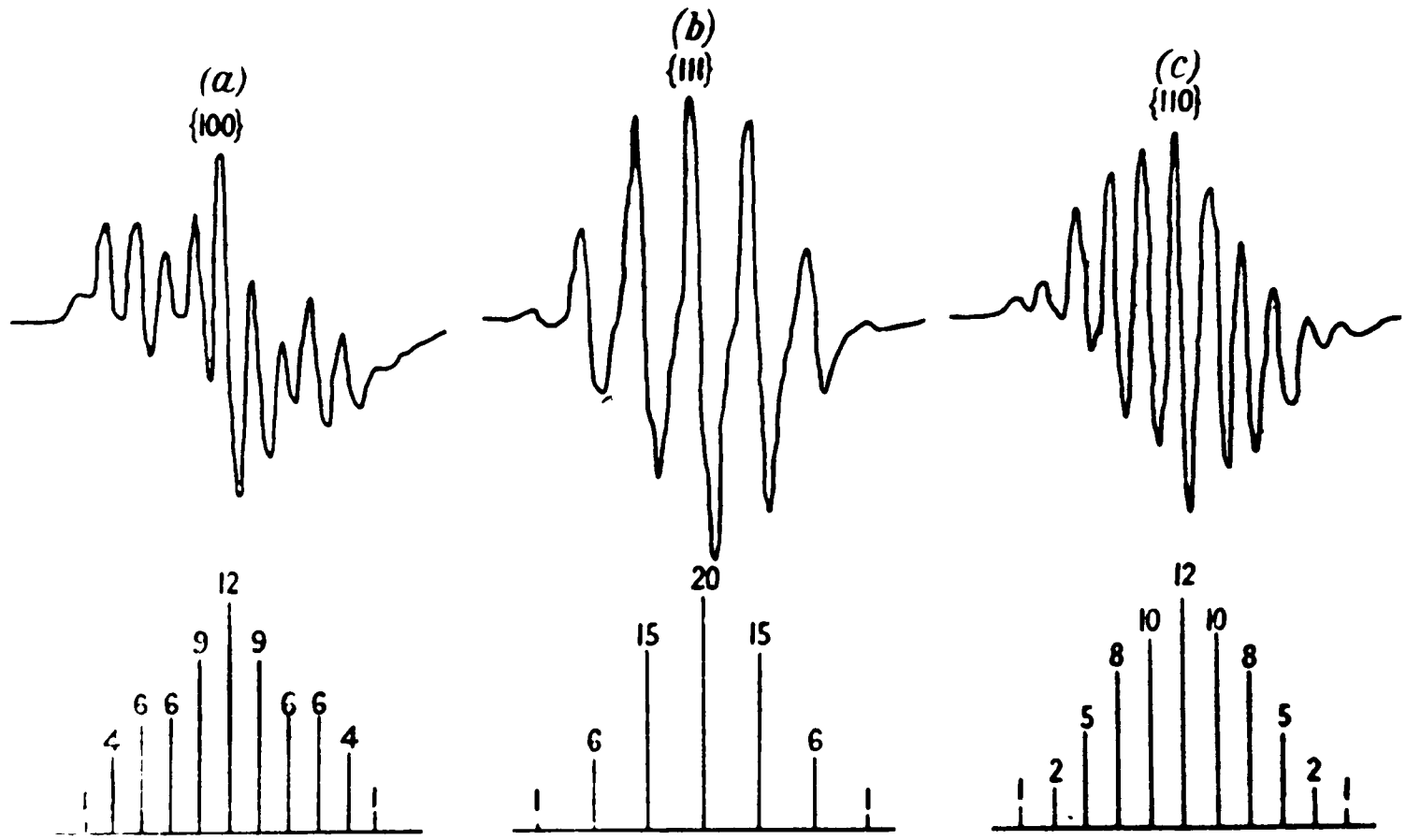



FIG. 2.2. Fluorine structure in the spectrum of $Fe^+$.

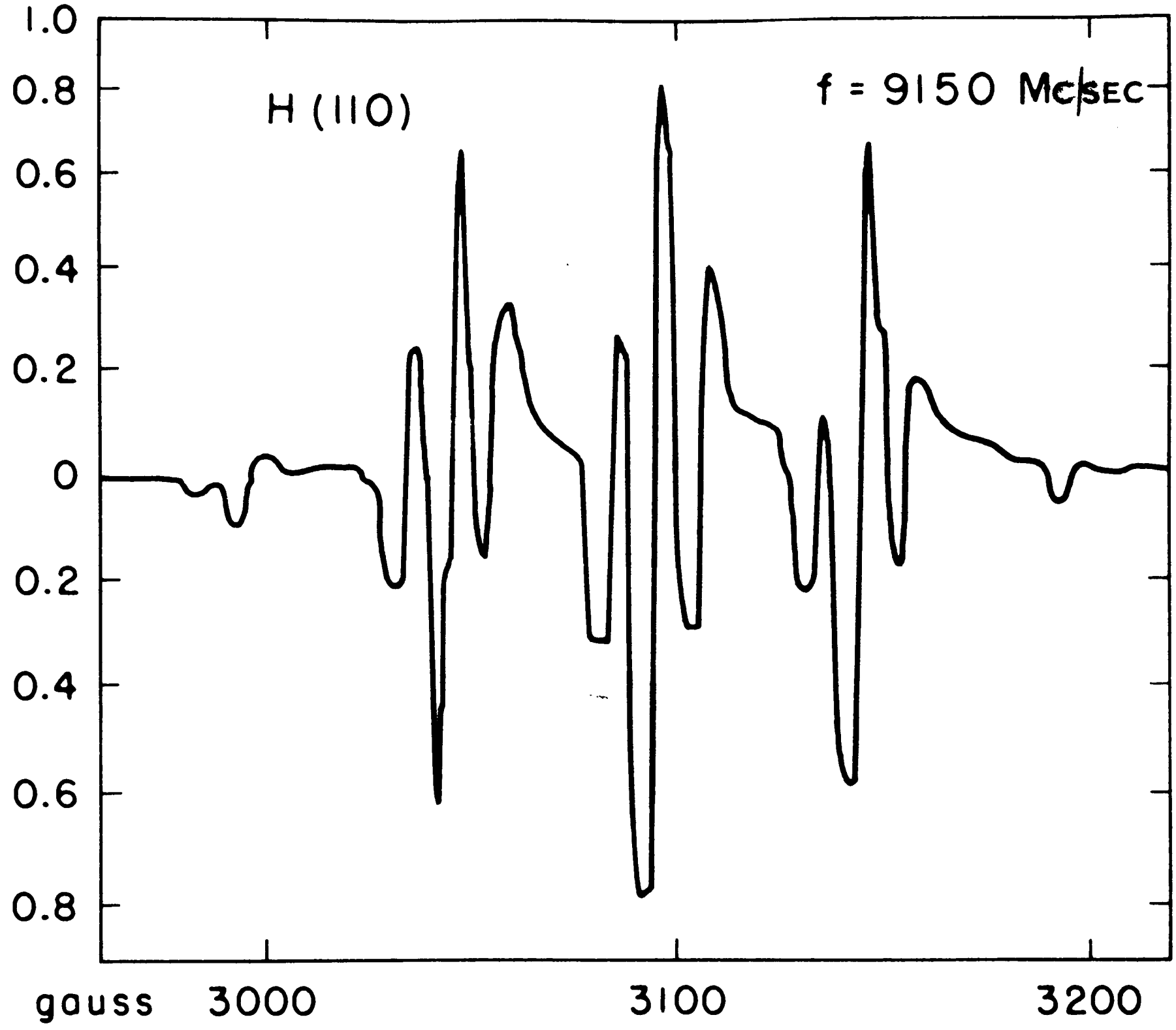



FIG. 2.3 FLUORINE STRUCTURE IN SPECTRUM OF $Ni^+$

# CHAPTER III

# NUCLEAR MAGNETIC RESONANCE IN $FeF_2$ AND $CoF_2$

## III.1 Introduction

The study of nuclear magnetic resonance (NMR) of diamagnetic atoms in paramagnetic crystals was first undertaken by Bloembergen[1,2]. The position, width and shape of the absorption lines are influenced by the magnetic environment of the nuclei and one must consider the microscopic field at the nuclei in addition to the externally applied field. We may expect a broad line from the large internal dipole fields[3]. However, strong exchange interactions may lead to a narrowing of the NMR line[4,5] and an ordered (antiferromagnetic) state at low temperatures.

When the temperature is lowered each paramagnetic ion acquires a considerable mean magnetisation in an external magnetic field. Exchange interactions among paramagnetic ions cause spins to fluctuate at a frequency $\omega_e \sim 10^{12}$ cs so that the mean magnetisation may be used in processes concerned with low frequency quanta ($\omega << \omega_e$)[6]. In the paramagnetic state the NMR line will be displaced from its normal field of $\omega/\gamma_N$ by the time averaged dipolar field of the magnetic ions at the nuclear positions ($\sim \frac{\mu^2 H_0}{3kT} \cdot \frac{1}{r^3}$) which is normally of the order of several gauss. Different displacements result for non-equivalent nuclear positions in the unit cell; the NMR line will therefore be split and the splitting will vary with the angle between the external magnetic field and the crystalline axis. In the ordered state an additional splitting will in general occur due to the relative proximity of nuclei to a spin of a

given orientation[7]. The shift of the NMR line is a measure of the magnitude and temperature dependence of the sub-lattice magnetisation.

In the case of nuclei of diamagnetic ions chemically bonded to paramagnetic ions, the effect of charge transfer is expected to cause shifts of the NMR lines much larger than dipole shifts. Such shifts have been observed in the resonance of $^{19}F$ nuclei in $MnF_2$[8] and in $CoF_2$ and $FeF_2$ [9,10]. The present chapter will be devoted to a discussion of the $^{19}F$ nuclear resonance in $FeF_2$ and $CoF_2$.

## III.2 Crystal Structure

Crystals of $AF_2$ (A refers to Mn, Fe, Co or Zn) have the rutile structure[11] which shows macroscopic tetragonal symmetry. This is a consequence however of having two A ions in the unit cell each with only orthorhombic symmetry whose axes differ by a $90^\circ$ rotation about the C-axis. The basic structure is given in fig. III.1(a) (The C-axis will also be referred to as the [001] or Z-axis; a similar interchange of nomenclature is used for the other principal orientations). Each A ion is surrounded by a distorted octahedron of fluorine ions and there are two distinguishable fluorine positions in the unit cell lying in (100) and (010) planes. Because of the $90^\circ$ rotation, the two types of fluorine are interchanged in going from one $A^{2+}$ ion to the next in the unit cell. Each $A^{2+}$ ion has four $F^-$ ions at a distance $X_1$Å and two $F^-$ ions at a distance $X_2$Å; values of $X_1$ and $X_2$ are given in Table III.1.

We shall use the nomenclature of Tinkham,[12] who, in his description of the paramagnetic resonance spectra of $Mn^{2+}$, $Fe^{2+}$ and $Co^{2+}$ ions present substitutionally as trace impurities in $ZnF_2$, called the four identical $F^-$

ions type I fluorines and the two identical $F^-$ ions type II fluorines. It follows that every $F^-$ ion has a type I bond to two $A^{2+}$ ions and a type II bond to one $A^{2+}$ ion. The $A^{2+}$ axes and the surrounding distorted octahedron of fluorines is shown in fig. III.1(b). From the relative $A^{2+}$ - $F^-$ positions in the unit cell it can be seen that when the external magnetic field is in the (110) or $(1\bar{1}0)$ planes the two $F^-$ positions are indistinguishable and only one NMR line will be observed; for all other planes, two resonances will in general be found.

TABLE III.1

LATTICE PARAMETERS IN THE ISOMORPHOUS SERIES $AF_2$

| A | $x_1$ Å | $x_2$ Å | d(F - F) Å |
|---|---|---|---|
| Mn | 2.11 | 2.14 | 2.62 |
| Fe | 2.10 | 2.03 | 2.59 |
| Co | 2.04 | 2.05 | 2.55 |
| Zn | 2.03 | 2.04 | 2.57 |

d(F - F) is the separation of the two nearest type I fluorines.

## III.3 Experimental Results

In order to find the field acting on a particular $F^-$ ion the contributions are considered separately from the portion of the specimen lying within a small spherical surface centred on the ion and from the portion lying outside.[13] The outer portion produces a field within the cavity greater than that in the absence of the cavity by a fraction $\frac{4}{3}\pi x_1$

where $\chi_1$ is the bulk susceptibility. However the field within the specimen is less than the externally applied field by a fraction $k\chi_1$ where k is a demagnetisation factor which depends on the shape of the specimen. If we neglect the ions within the cavity the resultant field is then

$$H = [1 + (\tfrac{4}{3}\pi - k)\chi_1] H_0. \qquad 3.1$$

For a spherical specimen k is $\frac{4}{3}\pi$ and the correction factor is zero. In the present case we must consider the paramagnetic $A^{2+}$ ions within the cavity and, of these, only the three bonded neighbours are of importance; they produce the shift of the NMR line we are at present investigating.

The crystals used in the experiments were about 0.05 cc. in volume and were of an irregular shape; because of their limited size they were not ground to a spherical shape. The dimensions were nearly the same in three mutually perpendicular directions and it is assumed that the field inside them is the same as it would be for a spherical sample (the correction will in fact be small since $\chi_1 = 2 \times 10^{-5}$ c.g.s.). There will be a contribution of a few gauss to the line width however due to lack of field homogeneity over the specimen. The crystalline c-axis was determined in the normal way for translucent uniaxial crystals using polaroids. All measurements were made at 30 mcs.

The temperature dependence of the paramagnetic shift was checked by making all measurements on each sample at two temperatures. No resonances were observed at 90°K in $FeF_2$ or at 20°K in $CoF_2$. At these temperatures the crystals will be in the ordered state and the position of the $^{19}F$

resonance will be outside the range of the spectrometer. The antiferromagnetic transition temperatures are variously given as 90°K for $FeF_2$ and 50°K for $CoF_2$ [14] and 78°K for $FeF_2$ and 38°K for $CoF_2$ [15]. The position of the single NMR line was measured with the field parallel to the c-axis. The mean shift and the angular dependence of the transitions were measured with the field in the (001) plane. In this plane a single resonance is observed when the magnetic field is parallel to the [110] or [1$\bar{1}$0] directions but in intermediate directions two lines are resolved; the splitting has a $\cos^2\varphi$ dependence where $\varphi$ is the angle between the magnetic field and the [100] axis.

In the case of $MnF_2$ it was found[8] that neither the anisotropy of the splitting nor the large isotropic contribution to the shift (about 7% of the applied field at 77°K) could be explained by dipolar interaction. A similar situation occurs with $FeF_2$ and $CoF_2$. In the case of $FeF_2$ an isotropic shift of about 5% of the applied field is observed at 195°K and in the case of $CoF_2$ an isotropic shift of about 8% is found at 90°K.

III.4 Interpretation

The large isotropic shifts arise because the covalency in the $A^{2+} - F^-$ bond produces large internal magnetic fields at the fluorine nuclei. Bleaney[16] showed how the fluorine NMR measurements in the paramagnetic crystals $AF_2$ could be correlated with the paramagnetic resonance measurements of Tinkham[12] on $A^{2+}$ ions present as substitutional impurities in the diamagnetic crystal $ZnF_2$. Tinkham found that the paramagnetic resonance lines of the $A^{2+}$ ion showed a resolved fluorine structure. He described the fluorine structure with the term $\sum_N I_o^N . A^N . S$ where the summation is

over the six nearest fluorine ions and wrote the principal values of the coupling constant $A^N$ in the form

$$A_i^N = A_s^N + A_\sigma^N (3\cos^2\theta_{i\sigma} - 1) + A_\pi^N (3\cos^2\theta_{i\pi} - 1) \qquad 3.2$$

where $\theta_{i\sigma}$ and $\theta_{i\pi}$ are the angles between the $i^{th}$ axis and the bond axis to nucleus N and the $\pi$ axis respectively. $A_s^N$ gives the isotropic interaction through 2s orbitals, $A_\sigma^N$ includes the direct dipolar term and the interaction through $p\sigma$ orbitals and $A_\pi^N$ gives a measure of the coupling through $p\pi$ orbitals. These expressions for the $ZnF_2$ lattice may be written as follows:

$$A_x^I = A_s^I - A_\sigma + 2A_\pi \qquad A_x^{II} = A_s^{II} + 2A_\sigma - A_\pi$$

$$A_y^I = A_s^I + 0.1A_\sigma - A_\pi \qquad A_y^{II} = A_s^{II} - A_\sigma + 2A_\pi \qquad 3.3$$

$$A_z^I = A_s^I + 0.9A_\sigma - A_\pi \qquad A_z^{II} = A_s^{II} - A_\sigma - A_\pi$$

The coefficients 0.1 and 0.9 apply to the bond angles in $ZnF_2$ but will not differ appreciably for the other $MF_2$ crystals. Tinkham detected a slight difference in the isotropic interactions between the type I and type II fluorine ions which he attributed to the slight difference in bond length ($\sim .01\text{Å}$) in the two cases. Tinkham's values for the fluorine structure parameters for $Mn^{2+}$ and $Fe^{2+}$ in $ZnF_2$ are given in Table III.2. In his measurements on $Mn^{2+}$ Tinkham could not measure $A_x$ owing to lack of resolution but he estimates $A_x^I$ is nearly equal to $A_y^I$ and $A_x^{II}$ is nearly 30% larger than $A_y^{II}$. In the case of $FeF_2$ only $A_z^I$ and $A_z^{II}$ were measured and the other values given in Table III.2 were estimated using

eq. 3.3 and the values of $A_g$ and $A_x$ measured for $Mn^{2+}$. Tinkham was unable to distinguish between the hyperfine structures of the two bond types in the case of $Co^{2+}$ and gives only a mean value $\langle A^N \rangle$ averaged over both types of neighbours. Using his g-values we calculate an average $A_x = 16$, $A_y = 32$ and $A_z = 21$ ( $\times 10^{-4}$ $cm^{-1}$).

TABLE III.2

Fluorine Structure Parameters in $ZnF_2$

| | $A_x^I$ | $A_y^I$ | $A_z^I$ | $A_x^{II}$ | $A_y^{II}$ | $A_z^{II}$ |
|---|---|---|---|---|---|---|
| $Mn^{2+}$ | 16.5 | 16.5 ± 0.7 | 18.2 ± 0.2 | 19.0 | 14.6± 1.2 | 12.5± 0.2 |
| $Fe^{2+}$ | 23 | 24 | 25 | 22 | 18 | 16 |

A values are in units of $10^{-4}$ $cm^{-1}$.

Extending Tinkham's nomenclature, Bleaney[16] wrote the Hamiltonian for the fluorine nuclear spin system as

$$\mathcal{H} = - g_n \beta_n H.I_o + \sum_N I_o . A^N . S^N \qquad 3.4$$

where $I_o$ is the spin operator for the fluorine nucleus and $A^N$ is the structure constant for the interaction between this nucleus and the $N^{th}$ $A^{2+}$ ion whose spin operator is $S^N$. The summation is taken over all $A^{2+}$ ions in the crystal but only the coupling to the three nearest ions need be considered.

Owing to the rapid change of spin orientation for the $A^{2+}$ ions we must take a weighted mean $\bar{M}$, of the different values of the projection $M$ of $S$ on the direction of the applied magnetic field. The measured

susceptibility may be related to $\bar{M}$ since, per mole,

$$\chi = N g \beta \bar{M}/H. \qquad 3.5$$

Fluorine NMR lines will therefore occur at a frequency

$$\nu = (g_n \beta_n H + \bar{M} \sum_N A^N)/h$$

$$= g_n \beta_n H (1 + a)/h \qquad 3.6$$

where $a = (\chi/Ng\beta g_n \beta_n) \sum_N A^N = \delta \sum_N A^N$ is the fractional field shift and $\delta = \frac{1338\chi}{g}$ if $A$ is in units of $cm^{-1}$.

It is seen from fig. 3.1(b) that because of the $90^\circ$ rotation about the z axis in going from one $A^{2+}$ ion to the next in the unit cell that the x and y directions for one $A^{2+}$ ion will be the y and x directions for the other. The components of A along the principle axes are, for the two fluorine resonances

| | line a | line b |
|---|---|---|
| $A_1$ (x-axis) | $2A_x^I + A_y^{II}$ | $2A_y^I + A_x^{II}$ |
| $A_2$ (y-axis) | $2A_y^I + A_x^{II}$ | $2A_x^I + A_y^{II}$ |
| $A_3$ (z-axis) | $2A_z^I + A_z^{II}$ | $2A_z^I + A_z^{II}$ . |

According to Shulman and Jaccarino[8], the angular dependence of the fractional shift of the resonant field for the resolved lines a and b in the (001) plane is, for the case $\delta A_1$, $\delta A_2 << 1$,

$$a_a = \delta\,[(2A_y^I + A_x^{II})\cos^2\varphi + (2A_x^I + A_y^{II})\sin^2\varphi]$$

$$a_b = \delta\,[(2A_x^I + A_y^{II})\cos^2\varphi + (2A_y^I + A_x^{II})\sin^2\varphi] \qquad 3.7$$

where $\varphi$ is the angle between the [100] axis and the external magnetic field. At $\varphi = \pm 45^\circ$ corresponding to [110] or [1$\bar{1}$0] both lines coincide at $\delta\,[A_y^I + A_x^I + \frac{1}{2}(A_y^{II} + A_x^{II})]$ which is the mean shift $a(xy)$ of the two lines for all values of $\varphi$. At $\varphi = 0$ the two lines are displaced by $\delta(2A_y^I + A_x^{II})$ and $\delta(2A_x^I + A_y^{II})$ and we shall call the difference between these displacements $\Delta a(xy)$. When the external field is along the z axis both lines are coincident and the displacement is $\delta(2A_z^I + A_z^{II})$; we shall call this displacement $a(z)$.

The shift parameters $a(z)$, $a(xy)$ and $\Delta a(xy)$ obtained from the measurements are given in Table III.3. Comparison of the observed shifts for $FeF_2$ and $CoF_2$ with the shifts calculated using Tinkham's data is more indirect than for $MnF_2$ because incomplete quenching of the orbital angular momentum makes the net spin component $\bar{M}$ in any direction no longer proportional to the susceptibility. This effect will not be serious in $FeF_2$ where Tinkham indicates that the only low lying levels are the five spin states ($S = 2$). These have an overall splitting of about $50^\circ K$ and at the temperatures of measurement, the susceptibility and $\bar{M}$ should be proportional to one another. The g-values used, $g_{//} = 2.25$ and $g_\perp = \frac{1}{2}(g_x + g_y) = 2.04$, were given by Tinkham. Niira and Oguchi[17] interpreted susceptibility measurements on $FeF_2$ using $g_{//} = 2.45$ and $g_\perp = 2.24$. If these values were used instead of Tinkham's all calculated values of $a$ and $\Delta a$ would be reduced by about 9 . Values

TABLE III.3

Observed and Calculated Value of the Paramagnetic Shift Parameter $a$

| Salt | Temp. $^{o}K$ | $a(z) \times 10^3$ Meas.[a] | $a(z) \times 10^3$ Calc.[b] | $a(xy) \times 10^3$ Meas.[a] | $a(xy) \times 10^3$ Calc.[b] | $\Delta a(xy) \times 10^3$ Meas.[a] | $\Delta a(xy) \times 10^3$ Calc.[b] |
|---|---|---|---|---|---|---|---|
| $FeF_2$ | 300 | 36.2 | 41± 3 | 30.3 | 38± 7 | 9.6 | 2± 8 |
| | 195 | 49.1 | 57± 5 | 39.0 | 51± 9 | 11.8 | 3± 12 |
| $CoF_2$ | 300 | 35.8 | 19± 3 | 30.7 | 19± 3 | 15.2 | 4± 5 |
| | | | (25± 5) | | (18± 4) | | (5± 5) |
| | 90 | 79.7 | 37± 5 | 82.0 | 52± 7 | 33.6 | 11± 7 |
| | | | (49± 9) | | (51± 9) | | (13± 9) |
| $MnF_2$ | 77 | | | 72.0[c] | 77± 6[d] | 19.6[c] | 7± 8 |

a The error in the measurements of $a \times 10^3$ and $\Delta a \times 10^3$ in $FeF_2$ and $CoF_2$ is ± 1.3 on all values.

b $CoF_2$ values are calculated by using Tinkham's g-values[12] (unbracketed) and Nakamura and Taketa's g-values[20] (bracketed)

c Shulman and Jaccarino's experimental results[8] without a demagnetising correction.

d Bleaney's calculated value[16].

of the molar susceptibility at 300°K and 195°K are respectively[18,19] in units of $10^{-3}$, $\chi_{11} = 10.6$, $\chi_{\perp} = 8.6$ and $\chi_{11} = 14.4$, $\chi_{\perp} = 11.6$.

In common with the measurements of Shulman and Jaccarino[8] on $MnF_2$ which are also included in Table III.3, the predicted shifts are a few percent larger than the observed shifts. This is probably due in part to the fact that in these salts the separation of the fluorine from its neighbouring $A^{2+}$ ions is generally greater than in $ZnF_2$ (see Table III.1) so that the values of $A^N$ are expected to be smaller. Part of the discrepancy may be due to the inadequacy of Tinkham's measurements.

In the case of $CoF_2$ the assumption that $\overline{M}$ is proportional to the susceptibility is a poor one, since the specific heat data of Stout and Catalano[15] suggest that another doublet lies some 240°K above the ground doublet. For this reason, the large discrepancy between the measured and calculated values of $a$ and $\Delta a$ is not surprising.

The molar susceptibilities at 300°K and 90°K are respectively[18,19], in units of $10^{-3}$, $\chi_{11} = 9.1$, $\chi_{\perp} = 8.3$ and $\chi_{11} = 18.4$, $\chi_{\perp} = 23.0$. Nakamura and Taketa[20] estimate g-values from the susceptibility measurements on the assumption that the ground state is an orbital singlet with small admixtures of other states and find g-values close to $2(g_{11} = 2.06$, $g_{\perp} = \frac{1}{2}(g_x + g_y) = 2.55)$. These values differ greatly from the measurements of Tinkham on the dilute salt ($g_{11} = 4.1$, $g_{\perp} = 4.3$). Values of $a$ and $\Delta a$ calculated from both sets of g-values are given in Table III.3. Using Nakamura and Taketa's g-values we get a better agreement with experiment but their theory would require considerable modification to fit the dilute salt and must be accepted with some reserve.

In both $CoF_2$ and $FeF_2$ the line width, measured between points of maximum slope was about 27 gauss; this is close to the value 28 gauss given for $MnF_2$ by Shulman and Jaccarino[8] who find $T_1 = 10^{-6}$ sec. It is interesting to note that Bloembergen and Poulis[2] failed to observe the $^{19}F$ resonance in $MnF_2$ and suggested that a value of $T_1$ shorter than $10^{-6}$ sec would explain the resonance not being visible with their equipment.

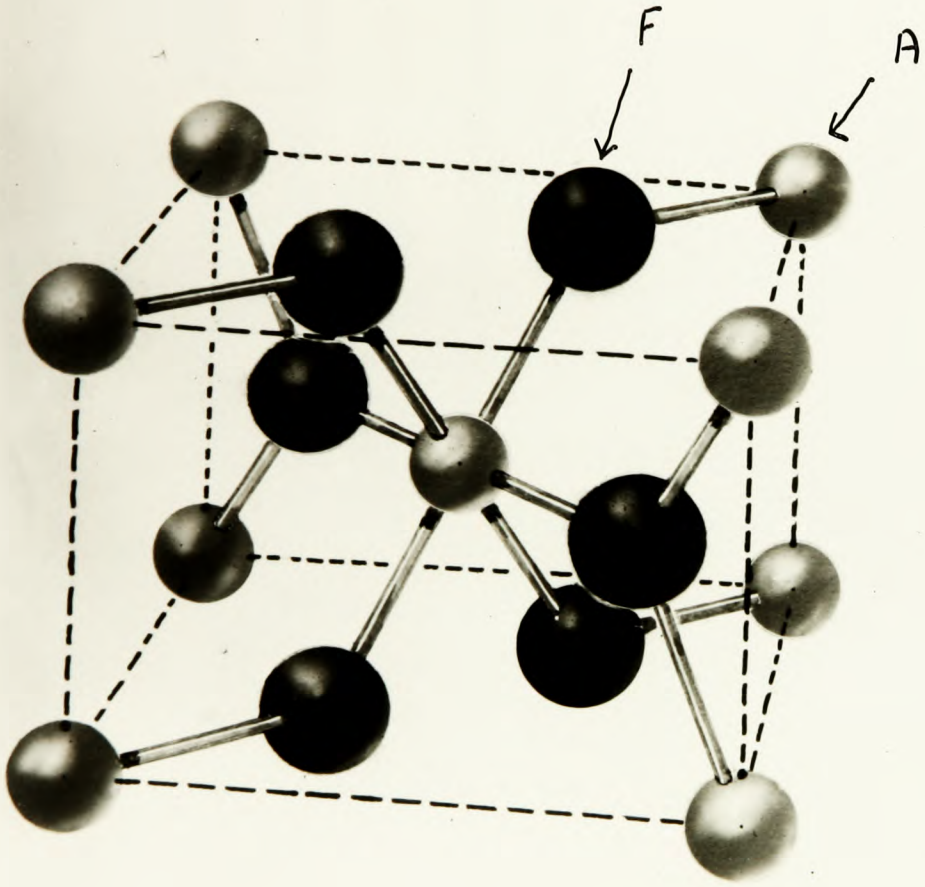
REFERENCES


1. Bloembergen, N., Physica, (1950), 16, 95.
2. Bloembergen, N., Poulis, N.J., Physica, (1950), 16, 915.
3. Bloembergen, N., Physica's Grav., (1949), 15, 386.
4. van Vleck, J.H., Phys. Rev., (1948), 74, 1168.
5. Anderson, P.W., Weiss, R.R., Rev. Mod. Phys., (1953), 25, 269.
6. Moriyo, T., Prog. Theor. Phys., Japan, (1956), 16, 23.
7. Poulis, N.J., Hardeman, G.E., Physica, (1952), 18, 492.
8. Shulman, R.G., Jaccarino, V., Phys. Rev., (1957), 108, 1219.
9. Shulman, R.G., Jaccarino, V., Phys. Rev., (1957), 106, 602.
10. Baker, J.M., Hayes, W., Phys. Rev., (1957), 106, 603.
11. Griffel, M., Stout, J.W., J.Am.Chem.Soc., (1950), 72, 435.
12. Tinkham, M., Proc. Roy. Soc., (1956), A236, 535, 549.
13. Debye, P., Polar Molecules, New York-Dover, (1945), p. 78, 116.
14. Erickson, R.A., Phys. Rev., (1953), 90, 779.
15. Stout, J.W., Catalano, E., J. Chem. Phys., (1955), 23, 2013.
16. Bleaney, B., Phys. Rev., (1956), 104, 1190.
17. Niira, Oguchi, T., Prog. Theor. Phys. Japan, (1954), 11, 425.

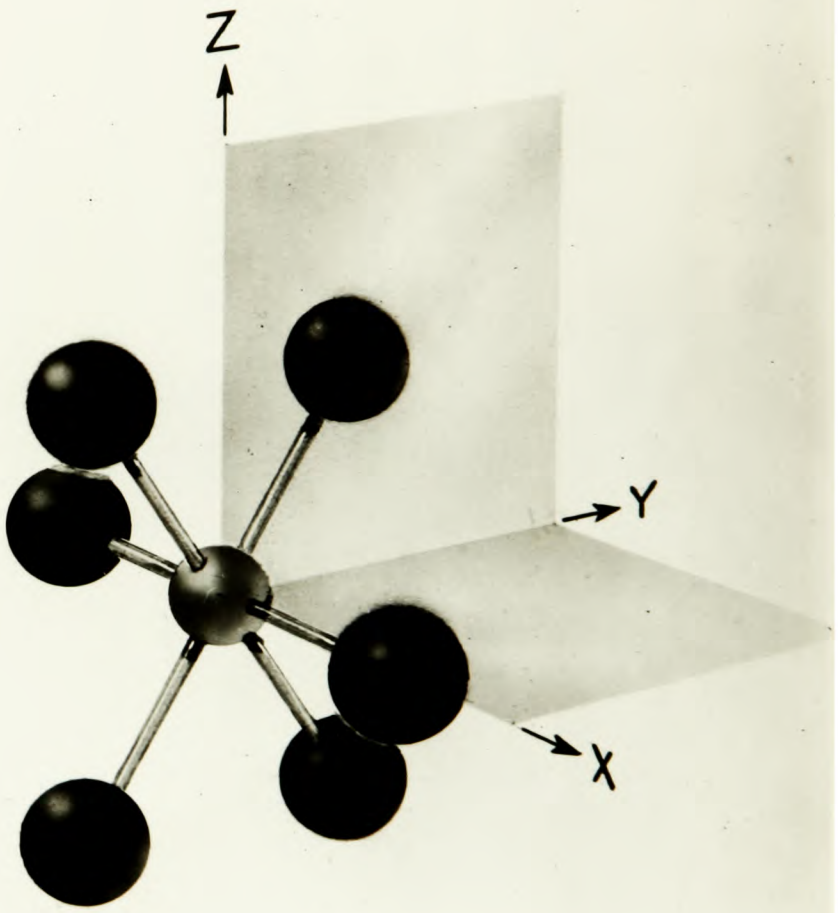
18. de Haas, W.J., Schultz, B.H., Physica (1939), 6, 481.

19. Stout, J.W., Natarrese, L.H., Rev. Mod. Phys., (1953), 25, 338.

20. Nakamura, T., Taketa, H., Prog. Theor. Phys. Japan, (1955), 13, 129.




(a)




(b)

Fig 3.1. Structure of $AF_2$ ( A is Mn, Fe, Co or Zn ).

# CHAPTER IV

# PARAMAGNETIC IMPURITIES IN $CaF_2$

## IV.1 Introduction

Naturally occurring fluorite ($CaF_2$) crystals are in many cases coloured and the optical spectra of these crystals have been the subject of many investigations[1]. The fluorescence and absorption spectra indicate the presence of samarium and europium ions in many specimens, and it seemed of interest to study the paramagnetic resonance spectra. However, the resonance spectra of the naturally occurring crystals were extremely complex because of the presence of many paramagnetic impurities and it was decided to introduce single impurities of the lanthanon (4f) and iron (3d) groups into crystals grown from a melt.

The structure of fluorite crystals may be regarded as a regular cubic array of fluorine ions with calcium ions at every other body centre (Fig. 4.1). Thus, each calcium ion is at the centre of a cube of eight fluorine ions ($Ca^{2+}$ - $F^-$ distance is 2.36 Å). If a doubly charged 3d ion were substituted for calcium and did not distort the lattice, then the impurity ion would be in a crystal field of cubic symmetry; its resonance spectrum would be of interest since ions of this group have been generally investigated in surroundings of nearly octahedral symmetry. The resonance spectrum of $Mn^{2+}$ has been observed; this exhibits a fluorine structure arising from covalent bonding with the surrounding cube of fluorine ions.

Lanthanon ions are in general trivalent and when they replace $Ca^{2+}$ ions, charge compensation must be achieved. Usually this takes the form

of an extra $F^-$ ion occupying the nearest vacant interstitial site (Fig. 4.1). This model was originally suggested by measurements of the lattice constant and crystal density by Zintl and Utgard[2] and later by the paramagnetic resonance measurements of Bleaney, Llewellyn and Jones[3] on $Nd^{3+}$ and $U^{3+}$ in $CaF_2$. A fluorine structure observed in the spectrum of $U^{3+}$ due to overlap of the 5f electrons onto the neighbouring fluorine ions indicates an interaction with an odd number of fluorines. The $F^-$ interstitial will introduce a tetragonal symmetry component into the crystal field acting on the impurity ion and this was observed in the resonance spectra of $Nd^{3+}$ and $U^{3+}$.

The lanthanon ions do not show the resolved fluorine structure characteristic of weak covalent bonding but do exhibit a fluorine satellite structure arising from the simultaneous transition of the electron spin and the spin of a neighbouring fluorine nucleus; this arises from weak magnetic coupling of the electron to the external nucleus. The effect of the charge compensating $F^-$ ion has been observed in this structure in the case of $Ce^{3+}$.

A list of impurities added to $CaF_2$ is given in Table IV.1. The molar concentration of impurity incorporated into the lattice, as estimated from the intensity of the resonance spectrum, is also given.

Many of the calculations mentioned in this chapter were initially carried out by J. M. Baker.

## IV.2 Manganese

All the $Mn^{2+}$ ions ($3d^5$, $^6S_{5/2}$) give an identical spectrum with cubic symmetry described by the spin Hamiltonian[4]

$$\mathcal{H} = g\beta H.S + \frac{1}{6}a[S_x^4 + S_y^4 + S_z^4 - \frac{1}{5}S(S+1)(3S^2 + 3S - 1)]$$

$$+ AI.S + \sum_N I_o^N . A^N . S \qquad 4.1$$

where S and I are both $\frac{5}{2}$ and $I_o = \frac{1}{2}$ is the fluorine nuclear spin. Measurements at 90°K and X-band yielded parameters

$$g = 1.998 \pm 0.003, \qquad A = (-)\ 97.8 \pm 1.0 \times 10^{-4}\ cm^{-1},$$

$$a = +\ 0.6 \pm 0.4 \times 10^{-4}\ cm^{-1}.$$

The sign of A has not been determined but is taken to be negative since its value is close to that of other measurements on manganese salts where the sign has been determined. The values of g and A agree with those of Low[5] for $Mn^{2+}$ in the same host lattice. The cubic field splitting parameter is so small it cannot be measured directly. Its effects are observed however in the fluorine structure pattern (the fluorine structure was not resolved in the crystals grown by Low). Together with the second order manganese hyperfine structure effects it causes small displacements of the fine structure components of each manganese hyperfine structure line (the manganese hyperfine structure in the present case is much larger than the fine structure so that the spectrum comprises basically six hyperfine lines). These displacements cause a slight confusion in the fluorine structure pattern on each line. The best resolution occurs in the third transition from the high field end of the spectrum which is $m = +\frac{1}{2}$ if A is assumed to be negative. From the formula for the second order hyperfine structure shifts[6] and the above spin Hamiltonian, 4.1, the displacements of the fine structure

TABLE IV.1

PARAMAGNETIC IMPURITIES IN $CaF_2$

| Salt Mixed with $CaF_2$ Powder | | Molar Conc. Added | Molar Conc. Estimated from Resonance |
|---|---|---|---|
| $MnF_2$ | B.D.H. Recrystallised | 0.01% Mn | 0.001% |
| $CeF_3$ | Thorium Ltd. | 0.01% Ce | 0.005% |
| $PrF_3$ | " " | 0.01% Pr | no resonance |
| $NdF_3$ | " " | 0.2% Nd | 0.01 % |
| $SmF_3$ | " " | 0.05% Sm | no resonance |
| $Eu_2O_3$ | Johnson Matthey | 0.01% Eu | 0.01% |
| $GdF_3$ | " " | 0.01% Gd | 0.01% |
| $Dy_2O_3$ | " " | 0.01% Dy | 0.0001% |
| $Er_2O_3$ | " " | 0.01% Er | 0.001% |

components from the $M = +\frac{1}{2}$ to $-\frac{1}{2}$ transitions have been calculated for the $m = +\frac{1}{2}$ hyperfine structure transition when the external magnetic field is along a cube edge. These are given below with the value of $M$ in brackets:

$$\mp 2a \pm 2b \ (\pm \tfrac{5}{2} \longleftrightarrow \pm \tfrac{3}{2}); \quad \mp \tfrac{5}{2}a \pm \delta(\pm \tfrac{3}{2} \longleftrightarrow \pm \tfrac{1}{2}); \quad 0(+\tfrac{1}{2} \longleftrightarrow -\tfrac{1}{2}).$$

In these expressions $\delta = A^2/2h\nu$. The fact that the two effects almost cancel in this transition indicates that the sign of $a$ is opposite to that of $A$ and is therefore probably positive. The value given for $a$ was obtained by calculating the value for complete cancellation in each fine structure component and then taking a mean weighted with the intensity of the component. The value of $a$ in $CaF_2$

is considerably smaller than the values found in other complexes[7] where $10 \times 10^{-4}$ cm$^{-1}$ is a typical value. The sign of a is in agreement with all other determinations and is in agreement with the theory of Watanabe[8] for S-state ions which predicts that the sign of a for $Mn^{2+}$ should be positive regardless of the sign of the cubic crystal potential.

If we apply the theory of Watanabe as in Chapter II.3 for $Cr^{+}$, we predict a value of a for $Mn^{2+}$ in $CaF_2$ of about $1 \times 10^{-4}$ cm$^{-1}$; this is close to the value observed. However, Watkins[9] finds $a = +8.3 \times 10^{-4}$ cm$^{-1}$ for $Mn^{2+}$ in ZnS. In ZnS there are four neighbours tetrahedrally bonded but they are doubly charged and since the separation of the ligands is the same as in $CaF_2$ they should give the same crystal field as in $CaF_2$. In fact the value of a in ZnS is larger by a factor of ten than in $CaF_2$. The lack of consistency may be due to the neglect of covalent bonding by Watanabe. The large effect of covalent bonding may be seen from the following values of A for $Mn^{2+}$ (in units of $10^{-4}$ cm$^{-1}$): 97.8 in $CaF_2$, 81.0 in MgO[5], and 63.7 in ZnS[9].

It is also interesting to note that although NaF and $CaF_2$ are both ionic and Dq (NaF) = Dq ($CaF_2$), the value of a for $Cr^{+}$ in NaF is about six times larger than that of $Mn^{2+}$ in $CaF_2$. (the parameter Dq is discussed in Chapter II.3). The theory of Watanabe does not account for the differences in the a values of $Cr^{+}$, $Mn^{2+}$ and $Fe^{3+}$ in the same type of environment.

As in the case of NaF, the fluorine structure term in the spin Hamiltonian, 4.1, arises from $\sigma$-bonds between the $Mn^{2+}$ and the $F^{-}$ neighbours and resonances are displaced by $\delta\nu$ where

$$\delta\nu = \sum_{N} I^{N}_{o\,z} \left[A_s + A_p \left(3\cos^2\theta_{zp} - 1\right)\right]; \qquad 4.2$$

here the summation is over eight nearest fluorine nuclei. When the external magnetic field is along the [100] direction, $(3\cos^2\theta_{z,p} - 1) = 0$ for all fluorines and we expect nine lines with equal spacing $A_s$ and with intensities in the ratio 1:8:28:56:70:56:28:8:1. Figure 4.2 shows the observed pattern in the $m = +\frac{1}{2}$ hyperfine component which as explained previously is best resolved. The observed pattern agrees close with the calculated one and the separation of the lines gives $A_s = 9.5 \pm 0.3 \times 10^{-4}$ cm$^{-1}$. Measurements in the [110] and [111] directions give $A_p = 2.7 \pm 0.5 \times 10^{-4}$ cm$^{-1}$ which is almost identical with the coupling constant $(2.5 \times 10^{-4}$ cm$^{-1})$ calculated from direct dipole-dipole interaction.

If we assume that the isotropic interaction with fluorine ions occurs through 2s orbitals, the fraction of the time the magnetic electron spend in the 2s orbital of one fluorine ion is given by the ratio

$$\frac{S(Mn)A_s}{S(F)\,A} = \frac{5A_s}{A} \qquad 4.3$$

where $S(Mn) = \frac{5}{2}$ and $S(F) = \frac{1}{2}$ and $A$, the hyperfine interaction of a single 2s electron on a fluorine ion is[10]

$$\frac{8\pi}{3} g\beta\gamma_N\hbar \left|s(0)\right|^2_{2s} = 1.57 \text{ cm}^{-1}; \qquad 4.4$$

the value of $|s(0)|^2$ has been given by Hartree[11]. We find $5A_s/A = .30$.

## IV.3 Impurities of the 4f Group

The crystalline electric potential acting on a paramagnetic ion may be written

$$V = \sum_{n\,m} V_n^m = \sum_{n\,m} A_n^m \overline{r^n}\, y_n^m(\theta,\varphi) \qquad 4.5$$

where $y_n^m$ denotes a surface harmonic, $A_n^m$ is a coefficient determined by the surrounding charges and $\overline{r^n}$ is the mean value of the $n^{th}$ power of the radial distance of the 4f electron[12,13,14,15]. In the present case the crystal field has either (a) cubic symmetry where the non-zero terms are $V_4^0$, $V_4^4$, $V_6^0$, $V_6^4$ or (b) tetragonal symmetry where the non-zero terms are $V_2^0$, $V_4^0$, $V_4^4$, $V_6^0$, $V_6^4$. In case (a) $A_4^4 = \sqrt{\frac{5}{14}}\, A_4^0$ and $A_6^4 = -\sqrt{\frac{7}{2}}\, A_6^0$ so that two independent parameters determine the potential[16]. In case (b) no such relationship exists and five different parameters are needed to specify the potential.

We have observed spectra only from ions containing an odd number of electrons and the states are at least doubly degenerate in the absence of a magnetic field. The $V_n^0$ terms split the ground state into a number of doublets $|\pm J_z\rangle$ and the terms $V_n^4$ admix states which differ in $J_z$ by 4 so that the ground state is a doublet of the form

$$a\,|\pm J_z\rangle + b\,|\pm (J_z+4)\rangle + c\,|\pm (J_z-4)\rangle + \ldots .$$

Transitions within this doublet may be fitted to the following spin Hamiltonian with $S = \frac{1}{2}$:

$$\mathcal{H} = g_{\parallel}\beta H_z S_z + g_{\perp}\beta(H_x S_x + H_y S_y) + A I_z S_z + B\,(I_x S_x + I_y S_y). \qquad 4.6$$

The g-values in the Hamiltonian are related to the coefficients a,b,c etc. specifying the ground state and these are in turn determined by the crystal potential. If the distribution of charges around the ion is known, then it is possible in principle to calculate the g-values if we assume a point charge model. The situation is somewhat different in the case of $Gd^{3+}$ and $Eu^{2+}$ where the free ion ground state is $^8S_{7/2}$ which is not split by the crystal field to first order. Higher order interactions produce a small fine structure splitting but the spectrum may still be described by a spin Hamiltonian with $S = 7/2$ .

IV.4 Cerium

A spectrum is observed at 20°K due to $Ce^{3+}$ ($4f^1\ ^2F_{5/2}$) and this has been measured at X and K-band. There are three similar ions in the magnetic unit cell each with axial symmetry about a different cube edge and the spectrum can be described by the spin Hamiltonian 4.6 with $g_{11} = 3.038 \pm 0.003$ and $g_\perp = 1.396 \pm 0.002$; there is no hyperfine structure. The g-values suggest a ground state

$$\cos\theta\ |\Gamma_7 \pm \tfrac{5}{2}\rangle - \sin\theta\ |\Gamma_7 \mp \tfrac{3}{2}\rangle \quad .$$

With $\cos\theta = 0.910$ one obtains $g_{11} = 3.11$ and $g_\perp = 1.43$. One may calculate the ground state by finding the A coefficients in the crystal potential, eq. 4.5, due to the eight nearest fluorines, the twelve next nearest calciums and the interstitial fluorine which gives rise to the tetragonal symmetry. Values of $A_n^m \overline{r^n}$ for $Pr^{3+}$ were estimated using the value $\overline{r^2} = .027 \times 10^{-16}$ for $Pr^{3+}$ given by Judd[16]. Values of $A_n^m \overline{r^n}$ for $Ce^{3+}$ were then estimated using the relationship[15]

$$V_n^m \propto A_n^m \overline{r^n} \propto (Z - 55)^{-n/4} \qquad 4.7$$

where $Z$ is the atomic number. For $Ce^{3+}$ we find $A_2^0 \overline{r^2} = 90\ cm^{-1}$, $A_4^0 \overline{r^4} = -100\ cm^{-1}$ and $A_4^4 \overline{r^4} = -606\ cm^{-1}$; the sixth order terms have no matrix elements within the ground manifold $J = \frac{5}{2}$. Using the tables of matrix elements of spin operators given by Stevens[12] and Baker, Bleaney and Hayes[17], we now calculate the ground state and find $\cos\theta \left|\pm \frac{5}{2}\right\rangle - \sin\theta \left|\mp \frac{3}{2}\right\rangle$ with $\cos\theta = 0.925$. The remarkably good agreement with the experimental value of 0.910 may be fortuitous since the extrapolation 4.7 is not very reliable. However, the calculation provides further evidence for the correctness of the proposed model for charge compensation.

## IV.5 Europium

Crystals of fluorite containing europium show a resonance spectrum characteristic of an $^8S_{7/2}$ state in a cubic field indicating the presence of europium in its divalent form ($Eu^{2+}$, $4f^7\ ^8S_{7/2}$). The spectrum may be described by the spin Hamiltonian[17]

$$\mathcal{H} = g\beta H.S. + B_4^0 O_4^0 + B_4^4 O_4^4 + B_6^0 O_6^0 + B_6^4 O_6^4 + AI.s \qquad 4.8$$

where the parameters $B_n^m$ are determined experimentally and are not related in any simple manner to the crystal field, and $O_n^m$ are spin operators. Expressions for these spin operators and their matrix elements have already been given[12,17]. The expression 4.8 is simplified in a cubic field since[16] $B_4^4 = 5B_4^0$ and $B_6^4 = -21\ B_6^0$ and only two general parameters $B_4$ and $B_6$ are required to specify the crystal field. The contribution of the crystal potential to the spin Hamiltonian 4.8 may now be written

$$B_4\,(O_4^0 + 5O_4^4) + B_6\,(O_6^0 - 21\,O_6^4).$$

The effective spin $S = \frac{7}{2}$ and $I = \frac{5}{2}$ for both isotopes $^{151}Eu$ and $^{153}Eu$. There are seven allowed fine structure transitions in strong external magnetic fields, which, when the field is parallel to the cubic axis of the crystal are given to second order by

| Transition | | Position | |
|---|---|---|---|
| $M = +\frac{7}{2} \leftrightarrow +\frac{5}{2}$ | | $h\nu = g\beta H + 20b_4 + 6b_6 + (\delta_1 - \delta_2)$ | |
| $+\frac{5}{2} \leftrightarrow +\frac{3}{2}$ | | $h\nu = g\beta H - 10b_4 - 14b_6$ | |
| $+\frac{3}{2} \leftrightarrow +\frac{1}{2}$ | | $h\nu = g\beta H - 12b_4 + 14b_6 + (\delta_2 - \delta_1)$ | |
| $+\frac{1}{2} \leftrightarrow -\frac{1}{2}$ | | $h\nu = g\beta H + 2\delta_1$ | 4.9 |
| $-\frac{1}{2} \leftrightarrow -\frac{3}{2}$ | | $h\nu = g\beta H + 12b_4 - 14b_6 + (\delta_2 - \delta_1)$ | |
| $-\frac{3}{2} \leftrightarrow -\frac{5}{2}$ | | $h\nu = g\beta H + 10b_4 + 14b_6$ | |
| $-\frac{5}{2} \leftrightarrow -\frac{7}{2}$ | | $h\nu = g\beta H - 20b_4 - 6b_6 + (\delta_1 - \delta_2)$ | |

where to avoid large numbers $b_4$ has been written for $60B_4$ and $b_6$ for $1260B_6$ and

$$\delta_1 = (\sqrt{35}b_4 - 3b_6)^2/4g\beta H$$
$$\delta_2 = (5\sqrt{3}b_4 + 7\sqrt{3}b_6)^2/4g\beta H. \qquad 4.10$$

In zero external magnetic field the ground octet splits into two doublets and a quartet as follows:

| | |
|---|---|
| doublet | $32b_4 - 8b_6$ |
| quartet | $20b_4 + 28b_6$ |
| doublet | 0 |

The experimentally determined splitting parameters are given in Table IV.2 together with the values of $g$ and $A$. It was not possible

TABLE IV.2

Constants of the Spectrum of $Eu^{2+}$ in Various Diluents

| Diluent | g | $\lvert A^{151}\rvert$ | $\lvert A^{153}\rvert$ | $\lvert b_4\rvert$ | $\lvert b_6\rvert$ | Ref. |
|---|---|---|---|---|---|---|
| $CaF_2$ | 1.971 ± 0.001 | 34.6 ± 0.1 | 15.4 ± 0.1 | - | - | 18 |
| $CaF_2$ | 1.992 ± 0.0010 | 34.07 ± 0.10* | 15.10 ± 0.10* | 55.75 ± 0.28* | 0.25 ± 0.06* | 19 † |
| $CaF_2$ | 1.989 ± 0.002 | 34.5 ± 0.2 | 15.3 ± 0.4 | 57.9 ± 0.2 | 0.5 ± 0.2 | present work † |
| $SrCl_2$ | 1.992 ± 0.003 | 33.1 ± 0.4 | 15.0 ± 0.4 | 12 ± 2* | - | 31 |
| KCl | - | 32.56 ± 0.06 | 14.38 ± 0.03 | - | - | 32 |
| SrS | 1.991 ± 0.001 | 30.8 ± 0.2 | 13.8 ± 0.2 | - | - | 33 |

Values of A, $b_4$, $b_6$ are given in units of $10^{-4}$ $cm^{-1}$.

* A calculated from the values given in gauss and $b_4$, $b_6$ from the quoted value of the overall splitting of the octet and the ratio of the separations between each doublet and quartet.

† $b_6$ has the opposite sign to $b_4$ and A.

* The cubic field splitting is smaller in $SrCl_2$, owing largely to an increase in lattice spacing by a factor 1.29.

to determine the sign of $b_4$ by observing the variation of the fine structure transitions with temperature since the spectrum became saturated at 20°K. From the position of the transitions the sign of $b_4$ is found to be opposite to that of $b_6$.

Previous measurements on this ion have been made by Manenkov and Prokhorov[18] and by Ryter[19] whose values are given in Table IV.2. The former use the expression

$$A^2/2g\beta H\,\{I(I+1) - m^2\} + A^2/2g\beta H\,\{m(2M - 1)\}$$

derived from Bleaney's formula[6] for the second order h.f.s. correction to the $(M,m \longleftrightarrow M-1,m)$ transition arising from the off-diagonal elements of $A(S_+I_- + S_-I_+)$; this is applicable only when the crystal field splitting is small compared with $h\nu$. In the present case this expression is inadequate and when allowance is made for the crystal field splitting, the correction becomes

$$\tfrac{1}{2}A^2\left[[I(I+1) - m^2]\left\{2\cdot\frac{S(S+1) - M(M-1)}{h\nu\ (M \longleftrightarrow M-1)} - \frac{S(S+1) - M(M+1)}{h\nu\ (M \longleftrightarrow M+1)}\right.\right.$$

$$\left.\left. - \frac{S(S+1) - (M-1)(M-2)}{h\nu\ (M-1 \longleftrightarrow M-2)}\right\}\right] + \tfrac{1}{2}A^2m\left\{\frac{S(S+1)-(M-1)(M-2)}{h\nu\ (M-1 \longleftrightarrow M-2)} -\right.$$

$$\left. - \frac{S(S+1) - M(M+1)}{h\nu\ (M \longleftrightarrow M+1)}\right\}.$$

This expression reduces to the simpler one used by Manenkov and Prokhorov if $h\nu$ in each denominator is replaced by $g\beta H$.

When the external magnetic field was parallel to a cube edge we found that the overall hyperfine structure was smaller in the extreme position

on the high field side. This corresponds to $b_4$ and A having the same sign and agrees with the work of Ryter. The corrected positions of the fine structure transitions are given in Table IV.3; each value is a mean of the corrected positions for the $^{151}Eu$ and $^{153}Eu$ isotopes. The corrected values of the overall hyperfine splitting (5A) for each isotope are also included.

The values of A for $Eu^{2+}$ in $CaF_2$ may be compared with the values given by various workers for this and other compounds listed in Table IV.2. The h.f.s. constant decreases noticeably in going from the fluoride through the chloride to the sulphide. This presumably arises from an increase in the covalent character of the bonds since similar but larger differences occur for $Mn^{2+}$ (see section IV.2).

As in $Mn^{2+}$ the h.f.s. in $Eu^{2+}$ arises from unpaired s-electron wavefunctions[20,21], but the effect is smaller than in $Mn^{2+}$. No fluorine structure due to overlap of the 4f electrons onto the surrounding fluorine ions is resolved and the full line width at half power in the $M = +\frac{1}{2} \longleftrightarrow -\frac{1}{2}$ transition is 2.5 gauss when the magnetic field is along a cube edge; this suggests that any covalent bonding to the fluorines by the $4f^7$ configuration is smaller by a factor of at least ten than by the $3d^5$ configuration. As both the h.f.s. and the bonding are smaller than in $Mn^{2+}$, the effect of changing the ligands is also smaller.

Partial breakdown of Russel-Saunders coupling will cause a small admixture of excited levels of the same J into the ground state[14]. We expect a small admixture of the first excited state $|^6P_{7/2}\rangle$ into the $|^8S_{7/2}\rangle$ ground state and this will contribute to the h.f.s. It also

TABLE IV.3

Positions of the Fine Structure Transitions and Values of the Overall Hyperfine Splitting (5A) for $Eu^{2+}$ in $CaF_2$ at 90°K ($\lambda$ = 3.215 cm) . H // [100]

| $\|M\| \leftrightarrow \|M-1\|$ | Fine Structure Transitions | Hyperfine Structure Splitting (5A) $^{151}Eu$ | $^{153}Eu$ |
|---|---|---|---|
| $\frac{7}{2} \leftrightarrow \frac{5}{2}$ | 4600.9 | 184.8 | 80.8 |
| $\frac{3}{2} \leftrightarrow \frac{1}{2}$ | 4091.7 | 186.7 | 83.3 |
| $\frac{5}{2} \leftrightarrow \frac{3}{2}$ | 3968.1 | 185.0 | 81.6 |
| $\frac{1}{2} \leftrightarrow \frac{1}{2}$ | 3328.8 | 186.1 | 83.2 |
| $\frac{5}{2} \leftrightarrow \frac{3}{2}$ | 2730.6 | 184.7 | 80.9 |
| $\frac{3}{2} \leftrightarrow \frac{1}{2}$ | 2574.1 | 185.4 | 82.5 |
| $\frac{7}{2} \leftrightarrow \frac{5}{2}$ | 2115.6 | 185.5 | 82.1 |

All values are given in gauss.

causes a departure of the g-value from the free spin g-value, $g_0$, and from the size of this departure the amount of admixture may be calculated. If we write the ground state as $\sqrt{(1-a^2)}\,|\,^8S_{7/2}\rangle + a\,|\,^6P_{7/2}\rangle$ then $g = g_0(1-a^2) + \frac{12}{7}a^2$ and with our measured g-value this gives $a^2 = 0.045$. The contribution of the $^6P_{7/2}$ state to the h.f.s. may be calculated using the expression[22]

$$A = \frac{2\beta_e\mu_n}{I}\left\langle\frac{1}{r^3}\right\rangle\frac{\langle J\|N\|J\rangle}{\langle J\|A\|J\rangle}\,g. \qquad 4.11$$

For the $^6P_{7/2}$ state, $\langle J\|N\|J\rangle = 8/35$,[16] $\left\langle\frac{1}{r^3}\right\rangle = 57\text{Å}^{-3}$[23] and $\langle J\|A\|J\rangle = 12/7$ and we find $^{151}A = 4\times10^{-4}$ cm$^{-1}$ or only 1% of the total h.f.s. It is therefore apparent that variations in a make only small contributions to variations in A.

IV.6 Gadolinium

The spectrum of $Gd^{3+}$ ($4f^7\ ^8S_{7/2}$) was observed at 90°K at both X and K-band but the second order effects arising from the very large zero field fine structure splitting made the interpretation of the spectrum impossible at X-band and extremely difficult at K-band. The spectrum draws three ions with similar spectra; the symmetry is tetragonal with principal axes parallel to the cube edges. It is presumed that the spectrum can be fitted to the spin Hamiltonian[17]

$$\mathcal{H} = g\beta H.S + B_2^0 O_2^0 + B_4^0 O_4^0 + B_4^4 O_4^4 + B_6^0 O_6^0 + B_6^4 O_6^4 \qquad 4.12$$

with $S = 7/2$. When H is parallel to the symmetry axis then transitions occur to second order at fields given by

| Transition | Position |
|---|---|
| $M = +\frac{1}{2} \leftrightarrow -\frac{1}{2}$ | $h\nu = g\beta H + 2\delta_1$ |
| $\pm\frac{1}{2} \leftrightarrow \pm\frac{3}{2}$ | $h\nu = g\beta H \pm 2b_2^0 \mp 12b_4^0 \pm 14b_6^0 + (\delta_2 - \delta_1)$ |
| $\pm\frac{3}{2} \leftrightarrow \pm\frac{5}{2}$ | $h\nu = g\beta H \pm 4b_2^0 \mp 10b_4^0 \mp 14b_6^0$ |
| $\pm\frac{5}{2} \leftrightarrow \pm\frac{7}{2}$ | $h\nu = g\beta H \pm 6b_2^0 \pm 20b_4^0 \pm 6b_6^0 + (\delta_1 - \delta_2)$ |

4.13

where $b_2^0 = 3B_2^0$, $b_4^0 = 60B_4^0$, $b_6^0 = 1260B_6^0$ and

$$\delta_1 = 1260\,(B_4^4 + 15B_6^4)^2/g\beta H$$
$$\delta_2 = 2700\,(B_4^4 - 7B_6^4)^2/g\beta H. \qquad 4.14$$

The positions of the energy levels are difficult to calculate when the magnetic field is perpendicular to the tetragonal axis because of the large off-diagonal elements. When the external field is parallel to the tetragonal axis, three nearly equal spaced transitions are identified as $M = \pm\frac{3}{2}$ to $\pm\frac{1}{2}$ and $M = +\frac{1}{2}$ to $-\frac{1}{2}$ and these may be followed into the perpendicular direction where two additional transitions, $M = \pm\frac{5}{2}$ to $\pm\frac{3}{2}$ are identified. The positions of these transitions are given in Table IV.4 Transitions in lower field could not be measured because of insufficient intensity due to line broadening and transitions in higher field were beyond the range of the magnet.

With the measurements available it is necessary to make some simplifying assumptions to obtain even a crude estimate of the crystal field parameters and we assume the $b_6$ terms are small and may be neglected. We now find $g = 1.99 \pm 0.01$, $b_2^0 = .12\ cm^{-1}$, $b_4^4 = .044\ cm^{-1}$ and $b_4^0 = .006\ cm^{-1}$. These estimates of the crystal field are not very reliable

but they do indicate an overall splitting of the octuplet in zero field of about 2-cm$^{-1}$. The results also indicate that $b_2^0$ is several times larger than $b_4^0$ and $b_6^0$. This is a feature in common with measurements on $Gd^{3+}$ in other salts[7], though our value of $b_2^0$ is much larger than that of most salts hitherto investigated.

TABLE IV.4

Positions of the Fine Structure Transitions of $Gd^{3+}$ at 90°K ($\lambda$ = 1.264 cm)

| $\|M\| \leftrightarrow \|M-1\|$ | Magnetic field | |
|---|---|---|
| $\frac{3}{2} \leftrightarrow \frac{1}{2}$ | 11601 gauss | H parallel to the tetragonal axis |
| $\frac{1}{2} \leftrightarrow \frac{1}{2}$ | 8533 " | |
| $\frac{3}{2} \leftrightarrow \frac{1}{2}$ | 5480 " | |
| $\frac{5}{2} \leftrightarrow \frac{3}{2}$ | 11236 " | |
| $\frac{3}{2} \leftrightarrow \frac{1}{2}$ | 9272 " | H perpendicular to tetragonal axis |
| $\frac{1}{2} \leftrightarrow \frac{1}{2}$ | 7711 " | |
| $\frac{3}{2} \leftrightarrow \frac{1}{2}$ | 6329 " | |
| $\frac{5}{2} \leftrightarrow \frac{3}{2}$ | 5212 " | |

These results are in contrast with the measurements of Ryter[19] and Low[24] on $Gd^{3+}$ in $CaF_2$. They find only one ion in the unit cell with cubic symmetry and a much smaller zero field splitting, 0.148 cm$^{-1}$, of the octuplet. In our case we may assume that the tetragonal distortion arises from the presence of a charge compensating fluorine ion in an adjacent interstitial site. The presence of $Gd^{3+}$ ions with cubic

symmetry may arise if the charge compensation is remote so that the immediate environment of the impurity ion is not distorted.

The line width in the $Gd^{3+}$ spectrum is 6 gauss which is considerably larger than in $Eu^{2+}$ possibly because of a small variation of the large fine structure splitting from one ion to the next.

IV.7 Erbium

In the case of $Er^{3+}$ ($4f^{11}\ {}^4I_{15/2}$) resonances were observed at 20°K at both X and K-band; the spectrum shows a hyperfine structure due to the odd isotope $^{167}Er$ ($I = \frac{7}{2}$, natural abundance 23%). There are three types of spectrum present:

(a) an isotropic line corresponding to one ion in the unit cell whose spectrum is described by equation 4.6 with $g_{11} = g_{\perp} = 6.78 \pm 0.01$.

(b) three lines corresponding to a single transition for three equivalent ions with axial symmetry about a cube edge. The spectrum is described by equation 4.6 with $g_{11} = 7.76 \pm 0.02$, $g_{\perp} = 6.253 \pm 0.006$, $A = 261 \pm 3 \times 10^{-4}\ cm^{-1}$ and $B = 219 \pm 3 \times 10^{-4}\ cm^{-1}$.

(c) three lines similar to (b) with $g_{11} = 6.76 \pm 0.02$ and $g_{\perp} = 9.11 \pm 0.01$.

The h.f.s. constants of $^{167}Er$ could not be measured for (a) and (c) because of the weakness of the lines and the complexity of the overlapping spectra. When the temperature was reduced from 20°K to 14°K, the intensity of (b) increased and (c) decreased indicating that both have the same origin and that (c) comes from an excited state about 36k above

the ground doublet (b).

Judd[16] has calculated that the ground doublet of $Er^{3+}$ in a cubic field is

$$\sqrt{\frac{77}{192}}\left|\pm\frac{13}{2}\right\rangle + \sqrt{\frac{65}{192}}\left|\pm\frac{5}{2}\right\rangle - \sqrt{\frac{39}{192}}\left|\mp\frac{3}{2}\right\rangle - \sqrt{\frac{11}{192}}\left|\mp\frac{11}{2}\right\rangle$$

for which $g = 6.80$. Correction for the breakdown of Russel-Saunders coupling makes $g = 6.77$ which is in excellent agreement with that found for (a). Because of the complexity of the calculations, no attempt has been made to find the crystal field states of the ground $J = \frac{15}{2}$ manifold which give rise to (b) and (c).

The forbidden quadrupole transitions of $^{167}Er$ were observed in (b) but were not resolved because of the large line width (13 gauss at $4^{o}K$); this arises from fluorine satellite structure which is unresolved in the low fields in which resonance is observed (see section IV.9).

## IV.8 Other Impurities

In addition to the measurements already described, experiments were also performed on crystals containing the following impurities:

Praseodymium, for which no resonance was observed down to $4^{o}K$.

Neodymium: it was not possible to measure the hyperfine structure constants of the odd isotopes $^{143}Nd$ and $^{145}Nd$ ($I = \frac{7}{2}$, natural abundance 12% and 8% respectively) because other impurities obscured the weak hyperfine lines. The g-values were previously measured[3].

Samarium: no resonance was observed down to $4^{o}K$ either because the g-values are too small or because it enters as $Sm^{2+}$ which has a ground state with $J = 0$. Optical evidence to show that samarium

enters $CaF_2$ at least in part as $Sm^{2+}$ has been summarised by Prsibram[1].

Dysprosium: a single weak anisotropic line was observed at $4^{o}K$ which was not investigated in detail because the apparatus was not sufficiently sensitive.

Spectra have also been observed in $CaF_2$ which have been tentatively assigned to $Co^{2+}$ and $Cr^{2+}$. These ions distort the lattice, presumably because their radii are considerably less than that of $Ca^{2+}$, and they are present in low concentration. The interpretation of the spectra presents difficulties and more experiments are required.

## IV.9. Fluorine Satellite Structure of Rare Earth Ions

In the spectra of $Ce^{3+}$, $Eu^{2+}$ and $Gd^{3+}$, satellites are observed on either side of the main resonance lines (see Plate 4.1). The spacing between the satellites and the main line is field dependent and is equal to the fluorine nuclear magnetic resonance frequency in the external magnetic field. This structure arises from a simultaneous flipping of the electron spin and a nearest fluorine nuclear spin due to weak magnetic coupling between them. Proton satellites of a similar nature have been observed in the paramagnetic resonance spectrum of atomic hydrogen produced by irradiation of acids at a low temperature[25] and by Bleaney, Hayes and Llewellyn[26] in the paramagnetic resonance spectrum of $NO_2$ molecules produced in lanthanum magnesium nitrate crystals containing radioactive isotopes.

A theory of the satellites has been developed by Dr. M.C.M. O'Brien assuming magnetic dipole coupling only between the electron spin and the fluorine nuclear spin[27]; this theory will be used in the present discussion

The relative intensity of a satellite associated with a single nuclear flip, and the main line is given by

$$P = \tfrac{1}{2}\,(H_S/H)^2 = \tfrac{1}{2}\left(\frac{\mu}{r^3 H}\right)^2 \left[(1+3\cos^2\varphi) - (\cos\alpha - 3\cos\varphi\cos\theta)^2\right] \qquad 4.15$$

where $\underline{H}_S$ is the component of the field of the electron moment $\underline{\mu}$ that is perpendicular to the applied field $\underline{H}$, $\underline{r}$ is the position vector of the nucleus relative to the electron, $\alpha$ is the angle between $\underline{\mu}$ and $\underline{H}$, $\varphi$ is the angle between $\underline{\mu}$ and $\underline{r}$ and $\theta$ is the angle between $\underline{H}$ and $\underline{r}$. If either $g$ is isotropic or the applied field is along a principal axis of $g$, expression 4.15 reduces to

$$P = \tfrac{1}{2}\left(\frac{\mu}{r^3 H}\right)^2 9\cos^2\theta\sin^2\theta. \qquad 4.16$$

If the spin is coupled to more than one external nucleus, then the expression for the satellite intensity must be summed over all nuclei. In this case extra satellites will be observed distant $n g_n \beta_n H$ from the main line corresponding to the flipping of $n$ nuclei as well as the electron spin. If the nuclei are not coupled together the probability of $n$ flips is the product of the probabilities of $n$ single ones multiplied by the number of ways of choosing $n$ nuclei. If an ion is equally coupled to $m$ nuclei with a relative probability of one nucleus turning over, then, the intensity of the main line and its satellites will be in the ratios

$$1 : Pm : P^2\,{}^mC_2 : P^3\,{}^mC_3 : \ldots\ .$$

A detailed investigation of the satellite structure was made in the anisotropic cerium spectrum. The spacing and relative intensities of

the satellites have been measured with the external field in several directions and at X and K-band so that measurements in different external fields are available. These are listed in Table IV.5. In some directions extra satellites are observed due to the flipping of more than one fluorine nucleus with the electron spin. Satellites were also observed in the spectra of $Eu^{2+}$ and $Gd^{3+}$ but these have not been investigated in detail because of the complexity of the spectra. Satellites were not resolved in the spectrum of $Er^{3+}$ because the lines occur in low field (H = 850 gauss at X-band) and were not observed in the case of $Nd^{3+}$, presumably because the spectrum was weak.

In all the lines studied the spacing of the satellites is equal to the fluorine nuclear magnetic resonance frequency in the external field to within the experimental error. In the case of $Ce^{3+}$ the intensities of the satellites are a factor 2 to 3.5 greater than calculated (see Table IV.5). The intensity of the first satellites relative to the main line should increase by a factor 2 when H is moved from the [110] direction to the [100] direction; an increase of 1.5 was observed at both X and K-band. This result indicates that about $\frac{1}{3}$ of the satellite intensity arises from an isotropic electron-extra nuclear interaction which presumably occurs through weak bonding with s orbitals on the fluorine ions. Inclusion of this effect will improve the agreement between the observed and calculated intensities slightly; the remaining discrepancy probably arises from a noticeable preferential saturation of the main line at $20^{\circ}K$, the assumption of a point charge model and the contraction of the lattice at low temperatures (the electron dipole field

## TABLE IV.5

### Satellites Observed in the $Ce^{+++}$ Spectrum

| Direction of Field | H gauss | Satellite Separation Mc/s | NMR freq. in Field H Mc/s | Ratio of Main Line to First Satellite Intensities | | Satellite Structure Intensities | |
|---|---|---|---|---|---|---|---|
| | | | | Observed | Calculated | Observed | Calculated* |
| ⊥ 100 axis | 4794 | 19.4 ± 0.5 | 19.2 | 5.7 | 11.9 | 100:17.5:2.5 | 100:17.5:1.3 |
| ⊥ 100 axis | 11915 | 46 ± 2 | 48 | 20 | 73.5 | 100:5 | |
| // 100 axis | 2197 | not resolved | | | | | |
| // 100 axis | 5380 | 21.0 ± 1.0 | 21.6 | 1.7 | 3.2 | 100:60:20 | 100:60:15.7 |
| // 111 axis | 3271 | 14.6 ± 2.0 | 13.1 | 1.2 | 2.9 | 100:85:55:25:5 | 100:85:29:5:0.5 |
| ⊥ 110 axis | 4794 | 19.6 ± 0.5 | 19.2 | 10 | 23.8 | 100:10 | |

*The intensities of the second, third and fourth satellites are calculated using the ratio of the main line to the first satellite to give the effective value of $1/h^6$, not by using the crystallographic value.

at the nucleus is determined by $r^{-3}$ and an effective reduction of r of about 17% would account for the entire discrepancy).

When calculating the intensities of satellites arising from multiple spin flips, any discrepancy between the observed and calculated values of P will be magnified in successive satellites. Accordingly, the intensities of the outside satellites are calculated relative to the first satellite using a value of P obtained from the intensity of the first satellite (see Table IV.5). The observed intensity falls off less rapidly than the theory predicts.

An interesting confirmation of the proposed model of charge compensation for lanthanum ions exhibiting tetragonal symmetry (see Fig. 4.1) has been observed in the spectrum of $Ce^{3+}$. When the external magnetic field is oriented along the [100] direction a splitting of the K-band resonance from those centres with their tetragonal axes along [100] is resolved (Plate 4.1(b)); this arises from the nuclear dipole field of the charge compensating interstitial fluorine ion which gives rise to the tetragonal symmetry. The field at the electron due to a fluorine nucleus is $\mu/r^3$ $(3\cos^2\theta - 1)$ and the contribution from the eight nearest fluorines vanishes when the magnetic field is in the [100] direction. The calculated contribution from the interstitial fluorine is $2\mu/r^3$ = 5.2 gauss and this agrees with the measured splitting of 5.2 gauss. The corresponding splitting for those $Ce^{3+}$ centres with their tetragonal axes along the [010] and [001] directions is 2.6 gauss and this has not been resolved. We do not observe the effect in the [100] oriented centres at X-band because the satellites are not resolved in the smaller

external field.

We observe a fluorine hyperfine structure with iron group ions and a fluorine satellite structure with rare earth ions because the greater covalent bonding in the former case produces a larger field from the magnetic electrons at the fluorine nucleus. Let us consider the case where the external field H is greater than the field of the electron at the nucleus, $H_e$, so that the resultant field is almost parallel to H (Fig. 4.3(a)). When the electron spin undergoes a transition from $S^+$ to $S^-$ the resultant field undergoes a small change in orientation from $H_a$ to $H_b$. As the field is essentially unchanged there is a negligible change in the energy of interaction of the field with the nucleus and the orientation of the nucleus makes almost no difference to the energy of the transition. Because of the small change in the axis of quantisation of the nuclear spin there is a small probability that the nucleus will undergo a transition at the same time as the electron and satellites are observed. This is the situation in the case of the rare earths and is illustrated in Fig. 4.3(b); the allowed transitions are marked with continuous lines and the satellite transitions with dashed lines.

If $H_e$ is greater than H so that the resultant field at the nucleus is almost parallel to $H_e$, an almost complete reversal of this field occurs, going from $H_c$ to $H_d$ (Fig. 4.3(a)), when the electron undergoes a transition. Hence the total energy change depends on the direction of the nuclear magnet and is larger by twice the nuclear magnetic resonance frequency in a field $H_e$ if the nucleus is initially

antiparallel to the field than if it is parallel; hence there are two separated h.f.s. transitions. In this case also the initial and final axes of quantisation of the nucleus are not quite parallel and there is a finite probability that the nucleus will undergo a transition at the same time as the electron. In both possible satellite transitions of this sort the relative directions of $H_0$ and the nuclear magnet do not change and both transitions are superimposed half-way between the hyperfine lines. Such lines have not been observed in the fluorine structure of iron group impurities in NaF or $CaF_2$ because the line width is too great a proportion of the hyperfine structure for them to be resolved. These transitions are illustrated in Fig. 4.3(c); the allowed hyperfine transitions are marked with continuous lines and the satellite transitions with dashed lines.

IV.10 Discussion

The paramagnetic resonance measurements indicate that the ions of $Mn^{2+}$ and $Eu^{2+}$ are incorporated substitutionally into the fluorite lattice without producing a distortion of the lattice symmetry (it is possible that the distance to the ligands is different from that in pure fluorite) while $Ce^{3+}$, $Nd^{3+}$, $Gd^{3+}$ and $U^{3+}$ produce a tetragonal distortion. In the case of $Er^{3+}$, ions are observed in the same crystal in both undistorted and tetragonally distorted surroundings. Low, using a crystal of $CaF_2$ containing $Gd^{3+}$ grown from a melt and Kyter using natural $CaF_2$ containing $Gd^{3+}$ find no distortion of the lattice. We have also observed $Er^{3+}$ ions in the cubic form only, in crystals of $CaF_2$ containing minute traces of the element.

When the trivalent ions are observed with a tetragonal distortion it appears that the distortion is produced by a charge compensating $F^-$ ion in the nearest interstitial site and our measurements indicate that the effect of this ion is large. It is therefore likely that when a specimen of cubic symmetry is observed, the charge compensation is not achieved locally. The type of charge compensation observed appears to be determined by the condition under which the samples were formed and the concentration of impurity added; it appears that cubic sites are initially occupied and at higher concentrations association with the compensating $F^-$ ion occurs.

A comparison of the cubic field splitting in the isoelectronic ions $Eu^{2+}$ and $Gd^{3+}$ shows that the splitting is larger in $Eu^{2+}$ in spite of the fact that the extra positive charge on $Gd^{3+}$ presumably tends to pull in the surrounding charges more and in spite of the larger spin-orbit coupling of $Gd^{3+}$. It appears that the decrease in $\overline{r^n}$ in going from $Eu^{2+}$ to $Gd^{3+}$ more than compensates for the other factors.

A striking difference between the spectra of rare earth ions and iron group ions in fluoride crystals is the presence of a resolved fluorine hyperfine structure in the latter; the rare earth ions do not show this structure because the deep-seated 4f electrons are too weakly covalent. However the spectrum of Uranium in $CaF_2$ shows a resolved fluorine structure[28] of the same extent as that of $Mn^{2+}$ indicating that the overlap of the 3d and 5f electron wavefunctions onto the ligands are comparable.

The spectrum of $Mn^{2+}$ has now been investigated in a number of

fluoride crystals. The measurements on $Mn^{2+}$ in NaF and $CaF_2$ described in this thesis may be compared with the work of Tinkham[29] on $Mn^{2+}$ in $ZnF_2$ and of Shulman and Jaccarino[30] on fluorine nuclear resonance shifts in $MnF_2$. The contact interactions are given in Table IV.6; included also are the amount of charge transfer to each fluorine 2s orbital and the separations of the bonding ions. Inspection of Table IV.6 shows a slight reduction of contact interaction with increased bond length in the octahedrally co-ordinated compounds $MnF_2$, $ZnF_2$ and NaF and a sudden change in $CaF_2$. However, in $CaF_2$ each $Mn^{2+}$ ion is at the centre of a cube of light fluorine ions so that the reduction in the total charge transfer is not so pronounced. The $\sigma$-bonding orbitals are now $d\varepsilon$ rather than $d\gamma$ because of the different symmetry involved. The inability to resolve $\pi$-bonding in NaF and $CaF_2$ indicates that the $\pi$-bonding is less than 30% of the $\sigma$-bonding.

TABLE IV.6

Contact Interaction of $Mn^{2+}$ in Fluoride Crystals

| | Mn:$ZnF_2$ | $MnF_2$ | Mn:NaF | Mn:$CaF_2$ |
|---|---|---|---|---|
| $A_s$ | 16.5± 1.5 | 15.7± 0.3 | 14.4± 0.3 | 9.5± 0.3 |
| Probability of occupation of a fluorine 2s orbital, % | .53 | .51 | .47 | .30 |
| Cation-anion distance, Å | 2.03 | 2.11 | 2.31 | 2.36 |

Values of $A_s$ are in units of $10^{-4}$ $cm^{-1}$.

## References


1. Pribram, K., Irradiation Colours and Luminescence, London Pergamon Press, (1956), Ch.14.
2. Zintl, E., Utgard, A., Z. Anorg. Chem., (1939), 240, 150.
3. Bleaney, B., Llewellyn, P.M., Jones, D.A., Proc. Phys. Soc., (1956), B69, 858.
4. Bleaney, B., Stevens, K.W.H., Rep. Prog. Phys., (1953), 16, 108.
5. Low, W., Phys. Rev., (1957), 105, 793.
6. Bleaney, B., Phil. Mag., (1951), 42, 441.
7. Bowers, K.D., Owen, J., Rep. Prog. Phys., (1955), 18, 304.
8. Watanabe, H., Prog. Theor. Phys. Japan, (1957), 18, 405.
9. Watkins, G.D., Phys. Rev., (1958), 110, 1956.
10. Moriya, T., Prog. Theor. Phys. Japan, (1956), 16, 23.
11. Hartree, D.R., Proc. Roy. Soc., (1935), A151, 96.
12. Stevens, K.W.H., Proc. Phys. Soc., (1952), A65, 209.
13. Elliot, R.G., Stevens, K.W.H., Proc. Roy. Soc., (1952), A215, 437.
14. " " " " " " " (1953), A218, 553.
15. " " " " " " " (1953), A219, 387.
16. Judd, B.R. (private communication).
17. Baker, J.M., Bleaney, B., Hayes, W., Proc. Roy. Soc., (1958), A247, 151.
18. Manenkov, A.A., Prokhorov, A.M., Dokl. Acad. Nauk. SSSR, (1956), 107, 402.
19. Ryter, C., Helv. Phys. Acta, (1957), 30, 353.
20. Abragam, A., Horowitz, J., Pryce, M.H.L., Proc. Roy. Soc., (1955), A230, 169.
21. Heine, V., Phys. Rev., (1957), 107, 1002.
22. Baker, J.M., Bleaney, B., Proc. Phys. Soc., (1955), A68, 937.

23. Bleaney, B., Proc. Phys. Soc., (1955), A68, 937.

24. Low, W., Phys. Rev., (1958), 109, 265.

25. Trammel, G.T., Zeldes, H., Livingstone, R., Phys. Rev., (1958), 110, 630.

26. Bleaney, B., Hayes, W., Llewellyn, P.M., Nature, (1957), 179, 140.

27. O'Brien, M.C.M., (private communication).

28. Llewellyn, P.M., Thesis, Oxford, (1956).

29. Tinkham, M., Proc. Roy. Soc. (1956), A236, 535, 549.

30. Shulman, R.G., Jaccarino, V., Phys. Rev., (1957), 108, 1219.

31. Hayes, W. (unpublished).

32. Abraham, M., Kedzie, R., Jeffries, C.D., Phys. Rev., (1957), 108, 58.

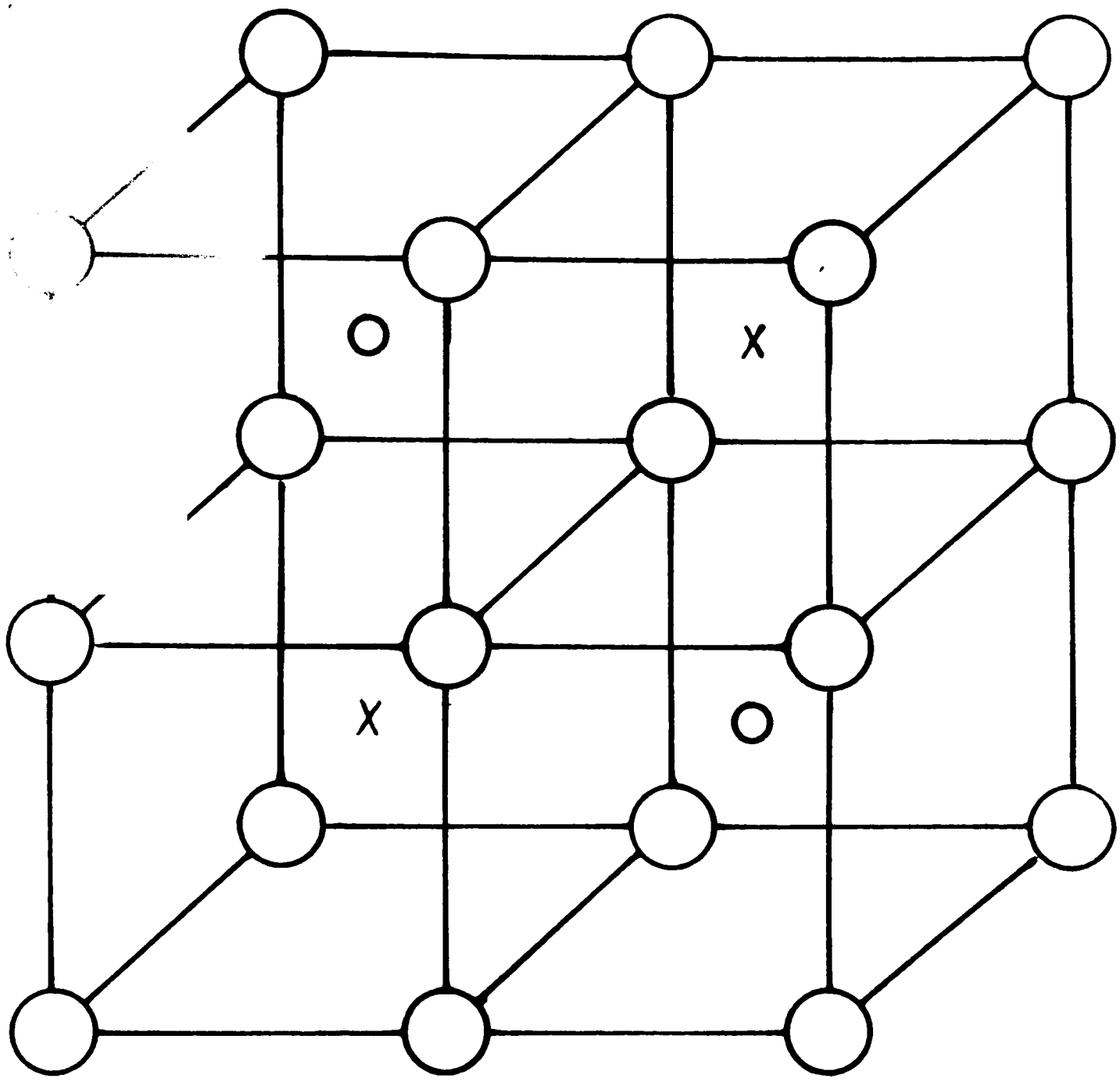
33. Bleaney, B., Low, W., Proc. Phys. Soc., (1955), A68, 55.

Fig. 4.1. One half on the $CaF_2$ unit cell. The second half lies behind and is similar to the half shown but with $Ca^{2+}$ and interstitial positions interchanged. A triply charged impurity ion may replace a $Ca^{2+}$ ion and a charge compensating $F^-$ ion may occur at a nearest interstitial position.

Fig. 4.2. Fluorine hyperfine structure of $Mn^{2+}$ in the $m = +\frac{1}{2}$ transition with H parallel to a cube edge. Theoretically there should be nine components with intensities in the ratios 1:8:28:56:70:56:28:8:1 but the outer components are so weak as to be barely visible.

Fig. 4.3. Fluorine structure transitions in the spectra of impurities in $CaF_2$; (b) satellite transitions when $H > H_\bullet$, (c) hyperfine transitions when $H_\bullet > H$ (see text).

Plate 4.1. Satellite structure in the spectrum of $Ce^{3+}$ in $CaF_2$. (a) the ion, at X-band whose tetragonal axis is perpendicular to the magnetic field showing first and second satellites. (b) the ion at K-band whose tetragonal axis is parallel to the magnetic field showing the splitting produced by the interstitial $F^-$ ion.




○ $F^-$ ○ $Ca^{2+}$

X INTERSTITIAL SITE

LATTICE STRUCTURE OF $CaF_2$

FIG. 4.1

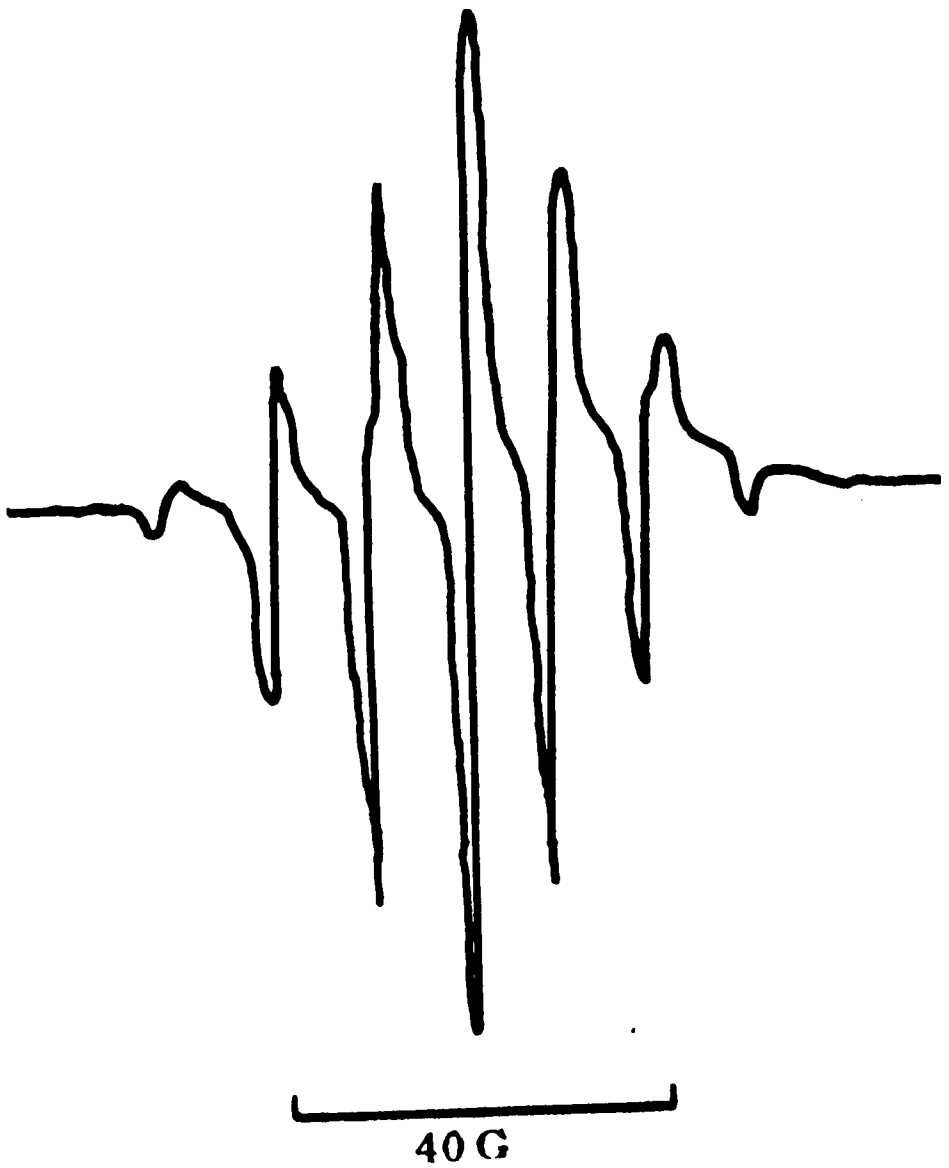
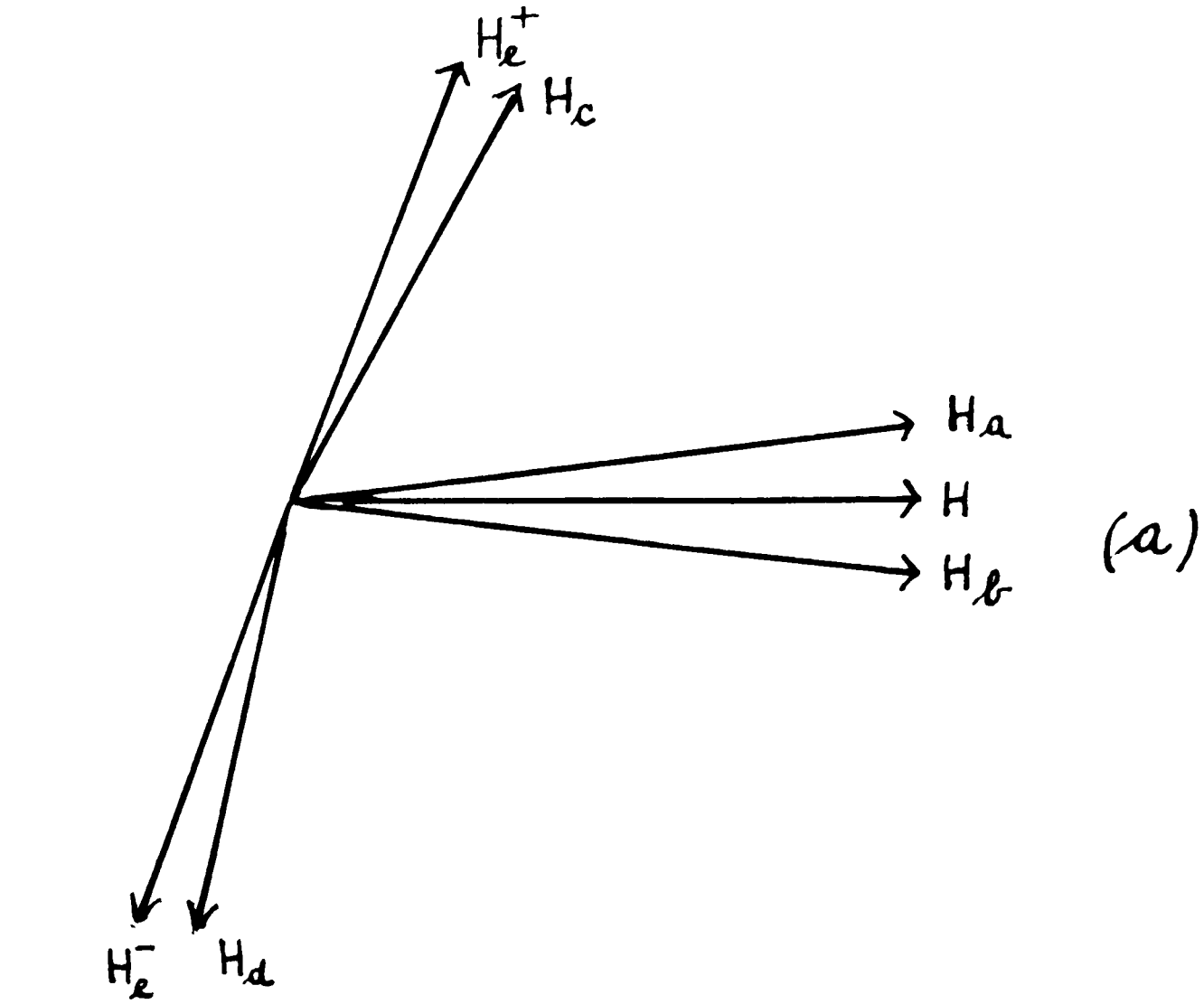



Fig. 4.2. Fluorine structure of $Mn^{2+}$.




FLUORINE STRUCTURE TRANSITIONS IN $CaF_2$

FIG. 4.3

(a)

(b)

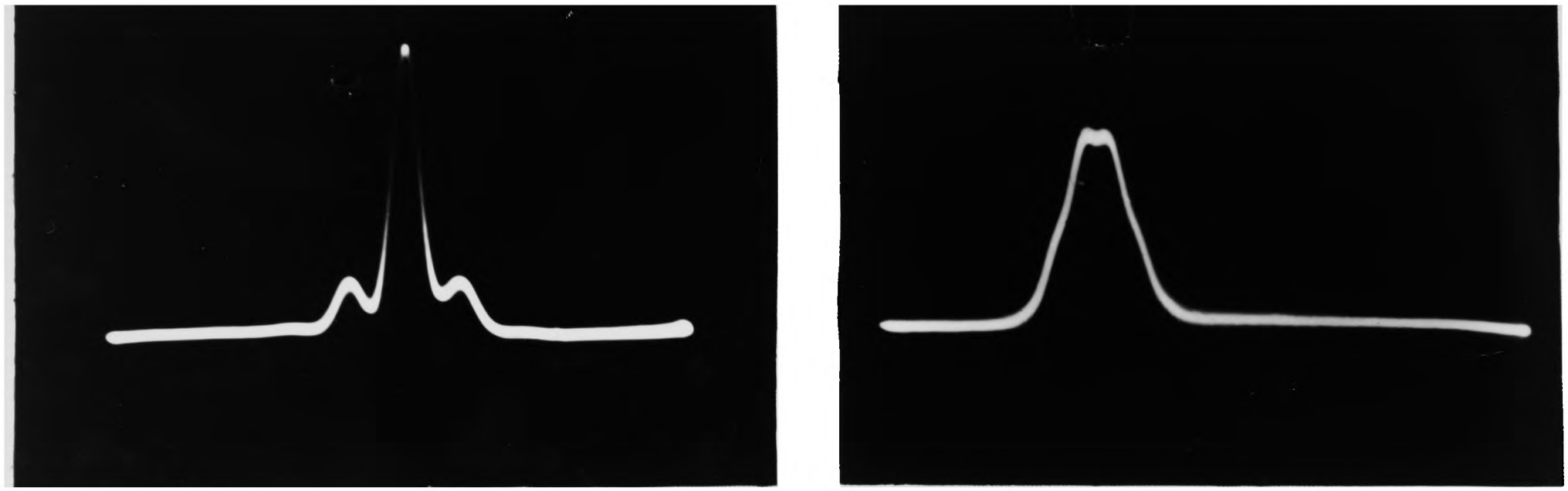


Plate 4.1. Fluorine satellite structure of $Ce^{3+}$.

# CHAPTER V

## V-CENTRES IN ALKALI HALIDES

### V.1 Introduction

Recently, the application of electron spin resonance techniques to the study of V-centres in alkali halides resulted in accurate descriptions of the structure of these centres[1,2]. V-centres may be defined as trapped positive holes. It has been shown that when crystals of KCl, NaCl, KBr or LiF which are pure or doped with $Ag^+$, $Tl^+$ or $Pb^{++}$ ions, are irradiated with X-rays at $77^oK$, complex electron spin resonance spectra are observed which may be assigned to the molecule ions $Cl_2^-$, $Br_2^-$ and $F_2^-$ (henceforth referred to in general as $X_2^-$). The optical absorption spectra of these defects have been investigated and correlated with their resonance spectra[2,3].

In the resonance spectrum of $X_2^-$ the hole is localised on two halogen nuclei and an extensive anisotropic h.f.s. is observed due to the interaction of the unpaired electron with these nuclei. An investigation of this structure showed that the molecule ion is accurately aligned along a [110] axis of the crystal (Fig. 5.1(a)). The symmetry of the centre is rhombic with two face diagonals and a cube edge as principle axes; six such combinations of axes are possible and there are six similar centres in the magnetic unit cell. In the case of $Cl_2^-$, a seven line h.f.s. is observed when the magnetic field is parallel to the axis of the molecule ion with intensities in the ratios 1:2:3:4:3:2:1. This structure arises because the chlorine nuclei are equivalent and each has a spin of $\frac{3}{2}$ so that the magnetic spin quantum

number $M(I) = M(I_1) + M(I_2)$ can take the values $-3, -2, -1, 0, 1, 2, 3$ weighted according to the above intensity ratios. The isotopes $^{35}Cl$ and $^{37}Cl$ occur in the ratio 3:1 and have slightly different nuclear moments so that three sets of spectra are resolved with intensities in the ratios 9:6:1 corresponding to the isotopic species 35-35, 35-37, 37-37. When the magnetic field is perpendicular to the axis of the ion, the h.f.s. is considerably collapsed and the degeneracy of the hyperfine lines is raised by second order hyperfine and quadrupole effects. In the case of $Br_2^-$ a spectrum with similar properties is found. Bromine has two equally abundant isotopes $^{79}Br$ and $^{81}Br$, each with a nuclear spin of $\frac{3}{2}$; three sets of spectra are resolved with intensities in the ratios 1:2:1 arising from the isotopic species 79-79, 79-81, 81-81.

The correlation of the optical and resonance spectra may be achieved by

(a) comparing the variation of intensities of the spectra with irradiation time

(b) observing the effect of bleaching in the optical absorption band with polarised light.

In the case of $Cl_2^-$, for example, an optical absorption band occurs at 365 mμ. After irradiation into this band with light polarised in the $[0\bar{1}1]$ direction at 77°K a dichroism is subsequently observed in the absorption spectrum measured with [011] and $[0\bar{1}1]$ polarised light. The optical and resonance measurements show that although some bleaching of the centres occurs due to recombination of electrons and holes, the main effect is a realignment of a large fraction of these centres into the

[011] direction from the other five possible orientations. This effect is expected to arise if the optical transition is only allowed for radiation polarised parallel to the axis of the molecule ion and if the excited state is unstable so that the centres become mobile. In this case [$0\bar{1}1$] polarised light will not excite [011] oriented centres but will excite centres in the five other orientations. It follows that if the excited $X_2^-$ centre is not very mobile and loses its excitation energy before annihilation there will be a reorientation of centres into [011] from the other five possible orientations.

A high intensity AH6 mercury arc lamp may be used for the polarized light bleaching experiments with a suitable combination of filters.

(c) measuring reorientation and decay curves for the two types of spectra.

At the reorientation temperature the dichroism begins to disappear in a crystal containing preferentially oriented centres due to the onset of movement of the centres through the lattice. The $Cl_2^-$ centres begin to reorient at 173°K but no appreciable decay of the centres is observed until the temperature reaches 203°K. The reorientation temperature is more sharply defined and lower than the decay temperature since reorientation may be achieved by a movement through one lattice spacing whereas, on the average, many lattice spacings are travelled before a hole meets an electron and is destroyed.

A pulse annealing technique is used for measuring reorientation and decay temperature. The starting temperature is normally that of liquid nitrogen. The sample is warmed to the required temperature in a suitable refrigerant, e.g. Freon 12, for two minutes, then cooled quickly to liquid

nitrogen temperature and the spectrum remeasured. The cycle is subsequently repeated at the next higher temperature. Steps of about 15°C are used.

The role of the impurities Ag, Tl and Pb in the production of $X_2^-$ ions has been investigated[2,3]. The production rate of $X_2^-$ ions in crystals containing these impurities is 100 to 1000 times faster than impure crystals. The impurities are efficient electron traps and prevent the recombination of electrons and holes during the irradiation (see Chapter VI). The impurities do not perturb the optical or resonance spectra of the $X_2^-$ ions in a measurable fashion and we may conclude that these centres are a property of the 'pure' lattice.

The effect of environment on the properties of the $Cl_2^-$ ion has been studied[4] by measuring the optical and resonance spectra in the series LiCl, NaCl, KCl and RbCl. Variations in the reorientation temperature and the peak position and width of the 365 mμ optical absorption band along the series have been explained in a qualitative manner by considering the effect of the lattice dimensions on the energy levels of the $Cl_2^-$ ion. The variation in the parameters of the resonance spectrum along the series is small. A careful investigation of the line width of the resonance spectra showed that the unpaired electron is not located entirely on the $Cl_2^-$ ion but spends about 0.8 of its time in orbitals on the surrounding positive ions.

Our present concern is with a new type of $X_2^-$ centre which is produced by low temperature X-irradiation of KCl and KBr crystals containing $Ba^{2+}$, $Sr^{2+}$ or $Ca^{2+}$ ions[5]. These centres have been assigned

to $Cl_2^-$ and $Br_2^-$ molecule ions but their properties differ from those of the centres described above. The work was done in co-operation with G.M. Nichols who carried out the optical experiments; he has kindly allowed his measurements to be quoted here.

The crystals were X-irradiated at 195°K, cooled to 77°K and transferred without warming to the microwave cavity. X-band measurements were made at 77°K.

V.2 Optical Absorption Spectrum of KCl

When crystals of pure KCl are X-irradiated at 195°K the optical absorption spectrum above 200 mμ consists of three bands: $V_2$ absorption occurs at 235 mμ, F-absorption at 540 mμ and K-absorption at 460mμ. The spectra of samples containing alkaline earth ions show a band in the near ultra violet in addition to those mentioned. The position of the new peak is determined, somewhat, by the divalent ion. In KCl:Ca the peak occurs at 323 mμ, in KCl:Sr at 321 mμ, in KCl:Ba at 335mμ. The ratio of F to $V_2$-absorption is significantly larger in the doped samples indicating that the new peaks in the near ultraviolet are trapped hole centres.

V.3 Paramagnetic Resonance Spectrum of KCl

After irradiation at 195°K, single crystals of KCl containing alkaline earth ions exhibit a resonance spectrum with a complex h.f.s. (Fig. 2). There are three distinguishable centres in the magnetic unit cell each with a similar spectrum and with approximate axial symmetry about a different cube edge. When the external magnetic field is parallel to the axis of one of these centres, the corresponding spectrum

consists of seven groups of lines in the region 3046 to 3617 gauss; in this orientation the external field is perpendicular to the axes of the other two centres and their spectra are identical and superimposed in the region 3200 to 3350 gauss. The centres are assigned to $Cl_2^-$ molecule ions alined approximately along a cube edge in contrast with the centres of Castner and Känzig[1] where the alinement is along a face diagonal.

It will be shown later that the two chlorine nuclei do not have identical environments and hence are not equivalent; this results in the raising of the degeneracy which might otherwise be present in the h.f.s. The seven line h.f.s. with intensities 1:2:3:4:3:2:1 observed for [110] oriented $Cl_2^-$ when the external magnetic field is parallel to the axis now becomes seven groups of lines. The characteristic three line isotopic structure with intensities 9:6:1 is observed in the extreme groups which are singly degenerate and therefore clearly defined.

We may describe the resonance spectrum approximately by the spin Hamiltonian

$$\mathcal{H} = g_{\parallel}\beta H_z S_z + g_{\perp}\beta(H_x S_x + H_y S_y) + AI_z S_z + B(I_x S_x + I_y S_y) \qquad 5.1$$

with $S = \frac{1}{2}$ and $I = I_1 + I_2$ where $I_1 = I_2 = \frac{3}{2}$ is the spin of the chlorine nucleus. The allowed transitions $(\frac{1}{2}, m) \longleftrightarrow (-\frac{1}{2}, m)$ occur when[6]

$$h\nu = g\beta H + Km + (B^2/4g\beta H_0)\left(\frac{A^2 + K^2}{K^2}\right)\{I(I+1) - m^2\} \qquad 5.2$$

where $K^2g^2 = A^2g_{\parallel}^2\cos^2\theta + B^2g_{\perp}^2\sin^2\theta$ and $\theta$ is the angle between the external magnetic field $H$ and the axis of the molecule ion. The

measured constants of the spin Hamiltonian for the isotopic species 35-35 are $g_{11} = 2.005 \pm 0.002$, $g_{\perp} = 2.04 \pm 0.01$, $A = 89.0 \pm 0.2 \times 10^{-4}$ cm$^{-1}$ and $B = 13 \times 10^{-4}$ cm$^{-1}$. The corresponding measurements for the [110] oriented centres are $g_{11} = 2.0010$, $g_{\perp} = \frac{1}{2}(g_x + g_y) = 2.0437$, $A = 94.3 \times 10^{-4}$ cm$^{-1}$ and $B = 8.4 \times 10^{-4}$ cm$^{-1}$.

V.4 Optical Absorption Spectrum of KBr

The results are similar to those of KCl. The spectrum of 'pure' KBr shows $V_2$-absorption at 275 mμ, F-absorption at 600 mμ and K absorption at 530 mμ. The position of the new peak in the doped samples occurs at 345 mμ in KBr:$Ca^{2+}$, 345 mμ in KBr:$Sr^{2+}$ and 360 mμ in KBr:$Ba^{2+}$. Again, the ratio of F to $V_2$ absorption is greater in the doped samples indicating that the impurity induced centres involve trapped holes.

V.5 Paramagnetic Resonance Spectrum of KBr.

Seven groups of lines are observed when the external magnetic field is oriented along a cube edge (Fig. 5.4). The spectrum is assigned to $Br_2^-$ ions and is the analogue of the $Cl_2^-$ spectrum; there are three distinguishable centres in the magnetic unit cell, each alined approximately along a different cube edge. The bromine isotopic structure is observed in the extreme h.f.s. components; the degeneracy of the inside components is raised by the inequivalence of the bromine nuclei and their large quadrupole moment. Of the parameters of the spin Hamiltonian, 5.1, only $g_{11}$ and A could be measured: $g_{11} = 1.991 \pm 0.003$ and $A = 419 \pm 3.0 \times 10^{-4}$ cm$^{-1}$. The measurements were made on the ion 81-81. The corresponding measurements on the [110] oriented centres are $g_{11} = 1.980$ and $A = 420 \times 10^{-4}$ cm$^{-1}$.

## V.6 Correlation between Optical and Resonance Spectra

A correlation between the 325 mμ bands in KCl, the 345 mμ bands in KBr and the $X_2^-$ resonance spectra has been achieved. Both the optical and resonance absorptions appear when KCl and KBr are doped with the divalent ions and irradiated at a low temperature and their intensities are proportional. The thermal stabilities of the two types of spectra are the same. The following decay temperatures were found: KCl:Ca at 236°K, KCl:Sr at 233°K, KCl:Ba at 231°K, KBr:Ca at 243°K, KBr:Sr at 253°K and KBr:Ba at 263°K. These temperatures correspond to the inflection points of curves relating optical density or resonance intensity to pulse annealing temperature. A typical plot is given in Fig. 5.5.

It was found that bleaching at 77°K with light polarised such that the electric vector is parallel to [010] results in preferential bleaching of those centres alined in the [010] direction. Similar effects have been observed with the [110] oriented $X_2^-$ ions[2,3]. Fig. 5.3 gives the results of an experiment on a KCl:Ca crystal which was bleached for 15 minutes at 77°K in the interval 300 to 400 mμ. The solid line shows th optical absorption in both the [100] and [010] directions before bleaching. The dotted lines show the absorption in these directions after bleaching with [010] polarised light. The optical density of centres in the [010] direction is reduced by a factor of more than two while that in the [100] direction has been slightly enhanced due to a reorientation of centres from the [010] direction. The largest ratio of [100] to [010] optical density which could be obtained was about 3 to 1.

Fig. 5.2 shows the paramagnetic resonance spectrum of KCl:Ca after bleaching with [010] polarised light. Fig. 5.2(a) was taken with the external magnetic field parallel to the [100] crystal axis and Fig. 5.2(b) with the field parallel to the [010] direction. A comparison of these spectra with the spectrum before bleaching showed that the bleaching did not decrease the number of [100] oriented centres while the number of [010] centres was reduced to one third of its original value. The optical and resonance measurements of the dichroism are therefore consistent and indicate that the optical transition is allowed only for radiation polarised parallel to the axis of the molecule ion and that the excited state of the optical transition is unstable.

The KBr crystals were usually badly strained and depolarised light to a degree which made it difficult to bleach preferentially the $Br_2^-$ molecule ions; the maximum ratio of [100] to [010] oriented centres which could be achieved was about 3:2.

Resonance and optical measurements gave identical reorientation temperatures. The following values were found: KCl:Ca at 193°K, KCl:Sr at 193°K, KCl:Ba at 193°K and KBr:Ca at 223°K. These values may be compared with 173°K for the [110] oriented $Cl_2^-$ and 143°K for the [110] oriented $Br_2^-$.

## V.7 Discussion

It has been established that the centres giving rise to the 325 mμ optical absorption band in KCl containing alkaline earth ions and the 345 mμ band in KBr containing the same impurities are $Cl_2^-$ and $Br_2^-$ molecule ions. These ions differ from the $Cl_2^-$ and $Br_2^-$ ions of Castner

and Känzig in that they have approximate axial symmetry about a cube edge. Experiments have been carried out with other alkali halides containing alkaline earths and with KCl containing $Cd^{2+}$ but the [100] oriented $X_2^-$ ions have not been found. The centres have not been found in pure crystals or crystals containing good electron traps such as Ag, Tl or Pb where the [110] oriented centres are readily formed.

There has been confusion over the degree of association of some divalent impurities and positive ion vacancies in alkali halides. Etzel and Maurer[7] suggest that in NaCl:Cd the $Cd^{2+}$ ions are almost completely associated at room temperature and Bean and Maurer[8] indicate complete dissociation of $Ca^{2+}$ ions in NaCl:Ca. On the basis of these results Etzel[9] concludes that free positive ion vacancies are effective hole traps whereas associated vacancies are not. On the other hand, Dryden and Meakins[10] do not find any evidence of association of $Cd^{2+}$ in their samples of NaCl:Cd and their results indicate a marked degree of association of $Ba^{2+}$, $Sr^{2+}$ and $Ca^{2+}$ in solid solution in KCl. Haven[11] also finds evidence for the prevalence of divalent-vacancy pairs in NaCl:Ca. Using these results one might draw conclusions opposite to those of Etzel.

In agreement with Dryden and Meakins we shall assume that the impurity ions enter the lattice substitutionally and a large fraction of them are associated with positive ion vacancies (Fig. 5.1(b)). It is suggested that upon X-irradiation at dry ice temperature a halogen ion is ionised and the electron is trapped as an F-centre; the positive hole is trapped as a $V_2$-centre or as an $X_2^-$ centre at a positive ion vacancy.

The presence of the vacancy may cause the molecule ion to move out of its normal [110] alignment and produce approximate alignment along the [100] direction; one possible way in which this may be achieved is illustrated in Fig. 5.1(b). We might then expect the anion-to-cation radius ratio of the host alkali halide to be of importance in the formation of the [100] oriented centres and the fact that we could not produce these centres in KI, NaCl, or NaBr may be due to the large value (~ 2) of this ratio in these salts. The variation in the position of the optical absorption band with the impurity ion supports the view that the impurity is closely associated with the $X_2^-$ centre.

The vacancy stabilised centres decay at a higher temperature than the [110] oriented centres and this largely accounts for the failure to observe the latter centres at dry ice temperature. When the samples are X-irradiated at liquid nitrogen temperature, $V_1$-centres are produced in addition to the [100] oriented $X_2^-$ centres; with the irradiation times used (~ 40 min.) the [110] oriented $X_2^-$ centres are not produced in observable quantities.

The g-shifts in the [110] oriented $Cl_2^-$ spectrum of Castner and Kanzig are described by them in terms of the theory given by Cohen[12] and Inui, Harasawa and Obata[13]. An energy level scheme for the $Cl_2^-$ ion with axial symmetry is shown in Fig. 5.6[14]; departures from axial symmetry will raise the degeneracy inherent in the $\pi$-levels but we neglect this. The ground state configuration involving valence shell orbitals is $(\sigma_g^2\ \pi_u^4\ \pi_g^4\ \sigma_u)\ ^2\Sigma_u^+$ and the first excited state involving an allowed transition from the ground state is $(\sigma_g^2\ \pi_u^4\ \pi_g^3\ \sigma_u^2)\ ^2\Pi_g$.

This transition is allowed for radiation polarised perpendicular to the molecular axis. The second excited state involving an allowed transition from the ground state is $(\sigma_g \pi_u^4 \pi_g^4 \sigma_u^2)\ ^2\Sigma_g^+$ and the transition is allowed for radiation polarised parallel to the molecular axis. It is likely that the ultra-violet band of the [100] and [110] oriented $X_2^-$ centres arises from this transition since it has the correct polarization properties; in addition, the $^2\Sigma_g^+$ state is expected to be unstable because of a net antibonding $\sigma_u$ electron and absorption of polarised radiation within the band may lead to the observed dichroism. A very weak transition of the [110] oriented centres has been observed at about 750 mμ which may be $^2\Sigma_u^+ \longleftrightarrow {}^2\Pi_g$ but the polarisation properties of this absorption have not been established[15]. Such a transition has not been observed in the case of the [100] oriented centres presumably because of insufficient intensity. Transitions of $X_2^-$ molecules have not been observed in the free state.

The unpaired electron of the ground state of $Cl_2^-$ is in the antibonding $3p\sigma_u$ orbital and the $g$-shifts are determined by the spin-orbit coupling to the $3p\pi_u$ level separated by a distance $\Delta$. Following Inui, Harasawa and Obata[13] we may write

$$\varepsilon_{11} = \varepsilon_0 - \frac{\lambda^2}{\Delta^2(1+\alpha^2)}, \quad \varepsilon_\perp = g_0 - \frac{2\lambda}{\Delta(1+\alpha^2)} - \frac{2\lambda^2}{\Delta^2(1+\alpha^2)} \qquad 5.3$$

where $\alpha$ determines the fractional s-character of the electron wave function and $\lambda$ is the spin-orbit coupling constant. The predicted value of $\varepsilon_{11} - g_0$ is negative ($g_0 = 2.0023$ is the free electron $g$-value) and

in the case of the [110] oriented $Cl_2^-$ centre is found to be - 0.001. In the present case the g-shift is +0.003. The positive shift may arise from the fact that the molecule ions are not alined accurately along a cube edge; the g-value measured with the magnetic field parallel to a cube edge will therefore include a small contribution from $g_\perp$. The observed shift indicates that the molecule ion makes an angle of about $2^\circ$ with a cube edge. The departure from axial symmetry results in an increase in the number of possible orientations and hence an increase in the number of distinguishable centres; however, the spectra from the centres distributed around a particular cube edge are not resolved.

Most of the crystals grown contained aggregates of impurity ions which caused cloudiness and scattering of light. Quenching from $650^\circ C$ to room temperature dispersed the impurity ions in the lattice and the number of $X_2^-$ centres which could be produced was increased by a factor of about 3. However, the strains produced by quenching caused shattering of the crystals, depolarization of polarized light and broadening of the resonance lines. These effects depend on the concentration and size of the impurity and were more pronounced in KBr than in KCl. The small $Ca^{2+}$ ions strain the KBr lattice more severely than $Ba^{2+}$ ions.

The effect of strains on the resonance line width is small in the parallel orientation since the variation of h.f.s. with angle is a minimum. The effect is expected to be less in KCl because of the smaller hyperfine splitting. With both KCl and KBr a sharpening and increase in amplitude of the lines from the [100] oriented centres occurs when the external magnetic field is moved parallel to the [100] orientation. In

the case of KBr:Ba the resonance lines disappear when the magnetic field is 18° off the [100] direction and with KBr:Ca cannot be observed even when the magnetic field is parallel to the [100] direction; it will be noticed in the spectrum of KBr:Sr (Fig. 5.4) that only lines from centres oriented parallel to the magnetic field are sufficiently narrow to be clearly visible.

In the parallel orientation, the $Cl_2^-$ and $Br_2^-$ line widths are 9.0 and 12.0 gauss respectively as compared with 1.3 and 2.5 gauss for the [110] oriented centres. Considerations based on dipole-dipole interactions with the nuclei of the surrounding ions suggest line widths of 0.5 and 1.0 gauss. It has already been shown[4] that in the case of the [110] oriented $Cl_2^-$ centre a large fraction of the line width arises from interaction with the nuclei of nearest neighbour ions through covalent bonding. This effect, the strained nature of the crystals and the misalignment of the centres may well account for the increased line width in the present case.

The ultraviolet optical absorption band of the $X_2^-$ centre in both KCl and KBr occurs at shorter wavelength than the bands of the corresponding [110] oriented centres. This effect is expected to arise largely from the influence of environment on the excited level of the transition. The effect of environment on the ground state in which paramagnetic resonance is observed should be less and only slight differences in the parameters of the resonance spectra from the two types of centre are observed.

REFERENCES


1. Castner, T., Känzig, W., J. Phys. and Chem. of Solids (1957), 3, 178.

2. Delbecq, C.J., Smaller, B., Yuster, P.H., Phys. Rev., (1958), 111, 1235.

3. Delbecq, C.J., Hayes, W., Yuster, P.H., to be published.

4. Hayes, W., Delbecq, C.J., Yuster, P.H., Bull. Am. Phys. Soc., (1958), Ser. II, 3, 325.

5. Nichols, G.M., Hayes, W., Bull. Am. Phys. Soc., (1958), Ser. II, 3, 178.

6. Bleaney, B., Phil. Mag., (1951), 42, 441.

7. Etzel, W., Maurer, R.J., J. Chem. Phys., (1950), 18, 1003.

8. Bean, C., Maurer, R.J., ONR Tech. Report No. 4, Contract N6 ONR-07129, University of Illinois, March 1952.

9. Etzel, H.W., Phys. Rev., (1952), 87, 906.

10. Dryden, J.S., Meakins, R.J., Disc. Faraday Soc., (1957), 23, 39.

11. Haven, Y., J. Chem. Phys., (1953), 21, 171.

12. Cohen, M.H., Phys. Rev., (1956), 101, 1432.

13. Inui, T., Harasawa, S., Obata, Y., J. Phys. Soc. Japan, (1956), 11, 612.

14. Herzberg, G., Spectra of Diatomic Molecules, Chapter 6, Van Nostrand, 1950.

15. Yuster, P.H., private communication.

Figure 5.1 (a) model for the [110]oriented $X_2^-$ molecule ion. (b) model for the [100] oriented $X_2^-$ molecule ion. In case (a) the two chlorine nuclei have identical environments whereas in case (b) they do not.

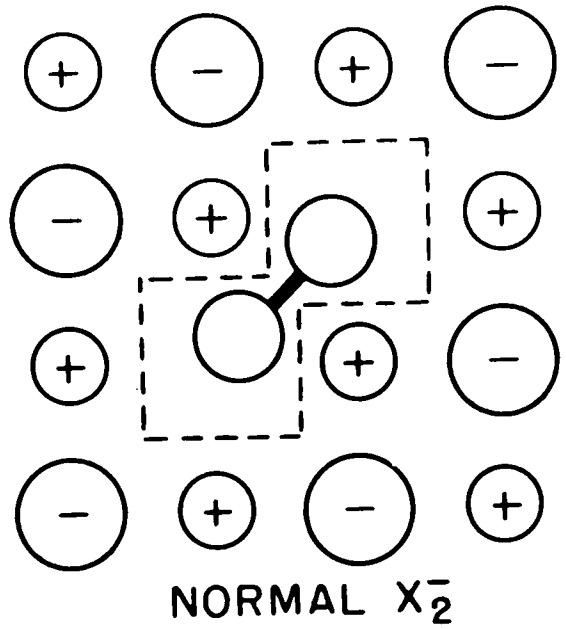
Figure 5.2. Spectrum of the [100] oriented $Cl_2^-$ after a polarised bleach (a) with the external magnetic field parallel to [010] (b) with the external magnetic field parallel to [100]. The strong lines in the region 3200-3300 gauss arise from centres alined perpendicularly to the magnetic field.

Figure 5.3. Effect of a polarised bleach on the 325 mμ absorption of $Cl_2^-$. The heavy line shows the absorption of [100] and [010] polarized light before bleaching and the dashed lines show the absorption after bleaching with [100] polarized light.

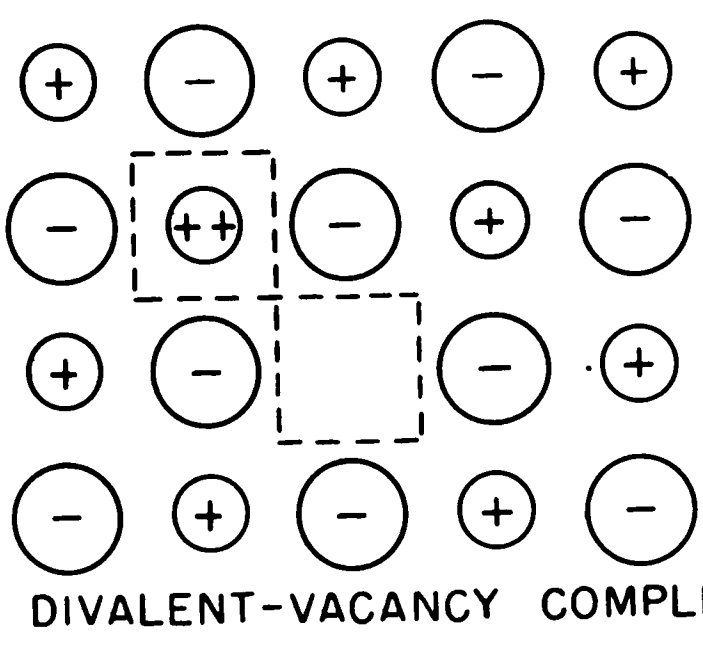
Figure 5.4. Spectrum of the [100] oriented $Br_2^-$. Only lines from centres oriented parallel to the magnetic field are sharp enough to be clearly visible.

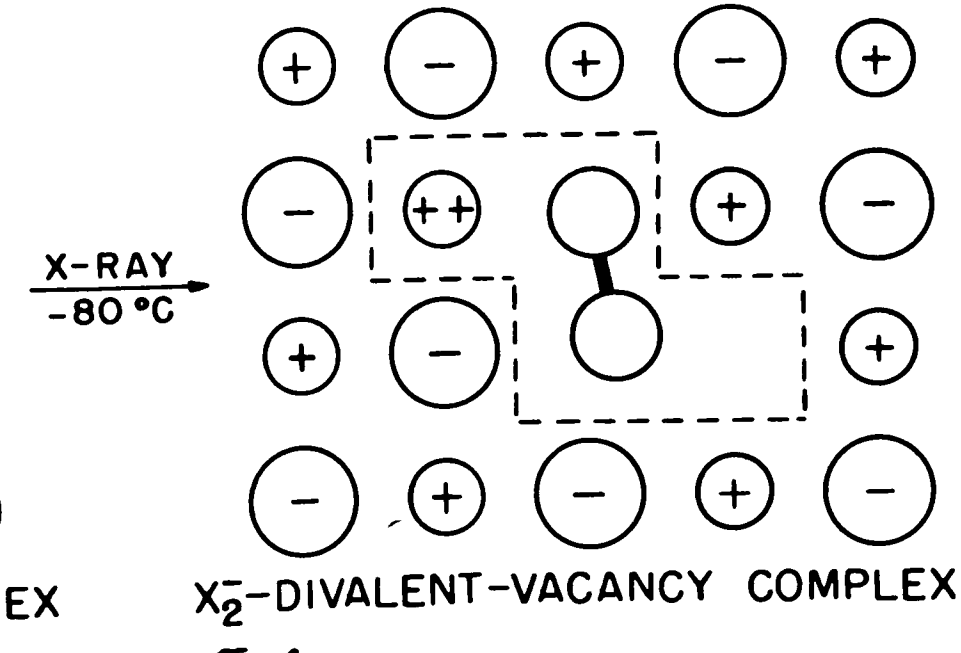
Figure 5.5. Plot of the intensity of the optical and resonance spectra of $Cl_2^-$ in KCl:Ca as a function of pulse anneal temperature; the decay temperature of the centres is taken to be the inflection point of the curve.

Figure 5.6. Schematic energy level diagram of $X_2^-$ ions in an axially symmetric crystal field.


NORMAL $X_2^-$

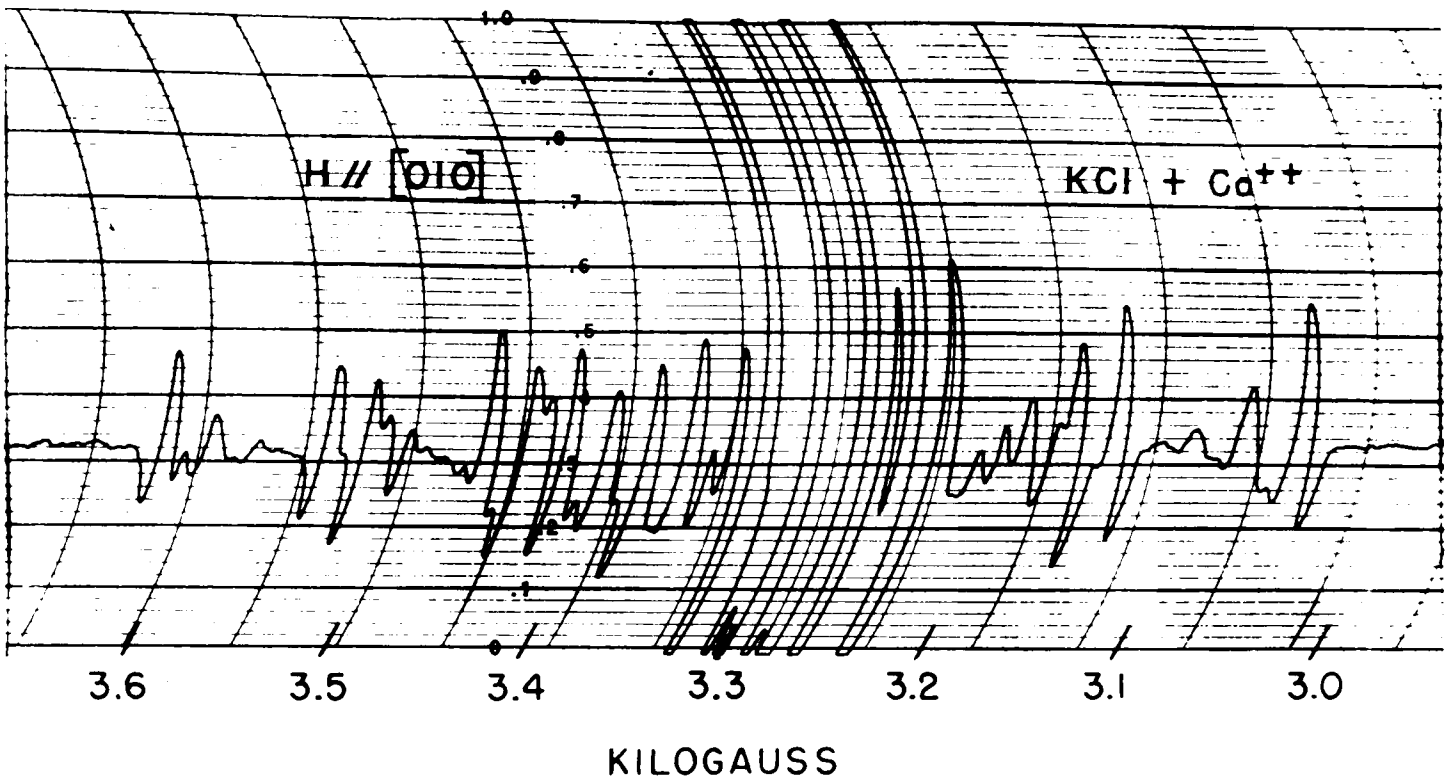
(a)


DIVALENT-VACANCY COMPLEX

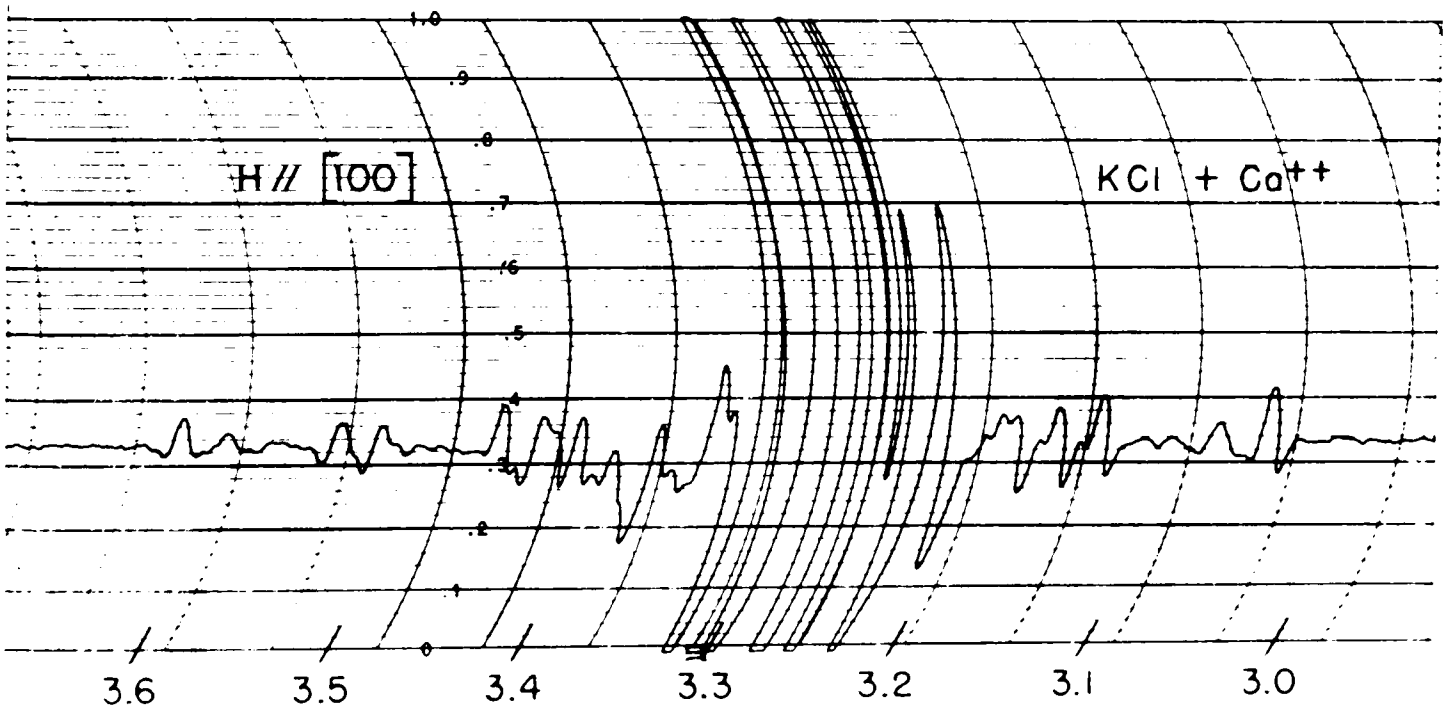

X-RAY
-80 °C
$X_2^-$-DIVALENT-VACANCY COMPLEX

(b)

FIG. 5.1




(a)

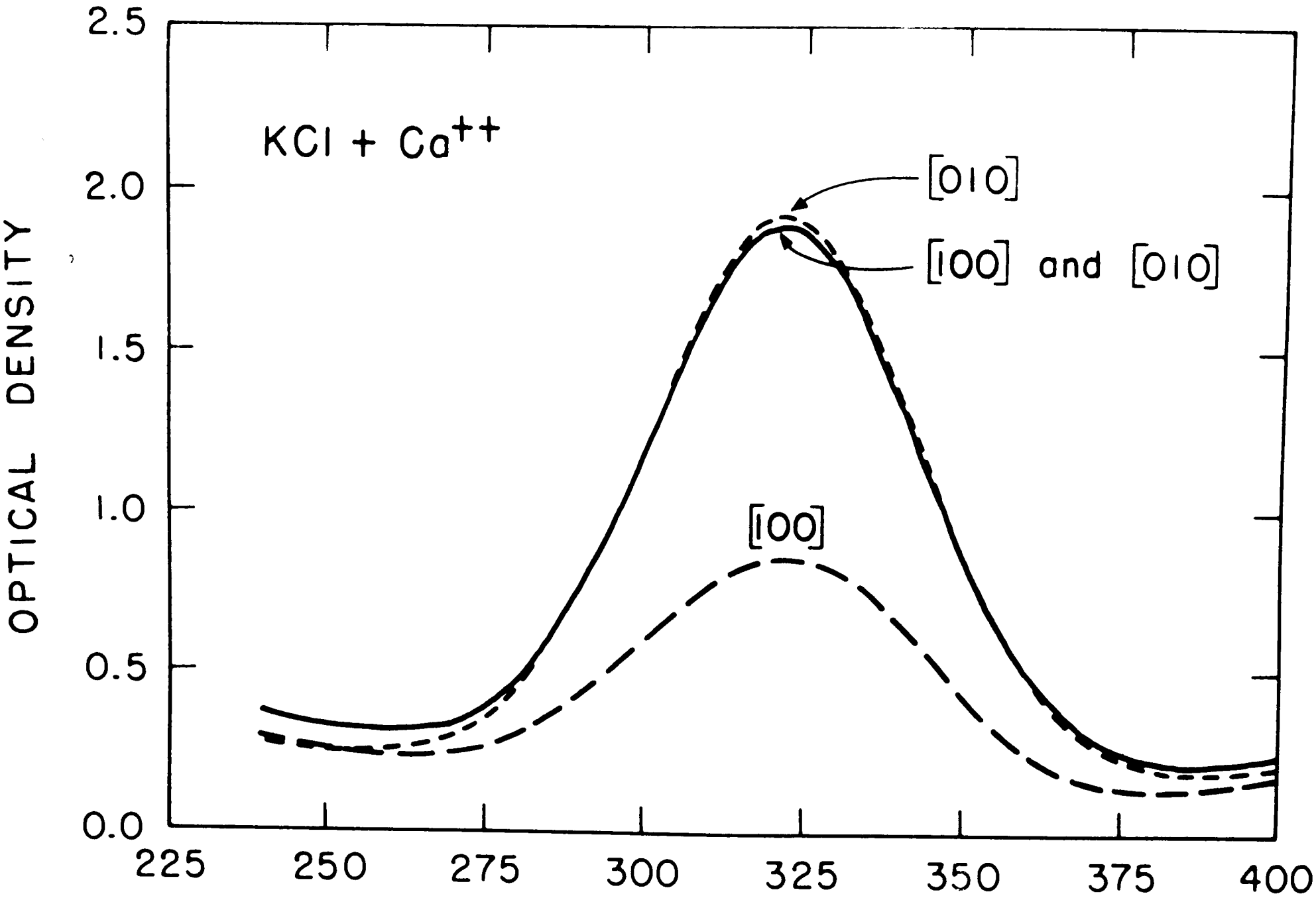



(b)

PARAMAGNETIC RESONANCE SPECTRUM OF $Cl_2^-$ IN KCl:Ca

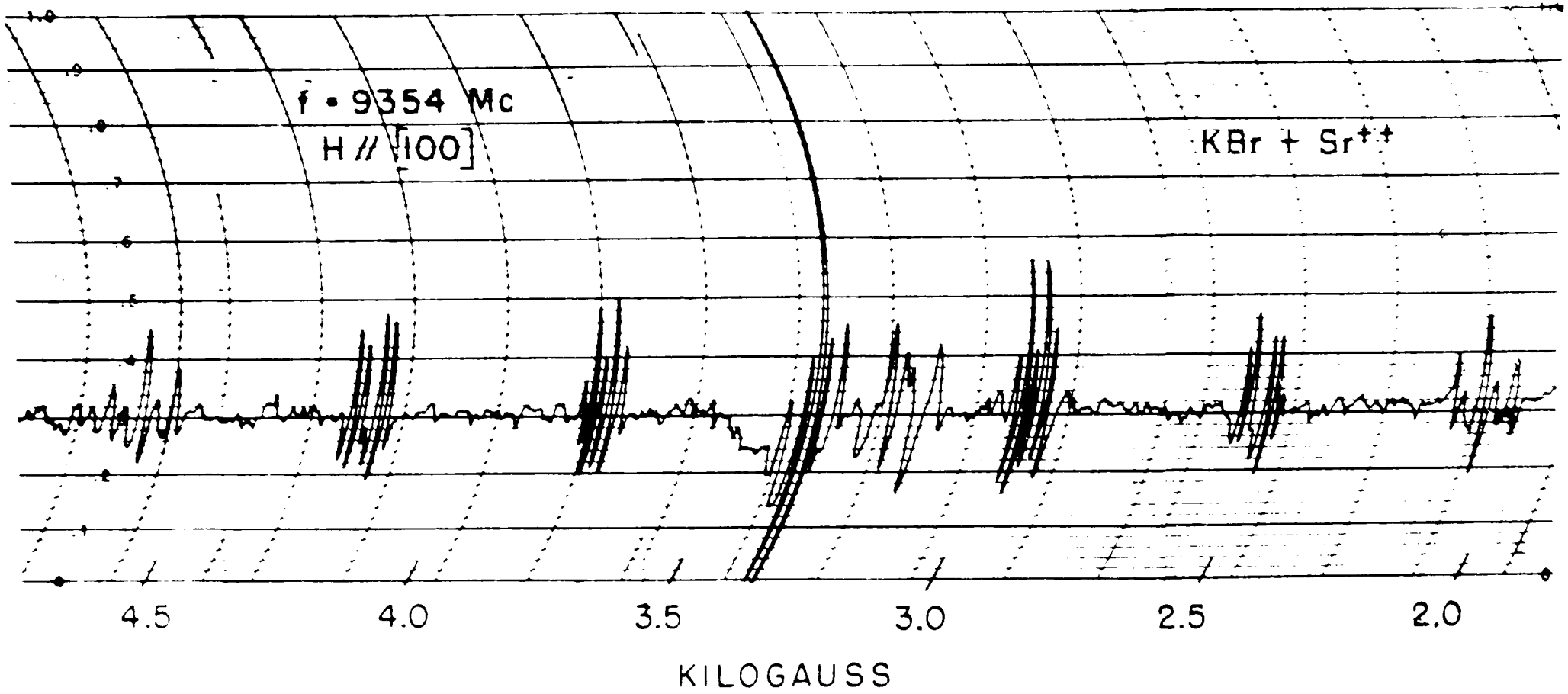
(a) H // [010] (b) H // [100]

FIG. 5.2



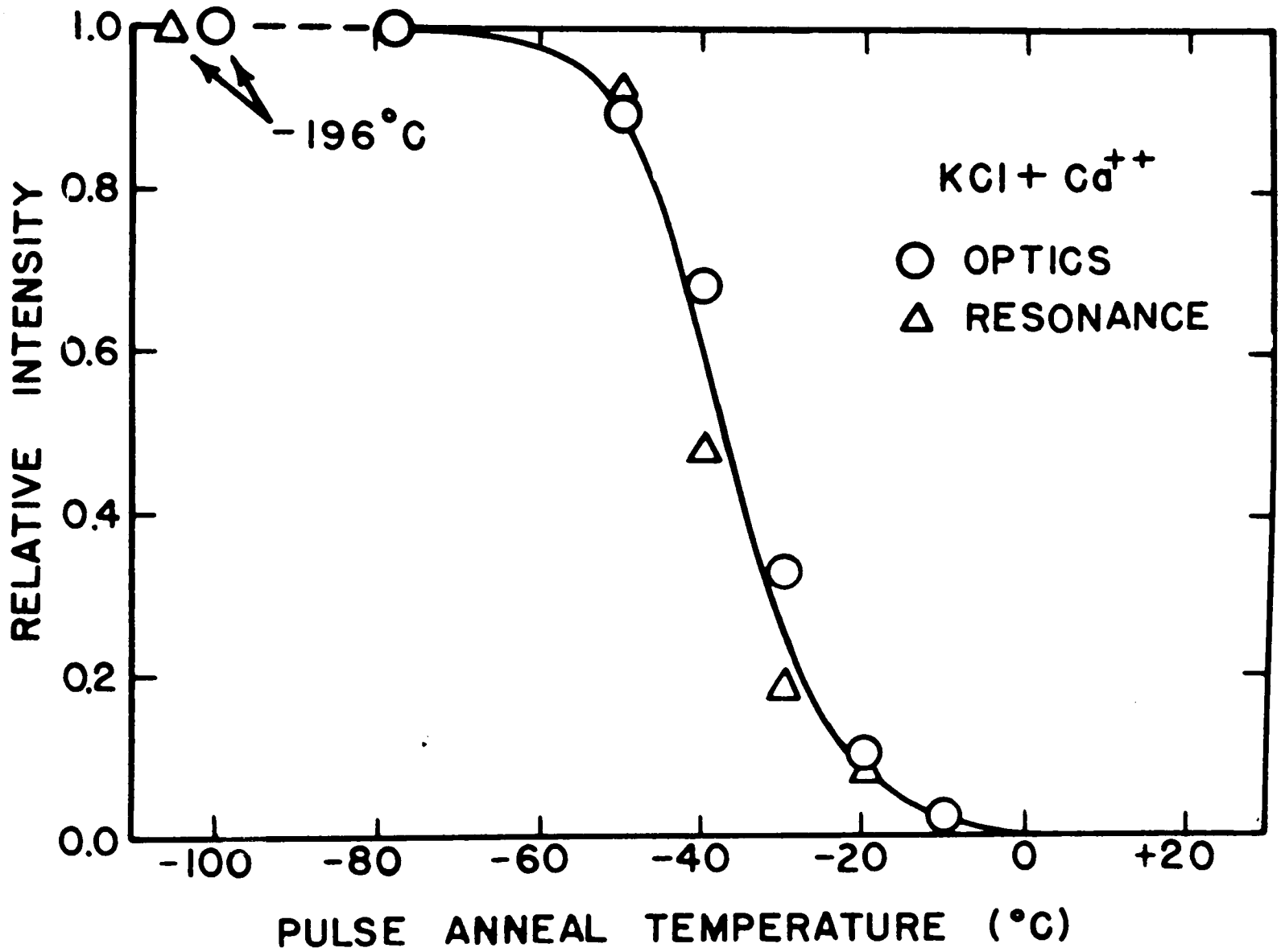

ULTRAVIOLET ABSORBTION BAND OF $Cl_2^-$ IN KCl: Ca (after Nichols)

FIG. 5.3



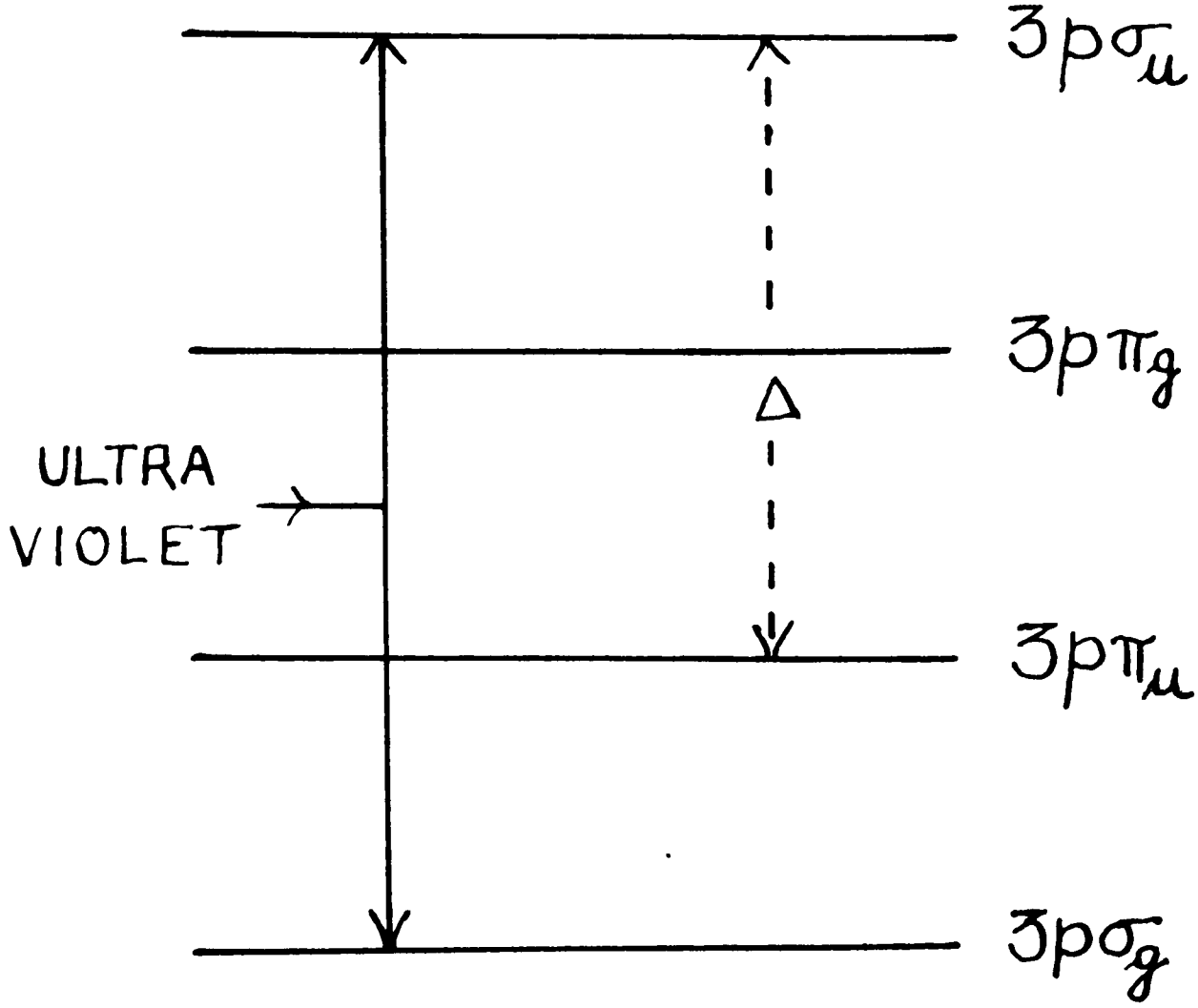

PARAMAGNETIC RESONANCE SPECTRUM OF $Br_2^-$ IN KBr:Sr

FIG. 5.4




DECAY OF $Cl_2^-$ IN KCl:Ca AS A FUNCTION OF TEMPERATURE

FIG. 5.5




SCHEMATIC ENERGY LEVEL DIAGRAM FOR $Cl_2^-$

FIG. 5.6

# CHAPTER VI

## POTASSIUM CHLORIDE CONTAINING SILVER

### VI.1 Introduction

An investigation of the properties of $X_2^-$ ions (X = F, Cl or Br) in alkali halides showed that the rate of production of these centres by X-irradiation at low temperatures is increased by a factor 100-1000 by the inclusion of impurities such as silver, thallium or lead into the halide lattice.[1,2] The rate of production of these [110] oriented $X_2^-$ centres is largely determined by the availability of electron trapping sites and in a 'pure' crystal the electron which is responsible for the hole on $X_2^-$ may be trapped at a negative ion vacancy forming F-centres. It has been suggested[1] that the impurities mentioned are extremely efficient electron traps and, if this is so, one expects changes in their properties after irradiation. Such changes have been observed in the case of KCl containing silver.[3] The investigation was carried out with Dr. Delbecq and Dr. Yuster and I am indebted to them for permission to quote their optical measurements here.

Crystals of KCl were grown by the Kyropoulos method from a melt containing about 1% by weight of AgCl.

### VI.2 Effect of X-irradiation on KCl:Ag at 77°K

Crystals of KCl containing $Ag^+$ ions were X-irradiated at 77°K for 10 minutes and the X-band paramagnetic resonance spectrum was subsequently examined at 77°K without warming the crystal; a strong $Cl_2^-$ spectrum was found flanked by two isotropic lines each with a similar

resolved chlorine structure. This suggests that the lines are due to a paramagnetic ion with a nuclear spin of $\frac{1}{2}$. Silver is the only element with $I = \frac{1}{2}$ present in appreciable concentration and one may conclude that during X-irradiation, electrons are trapped at $Ag^+$ sites producing neutral paramagnetic silver atoms in the lattice. This is the mechanism originally proposed[1] to account for the rapid production of $Cl_2^-$ centres in KCl doped with silver ions.

Silver atoms have a $4d^{10}\ 5s^1\ ^2S_{\frac{1}{2}}$ ground state and the g-value is expected to be near that of the free electron g-value. There are two naturally occurring isotopes, $^{107}Ag$ (51%) and $^{109}Ag$ (49%), each with $I = \frac{1}{2}$; the hyperfine splittings of the free atoms in zero field are 0.05719 $cm^{-1}$ and 0.06604 $cm^{-1}$ respectively. In the present case the silver h.f.s. is not resolved because of the presence of chlorine structure due to weak covalent bonding of the silver atoms with the surrounding chlorine ions. In order to make one set of accurate resonance measurements, a crystal of KCl was grown with enhanced $^{109}Ag$ (99.9%). The spectrum may be fitted to the spin Hamiltonian

$$\mathcal{H} = \beta \mathbf{H}.\mathbf{S} + \mathbf{A}\mathbf{I}.\mathbf{S} + \sum_N \mathbf{I}_o^N . \mathbf{A}^N . \mathbf{S} \qquad 6.1$$

where $S = \frac{1}{2}$, $I = \frac{1}{2}$, $I_o = \frac{3}{2}$ is the spin of the chlorine nucleus (chlorine isotope effects are not resolved), $g = 1.997 \pm 0.003$ and $A = 0.0620 \pm 0.0002$ $cm^{-1}$.

It was hoped to determine from an analysis of the chlorine structure whether the silver atoms were present substitutionally or interstitially. If the silver atoms are present interstitially, then each is surrounded by

an octahedron of chlorine ions. Chlorine hyperfine lines occur at fields displaced from the zero interaction position by

$$\delta H = \sum_N I_{ox}^N \left[A_s^N + A_p^N (3 \cos^2 \theta_{zp} - 1)\right] \qquad 6.2$$

where the symbols have the usual meanings (see Chapter II.2). When the external magnetic field is in the [111] direction, then $(3 \cos^2 \theta_{zp} - 1) = 0$ and a 19 line h.f.s. is expected with intensities in the ratios 1:6:21:56:120:216:336:456:546:580:546:456:336:216:120:56:21:6:1. Fifteen lines have been observed in the case of KCl:$^{109}$Ag which follow the above binomial intensity distribution closely (Fig. 6.1); the outside components were not observed because of insufficient intensity. The results indicate however that the silver atoms are present substitutionally. The measured values of the chlorine structure constants are

$$A_s = 12.0 \pm 0.2 \times 10^{-4} \text{ cm}^{-1}, \qquad A_p = 0.12 \pm 0.03 \times 10^{-4} \text{ cm}^{-1}.$$

The value of $A_p$ is close to the value $0.11 \times 10^{-4}$ cm$^{-1}$ calculated from pure magnetic dipole-dipole interaction.

The optical spectrum of the crystals irradiated at 77°K shows the $Cl_2^-$ absorption at 365 mμ and an absorption at 425 mμ due to $Ag^\circ$; the absorption bands are only partly resolved.

Ten minutes irradiation at 77°K produces $Ag^\circ$ centres with about 0.01 molar concentration. This represents about one fifth of the silver present in the lattice so that the defect centres now evident are $Ag^+$, $Ag^\circ$ and $Cl_2^-$. The silver atoms and $Cl_2^-$ ions are present with almost equal concentration.

## VI.3 Changes in the Properties of the Irradiated KCl:Ag Crystals with Increasing Temperature.

When crystals of KCl:Ag are X-irradiated at 77°K and warmed, the optical and resonance spectra do not change appreciably until the temperature reaches 208°K when a pronounced glow is observed. If the crystals are cooled to 77°K after the glow is extinct, the optical and resonance spectra are found to have changed. The $Cl_2^-$ resonance spectrum is completely absent and the intensity of the $Ag^0$ resonance is reduced by about 20%. A new resonance spectrum is observed which arises from three similar centres in the magnetic unit cell each with axial symmetry about a different cube edge, to within the resolution of measurement. The resonance observed with the external magnetic field along the [100] direction is shown in Fig. 6.2(a). The spectra with axial symmetry about [001] and [010] are superimposed and each has an eight line hyperfine envelope with intensities in the ratios 1:3:5:7:7:5:3:1. Such a pattern will arise from a hole localised on a silver ion and two chlorine ions, each occupying normal lattice sites, if the hyperfine interaction constants of the silver and chlorine ions are identical. The model for the centre is shown in Fig. 6.3. The line width is 20 gauss and each line is an envelope of partly resolved structure due to interaction of the unpaired electron with the remaining four chlorines in the octahedron. The centre with axial symmetry about the [100] direction gives rise to a h.f.s. consisting of two resolved lines; in this case the chlorine structure is unresolved and the two lines arise from the interaction of the electron with the silver nucleus. In future, for convenience, we shall refer to this high temperature hole centre as $AgCl_2$.

The spectrum may be fitted to the spin Hamiltonian

$$\mathcal{H} = g_{11}\beta H_z S_z + g_\perp \beta (H_x S_x + H_y S_y) + A I_z S_z + B(I_x S_x + I_y S_y)$$
$$+ A^1 [(I^I_{oz} + I^{II}_{oz}) S_z] + B^1 [(I^I_{ox} + I^{II}_{ox}) S_x + (I^I_{oy} + I^{II}_{oy}) S_y] \qquad 6.3$$

where $S = \frac{1}{2}$, $I = \frac{1}{2}$ is the spin of the silver nucleus, $I^I_o = I^{II}_o = \frac{1}{2}$ is the spin of the chlorine nuclei, $g_{11} = 2.196 \pm 0.006$, $g_\perp = 2.038 \pm 0.005$, $A = 39 \pm 2 \times 10^{-4}$ cm$^{-1}$, $B = 30 \pm 4 \times 10^{-4}$ cm$^{-1}$, $A^1 < 4 \times 10^{-4}$ cm$^{-1}$ and $B^1 = 30 \pm 4 \times 10^{-4}$ cm$^{-1}$. Silver and chlorine isotope effects are not resolved.

It may be mentioned here that preliminary measurements show that the behaviour of NaCl:Ag is similar to that of KCl:Ag. Optical experiments indicate the existence of $Ag^\circ$ and $AgCl_2$ centres. We have failed to detect the $Ag^\circ$ resonance for reasons which are not understood but a resonance from the $AgCl_2$ centres has been observed (see Fig. 6.2(b)). The constants of the spin Hamiltonian 6.3 in this case at 77°K are

$g_{11} = 2.189 \pm 0.007$, $g_\perp = 2.039 \pm 0.005$,

$A = 38 \pm 2 \times 10^{-4}$ cm$^{-1}$, $B = 30 \pm 4 \times 10^{-4}$ cm$^{-1}$,

$A^1 < 4 \times 10^{-4}$ cm$^{-1}$, $B^1 = 30 \pm 4 \times 10^{-4}$ cm$^{-1}$.

The line width in the spectrum with axis parallel to the magnetic field is 22 gauss and perpendicular to the magnetic field is 16 gauss. The interaction with the four chlorines in the plane perpendicular to the symmetry axis is not resolved in this spectrum.

When the resonance spectrum is investigated at higher temperatures

it is found that in the case of KCl the $Ag^{\circ}$ resonance does not change appreciably but the lines of the $AgCl_2$ centre begin to broaden at 153°K and are too broad to be observed at 178°K. However, if the crystal is warmed to room temperature for a few minutes and then cooled to 77°K, the $AgCl_2$ resonance is again observed with little loss of intensity. The line broadening may be due to a rapid reorientation of centres among the three equivalent orientations and a consequent short life time. In the case of NaCl the reorientation rate at a given temperature is more rapid and the resonance is too broad to be detected at 90°K. The poor resolution at 77°K is probably due to the onset of broadening at this temperature. The $AgCl_2$ resonance cannot be observed in either case at 20°K because of saturation.

Corresponding changes in the KCl:Ag optical spectrum are observed on warming past the first glow and subsequent cooling to 77°K. The $Ag^{\circ}$ absorption is found to have dropped in intensity by about 20 and the $Cl_2^-$ absorption has disappeared. On the other hand, two new bands are observed at 338 mμ and 460 mμ which have been assigned to the $AgCl_2$ centre. A dichroism is induced in both of these bands by irradiating into the 335mμ band at about 4°K with light polarized in the [100] direction. Subsequent examination near 4°K with light polarized in the [100] and [010] directions shows that the [100] oriented centres have been preferentially bleached. Both the optical and resonance spectra show that irradiation into the 335 mμ band with unpolarised light at 77°K causes dissociation of the $AgCl_2$ centres and the re-formation of $Cl_2^-$ centres.

In the neighbourhood of 373°K the $Ag^{\circ}$ and $AgCl_2$ centres in KCl

disappear rapidly and a glow peak is observed. The $AgCl_2$ centre is stable above 100°C in a crystal of KCl containing both $Ag^+$ and $NO_3^-$ ions due to the existence of a more stable electron trap than $Ag^+$. In the present case we conclude that the decay of the $AgCl_2$ centre is due to the thermal instability of $Ag^0$; the released electron is captured by an $AgCl_2$ centre with the emission of luminescence and the crystal is now in its original unirradiated state.

## VI.4 Discussion

The mechanism by which the $AgCl_2$ centre is produced is as follows. When the crystal is warmed to the first glow point the $Cl_2^-$ ions are moving rapidly through the lattice. If the silver atoms and ions are distributed at random throughout the lattice, then, about $\frac{1}{5}$ of the $Cl_2^-$ ions will encounter silver atoms and about $\frac{4}{5}$ will encounter silver ions. Electrons are removed from silver atoms by $Cl_2^-$ ions forming $Ag^+$ ions and normal $Cl^-$ ions. This accounts for the first luminescent glow and the partial reduction of $Ag^0$ concentration. The $Cl_2^-$ ions which encounter $Ag^+$ ions are trapped forming $AgCl_2$ centres.

A preliminary investigation of the theory of the $AgCl_2$ centre by Dr. M.C.M. O'Brien[4] indicates that the hole is localised on the silver ion for about 75 of the time. A hole trapped at $Ag^+$ is essentially $Ag^{2+}$ which is expected to have the configuration $4d^9$. This may be compared with the configuration of $Ni^+$ or $Cu^{2+}$ which is $3d^9$. The effect of a cubic crystal field on the $^2D$ ground state of these ions has been discussed in Chapter II.7 and it was pointed out that a Jahn-Teller distortion of the cubic field may occur. The contraction of the

octahedron of chlorine ions along a cube edge observed in the case of the $AgCl_2$ centre may be a similar effect.

REFERENCES

1. Delbecq, C.J., Smaller, ..., Yuster, P.H., Phys. Rev., (1958), 111, 1235.

2. Delbecq, C.J., Hayes, ..., Yuster, P.H., to be published.

3. Hayes, ., Delbecq, C.J., Yuster, P.H., Bull. Am. Phys. Soc., . (1958), Ser. II, 3, 178.

4. O'Brien, M.C.M., private communication.

Fig. 6.1. Paramagnetic resonance spectrum of $^{109}Ag^{o}$ in KCl showing resolved chlorine structure.

Fig. 6.2. Paramagnetic resonance spectrum at 77°K of the $AgCl_2$ centre in (a) KCl (b) NaCl. The eight line hyperfine envelope arises from centres with their axes perpendicular to the external magnetic field and the two line hyperfine envelope from centres with their axes parallel to the magnetic field.

Fig. 6.3. Model for the $AgCl_2$ centre. A distortion of the octahedron of chlorines surrounding the silver ion occurs so that the interaction of the silver ion with two chlorine ions is stronger than the interaction with the remaining four.

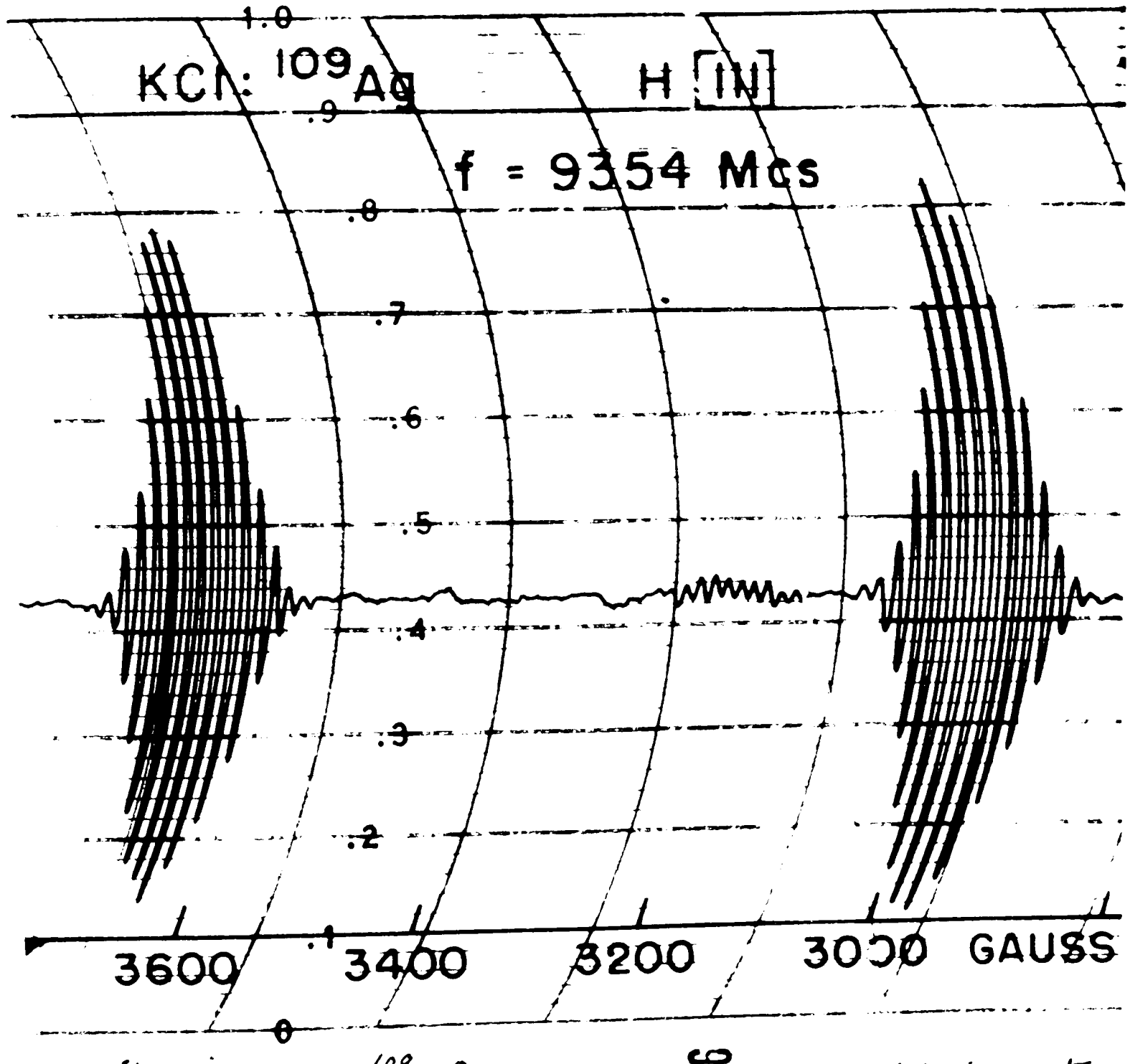
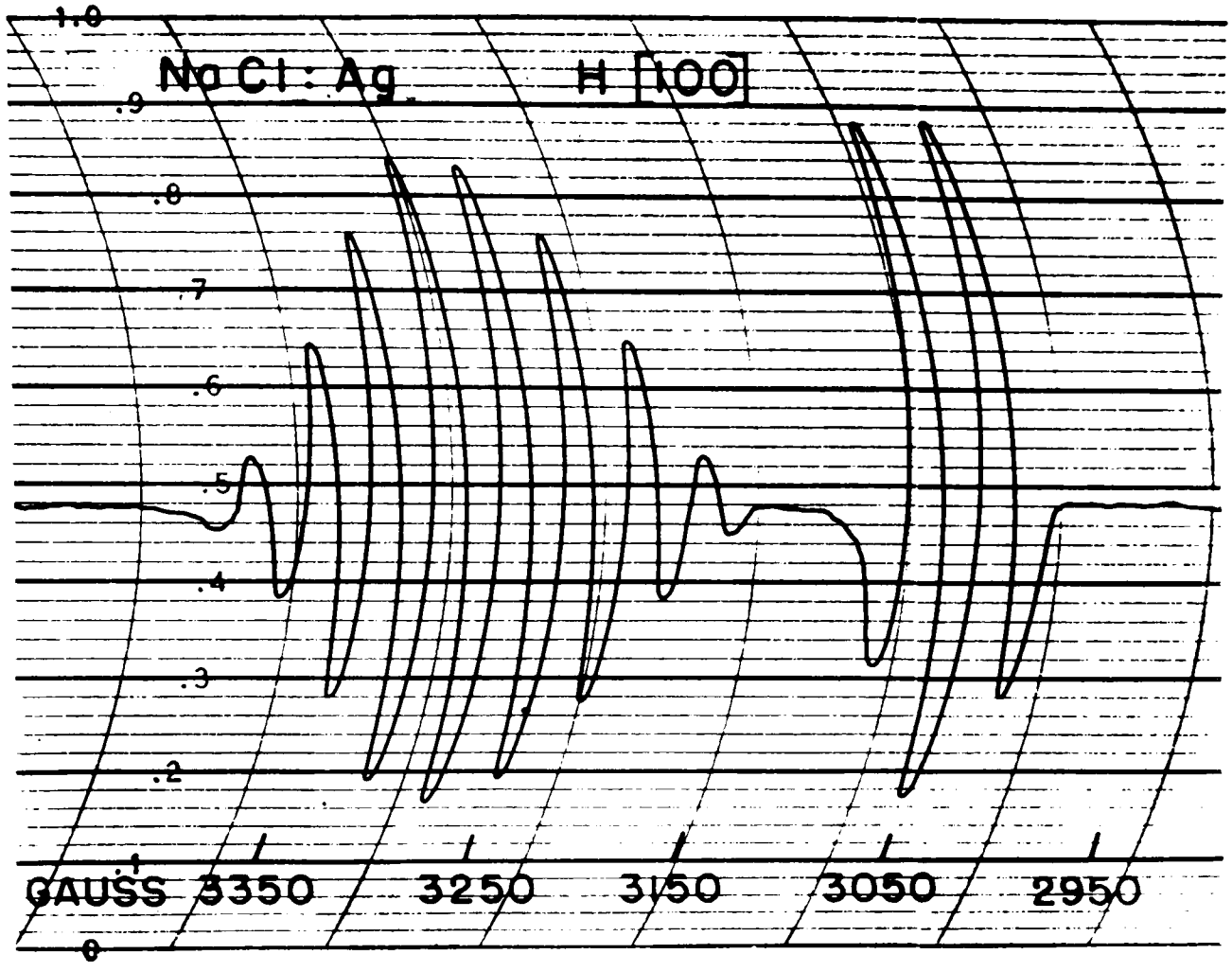



Fig. 6.1. Spectrum of $^{109}Ag^{0}$ in KCl showing chlorine structure



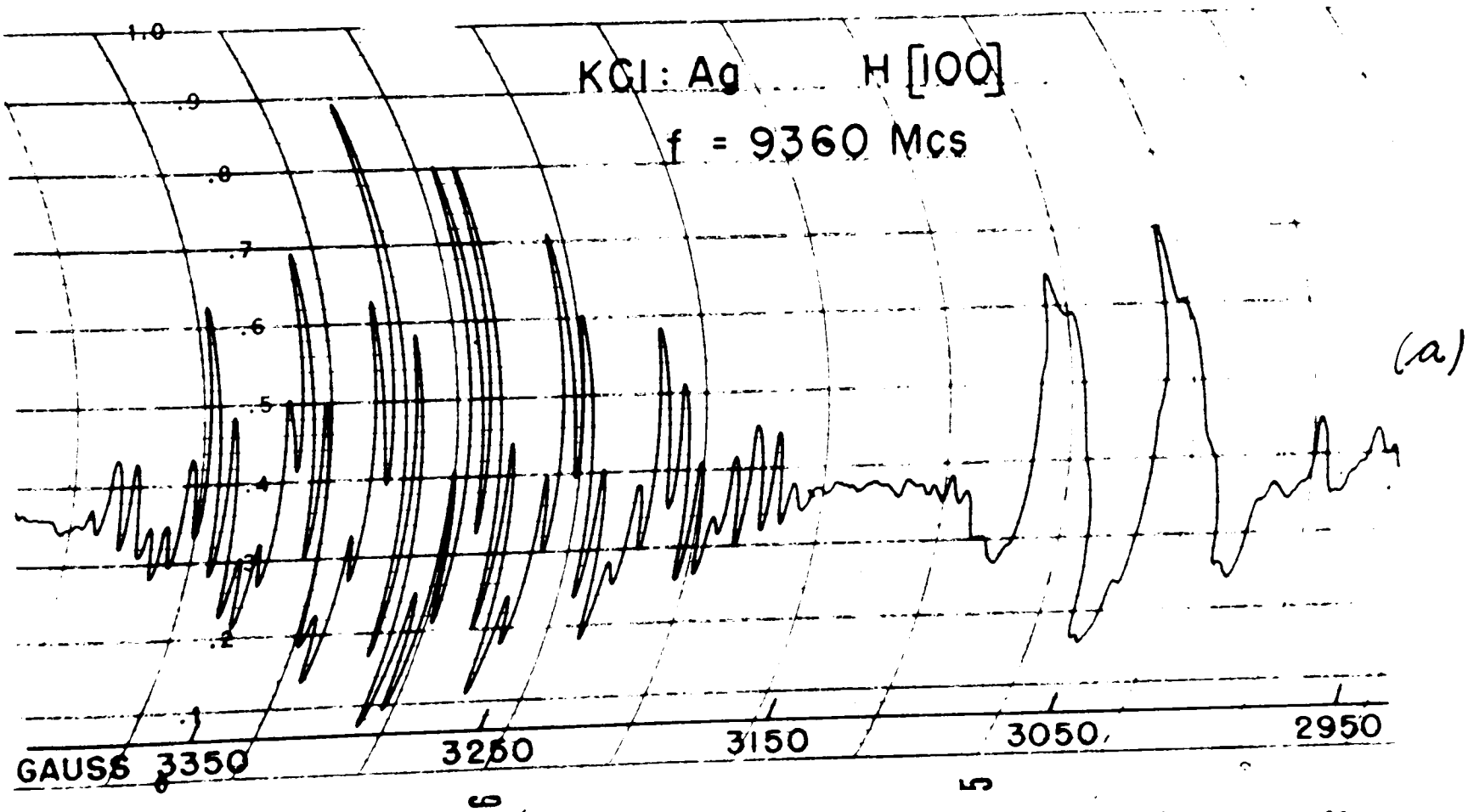
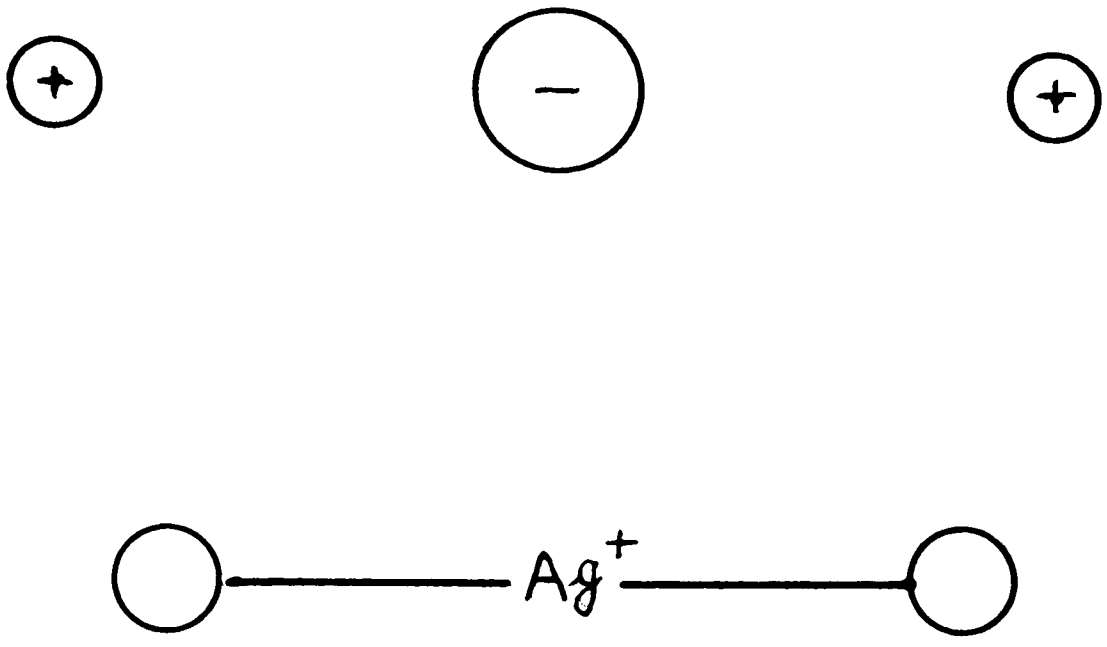
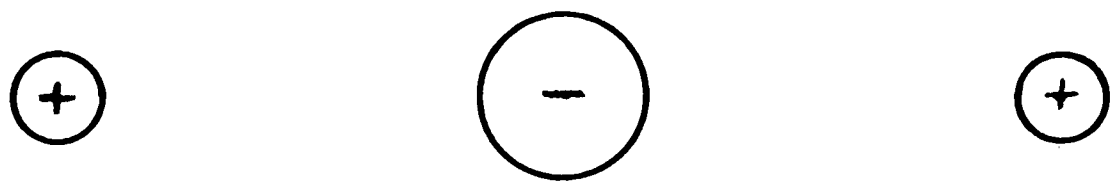




Fig. 6.2. Spectrum of the '$Ag Cl_2$' centre in (a) KCl, (b) NaCl.




MODEL FOR $AgCl_2$ CENTRE
IN KCl

FIG. 6.3